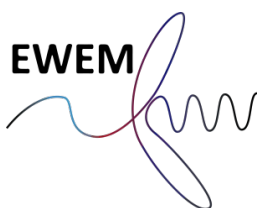




Integration methods for floating offshore wind farms

Master thesis

Florian Dach



Integration methods for floating offshore wind farms

MSc Thesis

by

Florian Dach

in partial fulfillment of the requirements to obtain the degrees of

[Master of Science](#) in Offshore and Dredging Engineering at the Delft University of Technology

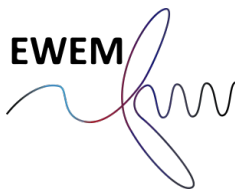
&

[Master of Science](#) in Technology- Wind Energy at the Norwegian University of Science and Technology

under the [European Wind Energy Master](#) programme

To be defended publicly on Tuesday July 18th, 2023

Student number:	5630894	TU Delft
	582209	NTNU
Submission date:	June 28, 2023	
Supervisors:	Prof. Dr. Zhen Gao	NTNU
	Dr. Xiaoli Jiang	TU Delft



Title picture ©Associated British Ports

Abstract

The amount of floating offshore wind farms under development has drastically increased over the past years as the technology becomes viable for pre-commercial and commercial scale projects. Projects of this size require a streamlined, efficient production of the complete floating offshore wind turbine (FOWT), not only for manufacturing the floater but also for assembling the complete system. Most assembly tasks could, in theory, take place in a port, which is generally preferred, but most ports do not have the sufficient port infrastructure to perform those tasks, while the required infrastructure upgrades are very expensive. This is a significant challenge for smaller-scale, first-mover floating wind farms, which do not have sufficient units to justify those substantial investments for the assembly. To overcome this issue, a jack-up type wind turbine installation vessel could be used nearshore to integrate the wind turbine on the floating unit. This would ensure the realisation of the project without major infrastructure investments. At the same time, it could utilise the sheltered area's advantages and be a kick-off for large-scale projects in the region.

This proposed concept has so far not been investigated in academic research. Therefore, this thesis aims to create a general understanding of the system and its characteristics. Based on the example of Port Talbot in the UK, it should be examined how the concept can be implemented in a location. Furthermore, a response analysis of the system is done in SIMA for the single blade installation to understand which motions characterise the integration task and which environmental conditions limit the operation. Those operational limits are then implemented in a Python model of the complete integration sequence to conduct an operability analysis which should also give estimates for the required installation time and costs of the system when subject to wind and wave loads. Based on the findings of those studies, the technical and economic feasibility of the concept should be investigated.

The study has found that the wave-induced floater motions are mainly governing the systems motions during the single blade installation, which leads to very strict operational limits for the waves during the mating procedure. The technical feasibility of the proposed system is given if it is not subject to large tides and if a sufficient control mechanism is implemented for the installation. The operability analysis has shown that the system can be economically feasible if smaller projects should be implemented. For large projects, it is likely more feasible to invest into the port infrastructure.

All used scripts and models can be found at <https://github.com/F10tastic/FDachMasterThesis>.

Keywords: Floating offshore wind turbine, Wind turbine integration, Port infrastructure, Turbine assembly, Single blade installation, Wind turbine installation vessel, Jack-up vessel, Response analysis, Operational limits, Operability analysis, Wind farm installation, Offshore wind

Preface

This master's thesis is submitted to fulfil the requirements for obtaining the master's degree in Offshore and Dredging Engineering at the Delft University of Technology, as well as the master's degree in Technology-Wind Energy at the Norwegian University of Science and Technology (NTNU) under the European Wind Energy Master (EWEM) programme. The work was conducted in collaboration between the Department of Maritime and Transport Technology at TU Delft, the Netherlands, and the Department of Marine Technology at the NTNU in Trondheim, Norway. The supervision from NTNU has been done by Prof. Dr Zhen Gao and from TU Delft by Dr Xiaoli Jiang.

I want to express my warm gratitude to my university supervisors for their guidance throughout my thesis. They helped me a lot to find orientation in my work and were great support whenever I encountered problems. I want to thank Zhen Gao for his extensive support during this past half year despite being 7890km and seven time zones apart. His insights were extremely helpful to determine the goals of this thesis and his expertise helped me tremendously throughout the past year. I am very thankful to Xiaoli Jiang for sharing her knowledge and supporting this work. I truly believe that thanks to her profound, critical questions, this work has gotten a much better academic work than I'd ever imagined creating.

A large thanks goes also to the industry experts I had the opportunity to talk to. I am thanking Hamish Armstrong and Trond Grytten from Moreld Ocean Wind, who substantially helped me in our elaborate conversations to better understand the characteristics of the assembly of floating wind turbines. Furthermore, I am thanking Yeray Solis Boado from Havfram for sharing his expertise on the installation of offshore wind turbines and Laura Sloomweg from Ørsted for our discussion about temporary shallow water moorings. None of the mentioned companies were directly involved in this work and no sensitive information has been shared. The experts were only consulted to gain a broader understanding of the very novel concepts.

I would like to thank everyone that has supported me throughout the past two years of this master's. I am incredibly grateful for my fellow EWEM students, who accompanied me on this journey. Without you, this master's would not have been possible and I truly believe that some of you will be my lifelong friends. Thank you for sharing with me your passion for wind energy and I am looking forward to collaborating with you throughout my professional career. I am very thankful for every single person I have met over the past two years while doing this master's. It is a true privilege to get to know so many amazing people in such a short amount of time and you enriched my life. Thank you to the master's students at the marine department at NTNU, who helped me through the daily struggles of the master's thesis and the hustle with SIMA. A special thank goes to my friends in Trondheim, who supported me through this past half year and always helped to clear and dance off my mind. I am very thankful to my friends in Germany, who always supported me on my journey to fulfil my dreams, even though it meant leaving them. Lastly, I'd like to thank my parents. Your infinite love and trust in me have supported me throughout my entire life and given me the confidence to do every step I did. It is the greatest privilege I can imagine to have you as my parents and none of this would have been possible without you.

*Florian Dach
Trondheim, June 2023*

Contents

List of Figures	v
List of Tables	vii
Abbreviations and units	viii
1 Background and objectives	1
1.1 Aim and scope	3
1.1.1 Assumptions and simplifications	3
1.1.2 Thesis structure	4
2 Introduction	6
2.1 Floating wind turbines	6
2.2 Market development	8
2.3 Port activities	13
2.3.1 Manufacturing port	14
2.3.2 Assembly port	15
2.4 Integration procedure	18
2.5 WTIVs for the turbine integration of floating wind turbines	20
2.5.1 Wind turbine installation vessels	21
2.6 Integration sequence	23
3 Case study	25
3.1 Site location	25
3.1.1 Wind farm site	27
3.2 Environmental conditions	27
3.3 Implemented components	31
3.3.1 Jack-up vessel	31
3.3.2 Floater	31
3.3.3 Wind turbine	32
3.3.4 Moorings	32
3.4 Setup	33
3.5 Implementation of the integration sequence	35
4 Modelling of the system	36
4.1 Literature review	36
4.2 Modelling method	37
4.2.1 Assumptions	38
4.2.2 Environmental loads	39
4.2.3 Equations of motion	40
4.2.4 Single blade installation criteria	42
4.3 Integration system	43
4.3.1 Jack-up vessel	43
4.3.2 Wind turbine blade	44
4.3.3 Floating wind turbine	45

4.3.4	Moorings	46
4.4	Applying the integration criteria	49
4.5	Numerical model	50
4.5.1	Jack-up vessel	51
4.5.2	Wind turbine blade	52
4.5.3	Floating wind turbine	53
4.5.4	Moorings	53
4.5.5	Load cases	54
4.5.6	Time-domain simulations	56
5	Simulation results	57
5.1	Blade motion	57
5.1.1	Crane motion	58
5.2	Blade root motion	58
5.3	Floater	62
5.3.1	Moorings forces	63
5.4	Hub	64
5.5	Relative motion	66
5.6	Alignment results	69
5.7	Mating phase	73
5.8	Discussion	76
5.9	Technical feasibility	78
6	Operability analysis	80
6.1	Literature review	81
6.2	Assumptions	82
6.3	Calm weather model	84
6.3.1	Parameters and input	85
6.3.2	Mathematical model	87
6.3.3	Results	88
6.4	Weather restricted model	89
6.4.1	Weather windows	90
6.4.2	Operational limits	91
6.4.3	Results	94
6.4.4	Sensitivity analysis	98
6.5	Discussion	102
6.6	Economic feasibility	103
7	Conclusion	106
7.1	Recommendations	107
	References	I
	Appendices	IX

List of Figures

1	Flow chart of the thesis content	5
2	Concept sketch of the different floater types	7
3	Long-term forecast of floating offshore wind	9
4	Expected annual new floating wind installations	10
5	Development of wind turbine models	11
6	LCOE prediction based on wind farm size	12
7	Anticipated LCOE reduction of floating wind	12
8	Cost breakdown of the total lifetime cost of a floating wind farm	13
9	Construction process of a floating wind farm	14
10	Load-out of the WindFloat floater with a semi-submersible	15
11	Concept art of the SK6000 ring crane	17
12	Turbine integration with a ring crane for the spar buoys of Hywind Tampen	17
13	The blade root with its guide pin and the hub	19
14	Concept art of a jack-up vessel used for the floating wind turbine integration	21
15	Mobile Port Solution of Fred Olsen 1848	21
16	Global WTIV fleet up to 2030	22
17	Map of the planned floating wind areas in the British Celtic Sea and adjacent ports	26
18	Current picture of the port of Port Talbot	26
19	Floating wind vision of the port Port Talbot	26
20	Location of the hindcast data	28
21	Scatter diagram Port Talbot	29
22	Wave rose Port Talbot	29
23	Wind rose Port Talbot	29
24	Monthly H_s distribution Port Talbot	30
25	Multicolored bathymetry profile of the Swansea Bay with the elevation profile of the green line	30
26	Bold Tern jack-up vessel with the upgraded crane	31
27	INO Windmoor 12MW concept	31
28	Storage of the Kin04 floater with horizontal mooring lines and bollards	33
29	Visualisation of the investigated integration operation in Port Talbot	34
30	Routes between Port Talbot, Swansea and Pembroke Dock	35
31	System and its coordinates from a side view	38
32	System and its coordinates from a top view	38
33	Illustration of a leg-encircling crane	44
34	Illustration of the yoke system	45
35	Results of decay tests for different mooring setups	47
36	Illustration of the different mooring angle setups	47
37	Hourly time series of the extrapolated MSL on site in 2015, data extrapolated from tidetimes.co.uk	49
38	Numerical SIMA model of the integration system	51
39	Coupled simulation method for blade loads	52
40	Overview of the structural model of the jack-up crane vessel	53
41	Investigated wind and wave heading angles	56
42	Spectral density functions of the blade motion for load case 14	58

43	Spectral density functions of the blade root motion for load case 14	59
44	Time series of the blade root motion radius and tracking of the blade root centre compared to its mean position at LC14	60
45	PSD of the motion radius of the blade root at LC14	61
46	Determination of the critical motion of the blade root motion	61
47	Spectral density functions of the floater motions at LC 14	63
48	Statistics of the mooring forces	64
49	PSDs of the hub motions in x- and z-direction at LC14	65
50	Time series of the hub motion radius and tracking of the hub centre compared to its mean position at LC14	66
51	PSD of the motion radius of the hub at LC14	66
52	Time series and tracking of the relative motion between the hub and the blade root in the xz-plane at LC14	67
53	PSD of the relative motion in the xz-plane at LC14	67
54	PSD of the motion radius of the blade root at LC14	68
55	Distance in y-direction between the hub and the blade root	69
56	Critical motion radii for all considered load cases	70
57	Impact of the alignment angle of the incoming wind on the critical outcrossing motion	71
58	Critical motions at different wind speeds for Case A	72
59	Number of simulations which have exceeded the y-limit out of six simulations	72
60	Time series and PSDs of the relative motion of LC14 when applying high pass filters of 0.5Hz and 0.3Hz	74
61	Critical pin-flange motion radii for all considered load cases with a filter of 0.5Hz	75
62	Integration sequence for the feeder concept	80
63	Integration sequence for the shuttling concept	81
64	Total installation time in the calm weather model	89
65	Total installation cost in the calm weather model	89
66	Exemplary integration sequence of a turbine for the weather data of 2016	91
67	Average total installation time in the weather-restricted model	95
68	Average total installation cost in the weather-restricted model	95
69	Average waiting time separated by wind and waves	96
70	Average operability of the different scenarios and cases under weather restriction	96
71	Waiting times of the different operations for all cases	97
72	Waiting times of the different operations for all cases	98
73	Average total installation time with different operational limits	99
74	Average total installation cost with different operational limits	99
75	Installation time of the mean feeder scenario when starting at different times	100
76	Installation times for the different amounts of turbines to be installed	101
77	Installation costs for the different amounts of turbines to be installed	101
78	Operability for the different amounts of turbines to be installed	102
79	Sketch of the different stabilization types for floating substructures	IX
80	Impact of co-location and proximity to site	X
81	Distance between White Cross site and Port Talbot	XI
82	Scatter diagram White Cross site	XII
83	Wave rose White Cross	XIII
84	Wind rose White Cross	XIII

85	Monthly H_s distribution White Cross	XIII
86	Velocity triangle of a 2D wind turbine blade	XIV
87	Time series of the blade decay test in all 6 DOF	XIV
88	Response amplitude operators of the blade decay test	XV
89	Time series of the crane tip motions at LC14	XVI
90	PSD of the relative crane time motion in the xz-plane at LC14	XVII
91	Critical blade root motion at LC14 for different turbulence intensities	XVII
92	Critical blade root motion at LC14 for different tug line pretensions	XVIII
93	PSDs of the floater motions from the decay test	XIX
94	Time series of the mooring line forces of line 2 at LC14 for different simulations . . .	XX
95	PSD of the relative motion in the xz-plane at LC14 when only considering wave loads	XXI
96	PSD of the relative motion in the xz-plane at LC14 when only considering wind loads	XXII
97	PSD of the relative motion in the xz-plane at LC14 when only considering currents .	XXII
98	Critical pin-flange motion radii for all considered load cases with a filter of 0.3Hz . .	XXIII
99	Detailed allowable sea states for the transition piece installation with different head- ing angles	XXIV
100	Operability with the different operational limits	XXV
101	Waiting time per month, separated by the different causes for the waiting time . . .	XXVI

List of Tables

1	Required parameters for a floating offshore wind assembly port	18
2	Main parameters of the jack-up vessel	43
3	Main parameters of the modified crane	44
4	Rotor scaling procedure with scaling factor s	45
5	Main parameters of the upscaled blade lifting system	45
6	Main parameters of the floater	46
7	Main parameters of the assembled FOWT	46
8	Main parameters of mooring line	48
9	Sea states with the highest probability for every wind speed	55
10	Examined load cases	55
11	Statistics of the blade root motion radius	60
12	Comparison of the natural floater periods	62
13	Outcomes of the alignment modelling	73
14	Outcomes of the complete single blade installation	76
15	Wind farm and vessel parameters	86
16	Operation task times	87
17	Operational limits of the integration sequence	92
18	Alpha factor for waves in the base case	93
19	Alpha factor for wind	93
20	Operational limits with applied alpha factor	93
21	Statistics of the hub motion radius	XXI

Abbreviations and units

Abbreviation	Long Version
AEP	Annual energy production
CAPEX	Capital expenditure
CAGR	Compound annual growth rate
COG	Centre of gravity
FCR	Fixed charge rate
FOWT	Floating offshore wind turbine
H_s	Significant wave height
LCOE	Levelized cost of electricity
MBL	Maximum break load
MSL	Mean sea level
OPEX	Operational expenditure
PSD	Power spectral density function
Spar	Single point anchorage
Std	Standard deviation
TLP	Tension leg platform
T_p	Peak period
U	Wind speed
WTG	Wind turbine generator
WTIV	Wind turbine installation vessel
WoW	Wait-on-weather

Unit	Description
deg	Degree
GPa	Gigapascal
GW	Gigawatt
Hz	Hertz
kg	Kilogram
kn	Knot
kNs	Kilonewton second
m	Meter
m/s	Meter per second
mm	Millimeter
MW	Megawatt
MWh	Megawatt-hour
N	Newton
s	Second
t	Ton

1 Background and objectives

In the context of the climate crisis and worldwide increase in demand for energy, it is essential to increase the global production of renewable, carbon-free electricity. Given the amount of required energy and the different characteristics of every renewable electricity resource, it is important that every potential resource is being utilised and that the suited technologies will be built out simultaneously to reach the global climate goals. Wind energy will be one of the key components of this energy transition, with wind resources being utilised both on land and on the sea. Compared to on-shore wind energy, offshore wind energy can utilise a more constant wind potential at lower heights with fewer restrictions in regard to the turbine size and the number of installed turbines. However, the technology has been so far limited to areas with shallow waters as the bottom-fixed foundations of the turbines are generally only deemed as economically feasible for water depths up to 60m.

Floating offshore wind turbines are promising to alleviate this problem as in this concept the turbines are installed on floating foundations which are kept in position by the use of mooring lines which are anchored to the seabed. Therefore, they can be utilised in water depths ranging from 60m up to 1000m, tapping into new wind potential as around 80% of all offshore wind potential lies in water depths deeper than 60m (Williams et al., 2022, p.96). However, in comparison to bottom-fixed offshore wind turbines, as of June 2023, floating offshore wind is still in a very early stage of development while a lot of large projects around the globe are already being announced and developed for the late 2020s and early 2030s. Realising those projects could impose several difficulties as, when compared to bottom-founded turbines, a floating wind turbine has significantly different requirements in regards to the manufacturing infrastructure for the foundations and the infrastructure for the turbine assembly.

The bottom-fixed wind turbine always needs to be installed at its designated location. Therefore, the foundation, in most cases a monopile, is either piled into the seabed or lowered to the ground when a gravity based foundation is used (Ramirez et al., 2021, p.27). The wind turbine is installed step by step onto the foundation with a crane vessel. This process is also called the integration of the wind turbine. Modern offshore wind projects are wind farms with several dozens of the largest wind turbine models with very specialised installation requirements. Therefore, plenty of specialised integration vessels have been built with several more under construction.

When it comes to floating wind turbines, depending on the foundation type, the integration does not need to take place on the wind farm site but can be located in a sheltered port location from where the assembled FOWT can be towed to the site. This is generally welcomed, as the on site integration can be very expensive and challenging as it is subject to much harsher environmental conditions. Those conditions reduce the utilisation rate of the vessel as it needs to wait for suitable weather windows. Given the very high day rates, this can get very costly. In contrast, the integration of the wind turbine in a sheltered port could, in theory, happen much faster with less specialised equipment. However, not many ports currently fulfil the required infrastructure needs for the turbine integration of a FOWT. The reason for this is that most shipyards and other port types are not suited for the size of the floating foundations, also called floater, and also the very large wind turbine size imposes new challenges. Furthermore, the assembly port needs to be in sufficient proximity to the floating wind farm site due to the operational limitations of the towing. In theory, it would be reasonable to build specialised floating wind ports in proximity to potential

floating wind areas. However, those large infrastructure investments are only made if a sufficient pipeline of floating turbine integrations can be predicted. Floating wind projects are still in an early phase, where the first projects in any location usually have only a handful of turbines with farm capacities of up to 200MW (Spearman et al., 2020, p.11). Those projects are too small to trigger dedicated infrastructure investments and thus, their realisation could be in danger (Associated British Ports, 2021, p.19). To overcome the problem of lacking infrastructure, a concept has been introduced where a jack-up vessel, which is designed for the integration of bottom-fixed turbines, would now be utilized for the integration of the floating wind turbine. In this case, the wind turbine installation vessels (WTIV) would be located in a sheltered area in proximity to the wind farm site, potentially the location of the future floating wind port, where the wind turbine is integrated on the previously assembled floater. Utilising this concept would be advantageous as it could ensure the realisation of early, small-scale floating wind projects in locations with little or no suitable port infrastructure. At the same time, this concept would show future investors the locations' clear commitment to floating wind, which can trigger more investments into the port infrastructure for future floating wind projects.

Even though companies and ports have proposed this integration method as a potential solution for the wind turbine integration, so far, no academic work has been published investigating the concept of using a jack-up vessel for integrating a wind turbine on the floating structure. The aim of this thesis should be to establish a basic understanding of the concept and its properties with a particular focus on the single blade installation, which is one step of the integration procedure. It should be investigated how the system is responding to environmental loads, determine the environmental limits and evaluate how those limits would affect the integration operation in an exemplary scenario.

Based on those findings, the feasibility of the concept should be determined. The feasibility describes if it is likely that a concept can be implemented based on given parameters. Doing a feasibility study can help to understand whether or not a technology is applying to the different goals of a project (Kendall & Kendall, 2011, p.62). The feasibility can be determined on many levels and criteria for offshore wind. In this study, the feasibility of the concept should be evaluated on two different levels: technical feasibility and economic feasibility. The technical feasibility describes if an operation is generally possible with the available resources, for instance, to check whether or not the nacelle integration is practically possible with the concept (Kendall & Kendall, 2011, p.63). The economic feasibility of a technology is looking at the cost and time of implementing the technology. The estimated costs often play a crucial role for the implementation as an exceedance of the planned project cost can make the technology economically unfeasible. However, also if an operation sequence stays within budget but takes too long based on the given time frame, the economic feasibility is not given (Kendall & Kendall, 2011, p.63). Assessing both levels of feasibility gives a comprehensive understanding of whether the technology is generally feasible. However, depending on the project, the different levels of feasibility can have different priorities. For example, if a technically feasible technology is on schedule and represents the only possible solution to ensure the successful implementation of a project, the financial aspect of the economic feasibility of this partial solution could be of less priority for the sake of the success of the total project. Other levels of feasibility could be a legal, social or environmental feasibility but those are of lower priority for an initial assessment of the concept (APMG, 2023).

Assessing the technical and economic feasibility of the wind turbine integration of the investi-

gated integration method in detail has the scope for multiple separate master theses. Therefore, several assumptions and simplifications have been made to better understand the concept's feasibility on a holistic level. When the technology should be implemented in a real application, detailed investigations of both levels of feasibility should be conducted.

1.1 Aim and scope

The work of this thesis has the main goal of understanding how the concept of using a jack-up vessel to integrate a floating wind turbine would perform in several aspects. One aspect is to understand the dynamics of the fixed-to-floating system are, with a particular focus on the single blade installation. Therefore, based on previous works of Zhao, Silva de Souza and Jiang, a fully coupled numerical model will be set up, which will be used for the study of the motion characteristics of the systems components during the single blade installation to understand if the operation is technically feasible (Zhao, 2019; Silva de Souza et al., 2021; Jiang et al., 2018b). Based on the model's outcomes, operational environmental limits should be established. Those operational limits should then be used to determine the economic feasibility of the concept. Therefore, they will be implemented in an operational model of the complete integration sequence with the jack-up vessel under weather-constrained operations to understand the concepts' limitations and determine the associated cost and time. During this process the following questions should be answered:

- What are the requirements for a port to integrate a floating offshore wind turbine?
- In which cases and how could a jack-up vessel help out for the integration?
- What are the characteristics of the system when using a jack-up vessel for the single blade installation?
- Which environmental conditions are especially challenging for the single blade installation?
- What are the operational limits of the single blade installation and how would they affect the integration sequence with a jack-up?
- What are the cost and time estimates of the integration sequence?
- Is it technically and economically feasible to implement the concept?

1.1.1 Assumptions and simplifications

If the feasibility of a new technology concept should be investigated in detail for every aspect, this would exceed the scope of one master thesis by a large extent. Therefore, several assumptions and simplifications have been made to limit the scope of the work. The most significant assumptions and simplifications are:

- Only the integration of one semi-submersible concept is investigated without regarding other floater types or concepts.
- Only a jack-up WTIV has been investigated with the specifications of one vessel.
- Only one mooring system is regarded in detail, no detailed investigation of a seabed or quay fixated floater.

- Focussing on one specific port location.
- Disregarding tides in the numerical simulation and the operational analysis.
- Only regarding a few selected load cases for the environmental conditions and not the full spectrum of all probable sea states.
- Focusing on the single blade installation, not studying the other integration tasks.
- Focusing only on the weather related downtimes of the integration sequence.
- Focusing only on the tasks, costs and times of the actual integration sequence without regarding the impact of preparations which are needed to realize the integration.

More assumptions are made for the specific modelling procedures and they will be examined and discussed in more detail in the chapters 4 to 6.

1.1.2 Thesis structure

This thesis is composed of seven chapters, which are briefly described here to understand the structure of this work:

Chapter 1: Background and objectives

This chapter provided a general introduction to the thesis topic with a description of the scope of the thesis, subquestions which should be answered and general simplifications of the following work.

Chapter 2: Introduction

This chapter introduces floating wind turbines and what infrastructure is required to assemble and integrate them. The technology of a jack-up vessel as a dedicated wind turbine installation vessel is being introduced and the integration procedure is examined in detail with particular interest on the single blade installation.

Chapter 3: Case study

To better understand in which situation and location a jack-up vessel can be used for the wind turbine integration, an exemplary study is made for the port of Port Talbot. The used technology and the site's environmental conditions are being introduced.

Chapter 4: Modelling of the system

This chapter introduces how the modelling of the single blade installation is done by examining the modelling method, the detailed properties of all components in the system and how the system is implemented in the numerical model.

Chapter 5: Simulation results

In this chapter, the outcomes of the numerical model are investigated by doing a dynamic response analysis of the components and determining the success or failure of the single blade installation based on environmental load cases to determine the operational limits of the process and the technical feasibility of the concept.

Chapter 6: Operability analysis

This chapter investigated the operability of the complete integration sequence of the system. Therefore, the sequence is implemented into a model which can conduct an operability analysis to estimate the installation time and cost of the integration sequence with and without weather restrictions. Based on those outcomes, the economic feasibility of the system is determined.

Chapter 7: Conclusion

This chapter will comprehensively discuss the outcomes of the work conducted in this thesis, give a conclusion and suggestions for future work.

Several different aspects of the investigated concept are considered in this work, therefore the flowchart in Figure 1 is presenting an overview of what aspect is tackled in which chapter.

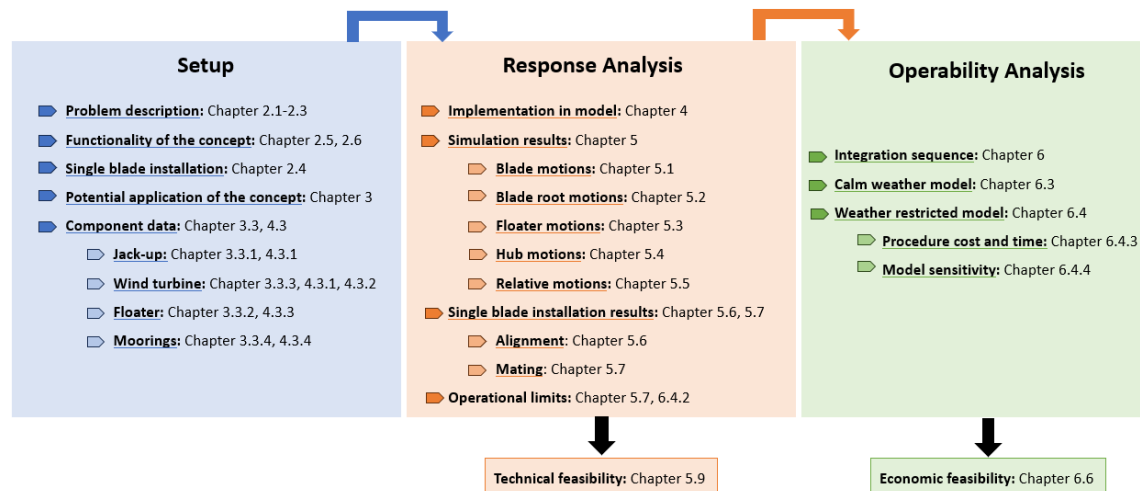


Figure 1: Flow chart of the thesis content

2 Introduction

This chapter will provide an extensive explanation of the investigated technologies and their associated challenges to profoundly understand why the proposed concept is needed in the first place.

2.1 Floating wind turbines

The concept of a floating offshore wind turbine exists since the late 1990s, where the first prototypes have seen their implementation in the late 2000s (Musial et al., 2003, p.1; Blue H, 2023). However, only in 2017 the first floating offshore wind farm with a total capacity of 30MW went online in Scotland (Equinor, 2023). Since then, the global interest in the technology has been steadily growing. This is due to the reason that it has the potential to unlock a completely new field of renewable electricity at large water depths, which the established bottom-founded offshore wind technology could not tap into due to economic and technology limitations (GWEC et al., 2022, p.15). In the most common case, a floating wind turbine consists of one horizontal axis wind turbine generator (WTG), which usually consists of three wind turbine blades, the hub, the nacelle and the tower. The WTG is placed on a floating substructure, either made of steel or concrete. To keep the floating wind turbine at its designated location in the wind farm, it is connected to mooring lines which are themselves connected to anchors. To transfer the generated electricity, the FOWT is connected to a dynamic cable, which can cope with the dynamic motions of the floater and transfers the electricity to a substation, where it is transformed to a higher voltage and then exported onshore for further use.

The floater can be separated into four different types: the semi-submersible, the spar-buoy, the tension leg platform (TLP) and the barge. A visualisation of those types can be seen in Figure 2. The barge can also be regarded as a subcategory of the semi-submersible as both are based on the same principle of maintaining stability. This principle takes advantage of having a sufficiently large water plane area, which creates a restoring moment that is sufficiently large to counteract the inclining moments of the wind and wave forces acting on the floater (Hannon et al., 2019, p.18). While the barge only creates the restoring moment based on a large water plane area, the semi-submersible has its columns more spread out for additional restoring moments. Meanwhile, the spar-buoy is mainly ballast-stabilised by having a large distance between the centre of buoyancy and the centre of gravity. To have this distance, the spar buoy is a slender cylinder with a large draft and both solid and water ballast at the bottom of the buoy. Therefore, this concept can not be implemented in shallow water locations due to the draft limitation, while the waterplane-stabilised types have much smaller drafts and thus can also be implemented in those locations (Hannon et al., 2019, p.18). The third stabilisation concept is the mooring-stabilised concept, which the TLP can be categorised in. In this case, the substructure has a very large submerged volume which correlates to a high buoyancy force. This force is counteracted by having very stiff, tensioned mooring lines connected to the floater. This design makes the concept more versatile for different water depths as the mooring line length is only scaling linearly with the depth. Meanwhile, the more slack mooring lines of the other types scale differently as the footprint has to be larger for very shallow sites but also in deep water sites, while the sweet spot for the mooring cost is somewhere in the range of 100m to 250m (James et al., 2018, p.42). A visualisation of the different stabilisation concepts can also be seen in Figure 79 in Appendix A. Even though the floater can be categorised into four different types, more than a hundred different designs have been proposed by companies where each

individual one has its up and downsides (QuestFWE, 2022).

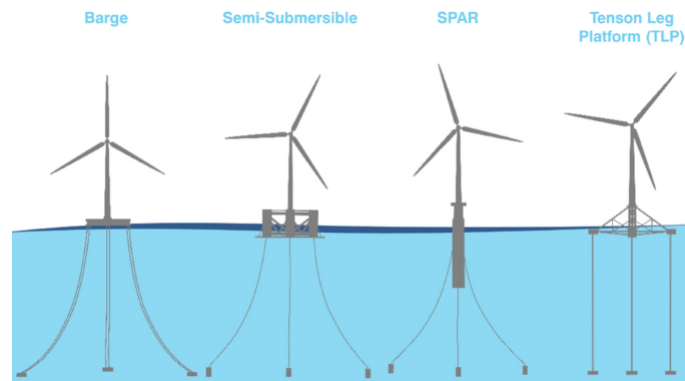


Figure 2: Concept sketch of the different floater types: barge, semi-submersible, spar-buoy and TLP (Ha et al., 2021, p.283)

For the waterplane and ballast-stabilized floater concepts, the mooring lines are usually in a catenary setup made out of chain, steel wire, synthetic fibre, or a combination of those types. When a TLP should be installed, the moorings are usually cables, tendon pipes or solid rods which can cope with the high required tension. The used anchors depend highly on the requirements of the mooring lines and the soil type and can range from drag anchors over driven piles to suction anchors (Ikhennicheu et al., 2020). Every floating wind turbine needs to have at least three mooring lines, connected to anchors (Hannon et al., 2019, p.18). Especially for large floating wind farms, this will require a substantial amount of moorings and anchors. Therefore, it can be economically very beneficial when several wind turbines share the same anchors and mooring lines. Dynamic cables are a fairly new application for subsea cables, where, previous to floating wind, usually the cables didn't have to adapt to the motions of the connection point, especially not at those high voltages. The catenary mooring systems are designed to keep the FOWT motions within the limitations of the cable, as a cable damage would have drastic consequences.

The different floater types are subject to a variation of different challenges. The spar buoys have a substantial operational draft in the range of 70-90m, while the structure, if made out of steel, also has a mass of 2500-5000t while concrete spar-buoys are even heavier (Crowle & Thies, 2021, p.3). Therefore, they can only be installed in water depths beyond 100m, while the draft also makes floater manufacturing and the wind turbine integration very challenging. Therefore, the integration of this type can only be done in deep water sheltered areas like the fjords of Norway or some regions of the Mediterranean Sea. A very expensive heavy lift vessel or a floating quay with a crane with far outreach needs would need to be utilized for the integration as it has been done in the Hywind projects (Snieckus, 2021).

The large buoyancy of the TLP concept makes it more challenging to install as its stability is very small before the mooring connection. The structure is lighter than the other concepts, whereby the port-based manufacturing will be simplified. Once the structure is loaded out into the water, additional stability needs to be added by either using a variable draft of the structure or using specialized transport vessels or temporary buoyancy solutions (Crowle & Thies, 2021, p.4). This

is especially crucial if the turbine should be integrated on the floater within the port before it is installed offshore to the moorings, as a loss of stability with the integrated turbine could have drastic consequences. Also, the increased requirements on the moorings and anchors make this floater type more challenging. Therefore, this floater technology is progressing a bit slower than the other concepts, with the first TLP-based floating wind farm getting installed at the end of 2023 in France (4C Offshore, 2023b).

For semi-submersibles and barges their substantial size become an issue, as steel concepts of modern turbines are in the range of 80 by 80m or even 100 by 100m with a weight of 2500-5000t, while concrete concepts are smaller (around 55x55m), but also substantially heavier (15000-18000t) (Torr, 2022, p.28; FOWCE & ORE Catapult, 2022b, p.3). In comparison to spars and TLPs, their draft allows a port based manufacturing and assembly, but only very few ports have the facilities to actually perform those activities for structures of this size.

2.2 Market development

The first offshore wind farm was installed in Denmark in 1991 with a total wind farm capacity of 5MW (Cordis, 2022). Since then, the global offshore wind capacity has grown to 64.3GW at the end of 2022 with an annual installation rate of 8.8GW (Hutchinson & Zhao, 2023, p.95). So far, most offshore wind projects are implemented with bottom-fixed foundations, of which more than 80% have monopiles as their foundation (Ramirez et al., 2021, p.27). Floating offshore wind is still in a very early stage, where, after the completion of the largest floating wind farm of 88MW, Hywind Tampen, the total global floating wind capacity installed will only be at 236MW at the end of 2023 (0.37% of total installed capacity) (QuestFWE, 2023). The vast majority of all energy that is being produced in the EU is still coming from fossil fuels, while renewable energy resources make up only 35.8% of the European electricity mix and only 17.2% of the total energy mix (Statista, 2023; EuroStat, 2023). However, due to the emerging threats of climate change and the general change of dynamics in the global energy market after the 2022 invasion of Russia in the Ukraine, governments across the globe have accelerated their plans to become carbon neutral. For instance, the EU is planning to reduce carbon emissions by 55% by 2030 and become fully carbon neutral in 2050 (Díaz et al., 2022, p.9). Those accelerated goals also impact the global offshore wind goals as the technology will be one of the foundations of the energy transition. Therefore, it is planned that by 2031 around 370GW of offshore wind should be installed globally. This means that the capacity that has been installed offshore over the past 30 years should now more than quintuple in the next eight years. Another example is the massive increase of the offshore wind targets of the European countries, where in 2023, targets of 120GW by 2030 and 300GW by 2050 were announced by the North Sea states after they just announced goals of 76GW/260GW in 2022 (Henley, 2023).

With Hywind Tampen, the first pre-commercial scale floating wind farm will come online this year. Previous projects were always demonstration or pilot projects which should prove the technology's suitability. Pre-commercial projects in the 50-200MW wind farm capacity range should test the supply chain and production at a larger rate (Spearman et al., 2020, p.11). However, floating wind farms will only be price competitive with other electricity resources when deployed at a commercial scale, where wind farms will most likely have much more than 200MW (Spearman et al., 2020, p.11). This is due to the economy of scale, where larger projects can be much more streamlined and thus are much more efficient. The learnings from the previous phases will also

be essential to optimise the technology and thus bring down costs. As the technology progresses, many commercial-scale floating wind farms are already being developed. The implementation of first GW-scale floating wind farms is expected from 2027 onwards (QuestFWE, 2023). As it has the potential to unlock entirely new markets, it is expected that floating wind will play an increasingly important role in offshore wind, where it is predicted that already 18.9GW will be installed by 2031, which would make up 5.1% of the market share (Williams et al., 2022, p.51). Under the assumption of a 15MW turbine, this would mean that 1260 floaters would need to be produced within the next eight years. This will be a substantial challenge for the so far merely existing port infrastructure, highlighting the importance of this research. An even longer forecast for the growth of floating wind can be seen in Figure 3, where a growth up to 250GW of floating wind by 2050 is predicted. In the context of IRENAS 2000GW offshore wind by 2050 prediction, this would make up a share of 15% of the global offshore wind capacity.

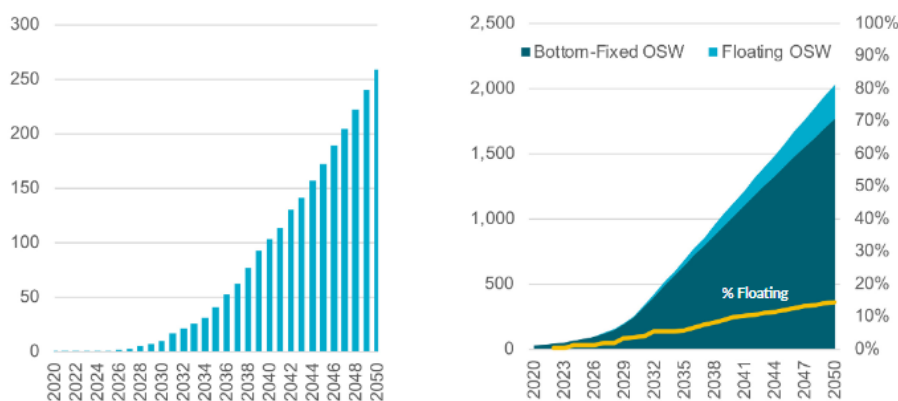


Figure 3: Left: Long-term forecast of floating offshore wind, Right: Those target in context of IRENAs forecasted 2000GW offshore wind scenario by 2050 (FOWCE & ORE Catapult, 2022a, p.4)

The main markets for the first commercial floating wind farms will be in Europe, Asia and North America (Williams et al., 2022, p.96). One important initial market for floating offshore wind will be the UK, as it can build upon its experience in bottom-fixed wind and oil and gas and already has a pipeline of 33GW of projects under development (RenewableUK, 2022, p.4). However, floating wind will also open up many new markets that have been so far unsuitable for offshore wind due to their water depth. Those markets include Japan, South Korea, Italy, Norway, the US west coast, Spain, France, Ireland and Sweden (Williams et al., 2022, p.52). A detailed forecast of the coming floating wind markets can be seen in Figure 4. It must be noted that those markets are just some preliminary examples where many more are potentially suitable for floating wind and more projects are getting announced regularly.

A further reason for the anticipated growth of (floating) offshore wind is a rapid increase in wind turbine capacity over the past and in the coming years. As Figure 5 shows, the rated capacity of the newest wind turbines from all turbine suppliers has drastically increased since 2016. In 2021, the average rating of the installed wind turbines was 8.1MW, which should already increase to 12MW in 2025. Much larger turbines of 14-15MW are already being tested, which are anticipated

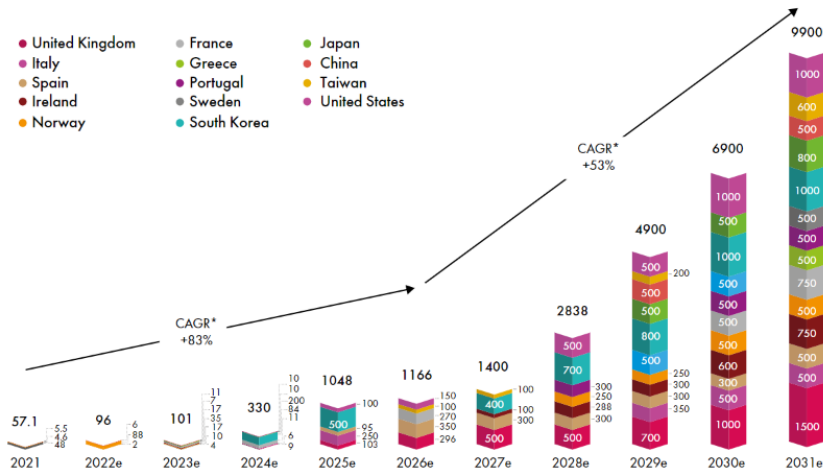


Figure 4: Expected annual new floating wind installations (CAGR = Compound Annual Growth Rate) (Williams et al., 2022, p.97)

to enter the broad market around 2025. As the projects have long development times where eventually, turbines of a certain size need to be selected, the average rating is always a bit behind the newest turbines. The growth of those turbines is not anticipated to stop at 15MW, as turbines of a rating of 17-20MW with rotor diameters of 250-275m are predicted to enter the market around 2030 (Williams et al., 2022, p.46).

The turbine size has drastically increased because of significant potential cost reductions. This is to a large extent as fewer turbines are needed to realize the wind farm with the same capacity. While the individual cost per turbine might increase, substantially fewer foundations, inter-array cables and moorings must be installed for the wind farm. This is potentially even more important for floating wind than for bottom-fixed wind turbines, as the foundations are much larger and more expensive due to their complexity. At the same time, also the moorings and cables are very expensive, totalling up to 25.1% of the project’s lifetime cost (BVG Associates et al., 2023d). In contrast, bottom-fixed turbines are only anticipated to have a share of 13.2% for the foundations and cables (BVG Associates et al., 2019). An estimation for a bottom-fixed wind farm of 1GW stated that increasing the turbine size from 10MW to 14MW could already save up to \$100m in foundation and cable cost (Flotre, 2020). Additionally, fewer wind turbines also mean that the maintenance costs reduce as fewer turbines result in fewer required technicians, vessels and major component exchanges. Also, the operational cost decrease as fewer turbines reduce the balancing cost, reduce the transmission expenditure and the power production can be more predictable (Williams et al., 2022, p.41). Furthermore, with the increase in the blade and tower size, the rotor also enters higher altitudes where stronger and more consistent winds occur, increasing electricity production.

However, the substantial increase also comes with some drawbacks. Wind farm developers always aim for the lowest project cost, so the demand for offshore wind turbines is high as they reduce the total cost of the wind farm. However, for the wind turbine manufacturers delivering the

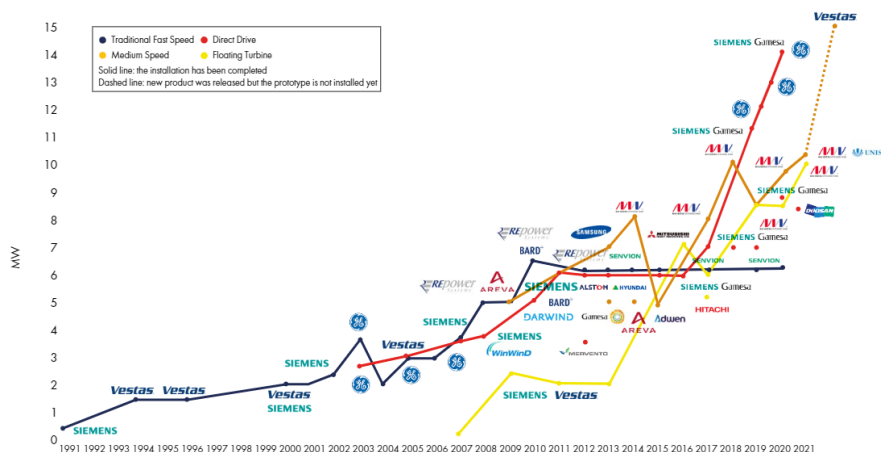


Figure 5: Development of wind turbine models (excluding Chinese market) (Williams et al., 2022, p.45)

newest and biggest turbines is very challenging as new turbines are always associated with very high research and development costs. Furthermore, their facilities need to be constantly upgraded while the turbine costs are also subject to a very fluctuating regime of material cost. Furthermore, the supply chain needs to adapt to the increasing size of the wind turbine components, making transporting and installing them more and more challenging. This is especially the case for the nacelle, which will be much heavier and have to be lifted at higher heights (Williams et al., 2022, p.46). Additionally, the rest of the floating wind turbine will need to be adapted to sustain the increased wind turbine weight and loads, but studies have found that the floater size is increasing much less than the turbine with increased rating, which makes the larger turbines even more favourable (Kikuchi & Ishihara, 2019, p.17).

Regarding the cost of a floating offshore wind farm, the wind farm is ultimately rated based on the levelized cost of electricity (LCOE), a metric to assess the cost of electricity generation that can also be used to compare the cost to other types of electricity generation. It is calculated with:

$$LCOE = \frac{(CAPEX \times FCR) + OPEX}{AEP_{net}} \quad (1)$$

where CAPEX is the capital expenditure [€/MW], FCR the fixed charge rate [%], OPEX the operational expenditures [€/MW/yr] and AEP_{net} is the net average annual energy production in MWh/MW/yr (Stehly & Duffy, 2022, p.14). For the US market, Stehly is estimating the current floating wind LCOE at around \$133/MWh, while bottom-fixed is estimated to be at \$78/MWh (Stehly & Duffy, 2022, p.11). The different technologies must always be compared based on the local market conditions and electricity prices. For instance, offshore wind is much more established in Europe than in the US, while fossil fuels like gas and oil are much cheaper than in Europe.

The LCOE of a floating offshore wind farm also highly depends on factors like the site conditions, the supply chain, the technology and the time. Regarding site conditions, factors like the water

depth, soil conditions, wind wave conditions, tides and distance to shore matter. For the supply chain, the mentioned issues with the growth of the wind turbine size can become a significant cost driver, as well as the material cost and the lack of sufficient port infrastructure. Also, the increase in wind turbine size and the general size of a floating offshore wind farm will have a huge potential for cost reduction. As Figure 6 shows, the LCOE of GW-scale offshore wind projects is much lower as many processes like the floater fabrication or wind turbine integration can be streamlined at scale, reducing the cost per unit. The FOWT technology is still in a comparably early stage, where mature, future large-scale projects are expected to reduce the LCOE significantly (BVG Associates et al., 2023d). The cost of early commercial scale projects starting 2027 is still likely to be in the range of £90-135/MWh, while already eight years later, it is anticipated to drop to £30-50, which also can be seen in Figure 7.

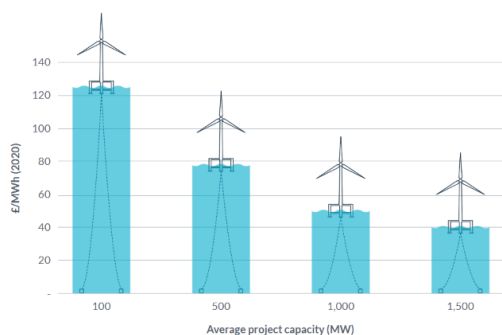


Figure 6: LCOE prediction based on wind farm size (FOWCE & ORE Catapult, 2021)

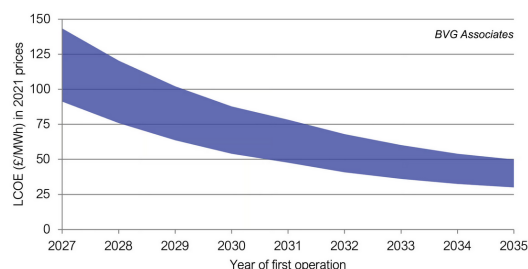


Figure 7: Anticipated LCOE reduction of floating wind farms starting in 2027 to 2035 (BVG Associates et al., 2023d)

While the net AEP might also increase due to larger and more efficient wind turbines, the largest factor for reducing LCOE will be a decrease in the total lifetime cost. The operational and maintenance cost make up a substantial share of the project cost over its lifetime of 20 to 25 years at around 36.6% as it is important to maximise the value of the asset by having an optimal performance at all times (BVG Associates et al., 2023d). Therefore, it is important to optimally operate the wind farm and maintain it regularly to ensure that it is running smoothly without any further delays. Fewer but larger turbines and increased understandings of the cost drivers of operating and maintaining a floating offshore wind farm and new monitoring and operation technology bear the potential to reduce the OPEX cost and, thus, LCOE drastically.

Figure 8 breaks down the total lifetime cost in its components. All cost assumptions are made for a commercial scale 450MW wind farm with a CAPEX of £3.52m/MW (\approx €4.12m/MW) where the entire required infrastructure is already assumed to be in place. It can be seen that 52.1% of all project costs come from the cost of the individual components, where the complete turbine makes up around 23% of all costs while the floater is estimated at 16.6% (BVG Associates et al., 2023d). Due to the novelty of all components in a floating application, large cost reductions can be expected for all component costs once the technology matures and scales up. The installation costs only make up 6.4% of the total project cost, where large portions are contributed to the installation activities happening offshore, from the cable and mooring installation to the substation installation offshore. In contrast, the cost associated with the assembly/integration of the wind turbine, which will be

the focus of this thesis, are comparably small with around 1.2% (1.9% of CAPEX, £68000/MW) (BVG Associates et al., 2023d). However, those cost estimates are assuming the entire required port infrastructure to be already in place. The cost breakdown for smaller, early-stage projects certainly differs from those estimates, especially when the existing infrastructure is insufficient. The estimation of the project CAPEX largely depends on the specific conditions and technologies used. Thus other floating wind CAPEX estimates are more in the range of $\approx \text{€}5.17\text{m/MW}$ (Stehly & Duffy, 2022, p.6).

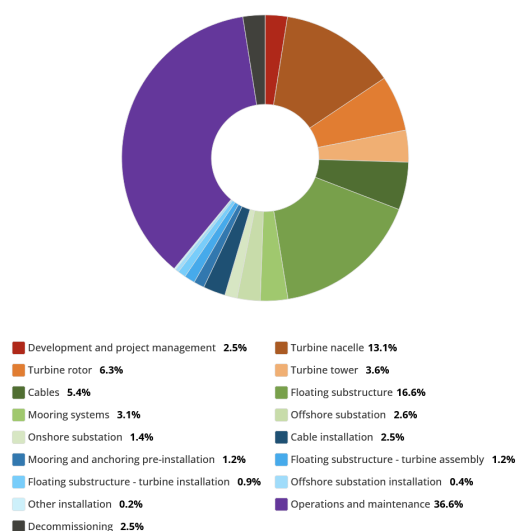


Figure 8: Cost breakdown of the total lifetime cost of a floating wind farm (BVG Associates et al., 2023d)

2.3 Port activities

As mentioned, many of the challenges of all floater types are associated with the ports. In general, it can be regarded as a significant advantage of floating offshore wind that, compared to bottom-founded wind turbines, a substantial amount of all installation activities can be performed at a port as any offshore operation is generally more expensive and challenging than an on-/nearshore activity due to the more challenging environment. For most of the floater concepts, it will be possible to completely assemble the FOWT in the port and only tow it to the wind farm's location, where it is connected to the previously installed moorings and cables. The entire construction process of a floating wind farm is displayed in Figure 9.

Ports do not only play an essential role during the construction phase but are also required as a supply base for the geotechnical and metocean survey in the development phase. In the operational phase, they can even function as maintenance harbours where the turbines simply could get disconnected offshore and towed to the port for major component replacements, thus reducing the number of offshore operations. When the wind farm comes to its end of life, a port is also needed to decommission the structures (Crowle & Thies, 2021, p.2). This chapter focuses on the assembly port, which will be utilized in one phase of the construction phase, as the proposed concept with the jack-up for the FOWT integration should be an alternative to an assembly port.

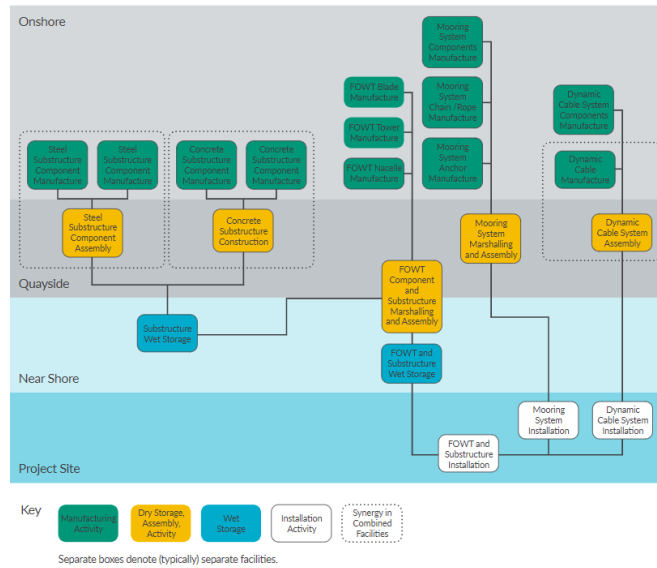


Figure 9: Construction process of a floating wind farm (Torr, 2022, p.22)

2.3.1 Manufacturing port

Initially, the manufacturing port is briefly introduced to understand what differentiates it from the assembly port. In the manufacturing port, the complete floater is assembled and loaded into the water. The manufacturing port can be separate from the assembly port as both have different facility and location requirements. Still, if both can happen at the same location, there are certainly synergy effects (Torr, 2022, p.33). Those synergy effects of co-location exist for all utilized port facilities throughout the project's lifetime and can be seen in more detail in Figure 80 in Appendix B, as well as the impact of the proximity to the wind farm site.

For the manufacturing port, shipyards will usually be utilized. Even though some expertise of the shipyard in large oil and gas (O&G) structures is beneficial, the procedures for floater production will be significantly different. For floaters, the focus is much more on the efficient and fast production of the units, while O&G structures are one of their kind and focus more on security as they are permanently manned (Torr, 2022, p.28). For floater manufacturing, it is therefore also important to create highly standardized procedures for their production, which is complicated by the large differences in the floater designs currently on the market.

It is very important to have suitable facilities and equipment, which can perform the manufacturing and assembly of the floater fast. A variation of cranes will be needed during the construction as also the individual floater components are very heavy (Matha et al., 2017, p.301). If the floater is made out of steel, specialized high-quality welding equipment is needed, which can connect the individual components. For concrete floaters, a mobile batching plant can be quickly set up at any appropriate site as the local requirements are much lower. The manufacturing facilities need a lot of space due to the sheer size of the floaters. The specific required area depends on the used manufacturing procedures and speed and also planned buffer spaces for storage and reworks (Borisade

et al., 2019, p.33). To transport the substructure components within the port, SPMTs will be used, which have good load-carrying capacities and can be adapted to the design but also come at a higher cost.

Ideally, dry docks would be used for the production of a floater as it could be easily streamlined and the float off of the structure once it has been assembled is also much easier. However, the number of dry docks with sufficient width and draft to produce several floaters is extremely limited (Matha et al., 2017, p.302). Therefore, most of the floaters will be produced not within a dry dock unless it is a few number of units with a small footprint and draft.

Not all components of the floater will need to be produced within the manufacturing port, as it can be much more efficient to produce the floater components in specialized facilities, which are then transported to the manufacturing port (Eatough, 2021, p.46). Given the size and complexity of the floater, the production of the unit will still take time, where the construction of one floater per week would be the gold standard for the industry. As this is still a fairly slow production rate, it can be also possible to manufacture floaters for one project at several facilities at the same time, which would be beneficial for the faster realization of larger wind farms (Borisade et al., 2019, p.24).

Once the floater assembly is completed, it needs to be lowered into the water, which is called load-out. The size and weight of the structure can make this procedure quite challenging. As it can be seen in Figure 10 or semi-submersibles, TLPs and barges the most common way is to transport the structure onto a submersible barge vessel, which will then be lowered with ballast tanks until the structure is floating. This roll-on operation is fairly complex, especially when the port has a location with high tidal range, but also the draft of the floater makes it challenging as a sufficient water depth needs to be given at the load-out location. Those launching barges are limited in availability and relatively expensive. Thus alternatives like a floating dry-dock or a load-out with a sufficiently strong crane might also have some potential (Rodrigues, 2023; Tugdock, 2023). After the load-out is successful, the floater is either transported directly to the turbine integration or stored in a wet-storage location to free up the manufacturing space. For spar foundations, they are either constructed in an upright position in deep waters or loaded out from the port horizontally and then are uplifted in a vertical position in a suitable location.

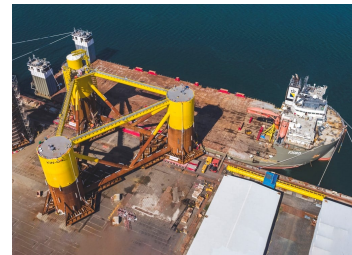


Figure 10: Load-out of the WindFloat floater with a semi-submersible (Mammoet World, 2021a, p.22)

2.3.2 Assembly port

After the floater is manufactured and loaded out, the structure can be transported to the assembly port. While the manufacturing port only needs sufficient access to load-out the floater in a location near the port, the assembly port requires a sufficient quayside draft and length to realize the integration as the floater would be directly moored to the quay to minimize the relative motions (Eatough, 2021, p.36). For the integration port, it is also important to have a sufficient storage area for all wind turbine components, which can make up substantial areas, especially for large projects (Crowle & Thies, 2021, p.2). Optimally, the port would also be utilized for storing the moorings,

cables and anchors, increasing the required space (Ramirez et al., 2020, p.21).

The proximity to the assembly port to the wind farm site must be given, as the tow-out of fully assembled FOWT is subject to weather restrictions. As the acceptable acceleration and motions of the turbine depend highly on the wind turbine type, standardised requirements and procedures have not been established so far (Harvey et al., 2022, p.25). Therefore, general operational limits are still fairly conservative. The weather forecasts are sufficiently accurate for three days with modern modelling techniques. Therefore, the maximum towing time can only be 2.5 days as the floater must also be connected to at least two mooring lines within the predictable weather window, which takes around eight hours per mooring line (Eatough, 2021, p.34). The uncertain acceptable accelerations limit the towing speed to 3kn, thus, the assembly port can be only 180nm (333.36km) away from the wind farm site if the tow should be direct. For longer tows, a staging port in case of bad weather would need to be included in the plans, which substantially increases the cost of the operation (Crowle & Thies, 2021, p.6).

Arguably the most essential part of the assembly port is to have a crane that can execute the turbine integration, where the integration procedure itself will be examined in more detail in chapter 2.4. Floating offshore wind turbines will usually have turbine ratings of 10-15MW or even 20MW after 2030. Those turbines will have hub heights of 150m or more, which are added to the floater height above the water lines. Therefore, the cranes need a sufficient boom length to reach this height and also the carrying capacity to lift the nacelle of 500-700t (Ramirez et al., 2020, p.21). This gets further complicated based on the floater design, as a design with the turbine in the centre requires a further outreach, which could be up to 55m (MammoetWorld, 2021b). The cranes that can execute those operations are landside cranes or wind turbine installation vessels. Regarding the landside cranes, the floating wind turbine integration has been done in the past with crawler cranes or ring cranes. Crawler cranes are faster to set up but are limited in their reach, whereas the mobilisation time of a ring crane is much longer, around five to six weeks, but their high load moment capacity enables high capacity lifts at large reach (Cranes Today, 2021; Mammoet, 2023). However, with the turbine specifications of the most recent and upcoming wind turbines, the limitations of many existing landside cranes are exceeded so that only a hand full of mobile cranes exist that could perform the floating wind turbine integration. New, upgraded cranes are currently under development, like the SK6000 ring crane of the Dutch company Mammoet displayed in Figure 11. The crane has been partially designed for floating wind turbines up to 20MW and should be able to lift 4000t up to 175m with a maximum reach of 144m (Mammoet World, 2021a). This ring crane would also be capable of loading lighter floaters into the water, which would increase the utilisation rate, which given the long mobilisation time of up to one month, would be preferable (Ramirez et al., 2020, p.21). However, given the design's novelty and the crane's massive size, the rental cost of such a crane would be substantial and could reach up to £14 million per project (ORE Catapult, 2020, p.21).



Figure 11: Concept art of the SK6000 ring crane (Mammoet World, 2021a)

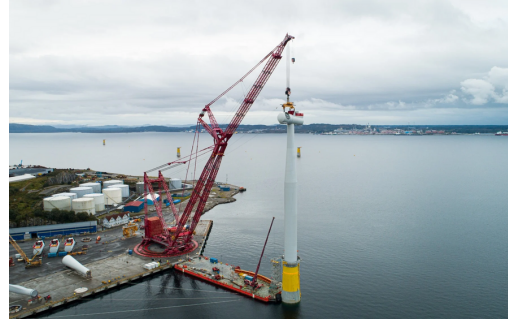


Figure 12: Turbine integration with a ring crane for the spar buoys of Hywind Tampen (Mammoet, 2022)

Due to their large draft, spar buoys can not be integrated directly next to the quay. Therefore, they either need to be integrated with a ring crane with a very far outreach, as it can be seen Figure 12 from the Hywind Tampen project or a costly heavy lift vessel needs to be used like in the Hywind Scotland project. For all onshore-based cranes, it will also be crucial to have a quay with sufficient load-bearing capacities, as the large floater weight requires a minimum surcharge load of 15t/m^2 for the area. If now a large crawler or ring crane is used, the area below the crane needs to sustain a distributed load of $30\text{-}40\text{t/m}^2$ and a maximum surcharge during heavy lifts of $50\text{-}80\text{t/m}^2$ (Ramirez et al., 2020, p.22). If the quay is too weak, temporary bearing upgrade mats could increase the bearing capacity up to 50t/m^2 (MammoetWorld, 2021b).

Due to the low availability, high price and complexity of using landside cranes, most assembly ports are expected to utilize a wind turbine installation vessel for the wind turbine integration instead (BVG Associates et al., 2023b). In this case, the WTIV would be positioned in a previously prepared location along the quay, from where it will be supplied with the wind turbine components, which are then integrated on the floater, which is moored against the quay to limit the floater motions. In this case, also older jack-up vessels or barges (not self-propelled) could be utilized, as their smaller crane could be compensated by further jacking-up and their deck area would be irrelevant in this case. To prepare the quay for this operation, it would be important to level the seabed in front of the quayside and to ensure a sufficient load-bearing capacity for the jack-up legs. An alternative to the large onshore and offshore cranes could also be a self-erecting climbing crane. Several concepts like the ones of SENSEwind or WindSpider also exist for floating wind turbines. Still, the technology is at a too early stage to know if it will see future implementations at large scale (SENSEWind, 2023; WindSpider, 2023).

To understand which requirements an assembly port for floating wind would need to fulfil, Table 1 is giving estimates for the required port infrastructure based on the floater type for floating wind projects with turbines in the range of $15\text{-}20\text{MW}$. Other literature gives very different estimates as a different floater design and different integration plans will have different requirements for the port infrastructure.

Primary Criteria	Semi-sub (minimum)	Semi-sub (preferred)	Spar	TLP
Navigation channel width	100m	200m	60-90m	90-135m
Quay/Navigation channel depth	10m	15m	6-9m (horizontal), 90m (if vertical)	10-12m
Quay Berth Length (assembly)	300m	600m	-	-
Quay Berth Length (with manufacturing)	600m	900m	-	-
Air draft Area	Unlimited 15-20ha	Unlimited 15-20ha	Unlimited 4-6ha, 20-40ha ideal	Unlimited 4-6ha, 20-40ha ideal
Laydown area assembly (+ manufacturing)	6ha (34ha)	12ha (50ha)	-	-
Wet Storage Area, 10 units (with assembled WTG)	30ha (80ha)	70ha (200ha)	-	-
Quayside bearing capacity	15 t/m ²	50 t/m ²	15 t/m ²	15 t/m ²
Laydown bearing capacity	7.5 t/m ²	> 20 t/m ²	-	-
Crane lifting capacity	1000 ton	1000 ton	1000 ton	1000 ton
Number of deep draft berths (>7.6m)	1-2	1-2	1-2	1-2

Table 1: Required parameters for a floating offshore wind assembly port (no info found for empty cells) (ORE Catapult, 2020, p.22; Gibson & O’loan, 2022, p.39; BVG Associates et al., 2023c)

2.4 Integration procedure

The wind turbine integration can be separated into the integration of the three main components: the tower, the nacelle and the rotor. As mentioned, the floater will be moored against the quay to integrate the turbine. For enhanced stability, it could even be lowered to the sea bed on a previously prepared area (BVG Associates et al., 2023a). As an initial step of the wind turbine integration, the tower will be lifted with a crane onto its position (Jiang, 2021, p.17). For modern wind turbines, the tower weight is around 25% higher than the one of the assembled nacelle and hub and has a length of up to 140m (Armstrong, 2023). Therefore, installing the tower in two to three sections would make more sense, especially for onshore cranes with limited lift capacity (Bessone et al., 2022, p.6). WTIVs are designed for integrating bottom-fixed wind turbines offshore, where critical lifting operations play a more important role than within the port. Every lift that can be reduced means that one risk event is reduced as any heavy lift and material movement offshore always is dangerous and has a high potential to damage objects (Armstrong, 2023). Therefore, the crane capacity of WTIVs is usually higher than the one of landside cranes as this reduces the number of critical lifts. Therefore, the tower can also be integrated in one piece. Offshore operations are often subject to long waiting times due to weather restrictions, therefore a reduced number of lifts also represents potentially less waiting time.

After the tower has been successfully installed, the assembled combination of nacelle and hub will be lifted on top of the tower. This lift will be very heavy (500-700t for 15MW) and needs to take place in one piece. The nacelle needs to be aligned with the tower, while besides using the lift wire and potentially some ropes only very little guidance mechanisms could be utilized. Already for bottom-fixed turbine integrations, this is a fairly complicated operation as the allowable displacements between the tower and the nacelle are very small, where also the tower oscillations play an important role (Jiang, 2021, p.17). When the nacelle should be integrated on a floating wind turbine, the floater's wave-induced motions, unless lowered to the seabed, complicate the nacelle integration as the allowable displacements are small. Due to the large height of the tower, even small rotational motions of the floater lead to large motions of the tower top. The problem of the relative motions only gets amplified if the tidal range in the port is large, whereby the nacelle also would need to be adjusted in the vertical position during the integration.

As the next step, the rotor needs to be integrated. In theory, it would also make sense to reduce the number of lifts if the operation takes place offshore, wherefore previous smaller offshore wind farms have already performed a rotor integration where two or three blades are already assembled onto the hub (Jiang, 2021, p.14). However, with the increased wind turbine size, the blade length also substantially increased to around 115m for 15MW while still being relatively light with below 100t, making integrating a preassembled rotor very complicated. Thus the single blade installation is the preferred method for modern wind turbines. The single blade installation is commonly regarded as one of the most critical integration operations and, therefore, will also be the focus of this thesis. In this procedure, the yoke first grabs the blade and lifts it to the hub level (Jiang et al., 2018b, p.1043). The orientation of the blade depends on the yoke equipment, where the leading edge of the blade is facing either downwards or is aligned horizontally. The blade direction during installation also depends on the equipment and turbine. Generally, a horizontal blade installation is preferred, but the wind turbine hub usually can't rotate by itself when a direct drive generator is used. Therefore, specialized hydro-mechanical tools must rotate the hub for the connection point in a horizontal position (Miceli, 2019). Other yoke systems are designed for the vertical or tilted integration of the wind turbine blade, but this thesis focuses on the horizontal integration.

After the blade gets lifted to hub height, the single blade installation enters the alignment phase. The blade is brought closer to the hub by slewing the crane and adjusting the tugger lines connected to the blade yoke (Jiang et al., 2018b, p.1043). During this phase in a floating wind application, both the blade root and the hub motion need to be carefully monitored to check if the motions are too large for the blade mating. If the motions are too large, the blade will keep hanging close to the hub until the conditions are acceptable. If the conditions remain harsh, after around 30 minutes, the blade will be lowered again and the operator waits for better conditions (Jiang et al., 2018b, p.1043).

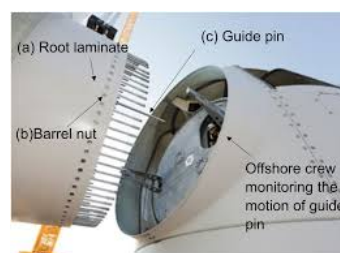


Figure 13: The blade root with its guide pin and the hub (Verma et al., 2019, p.211)

Once the alignment criterion is met, the mating phase initiates where the guide pin of the blade root enters its designated flange hole. The guide pin can be seen in Figure 13 and is a longer-sized

pin, which should help the worker in the hub to visually control the mating procedure before all bolts enter their flange. Once the mating of the guide pin is successful, the blade root is docking to the hub, where all blade root connections are bolted as T-bolt connections and the guide pin is replaced with a conventional bolt. Then the bolting connections are pre-tensioned and the yoke can disconnect from the blade.

Due to the small diameter of the guide pin and the flange hole, the maximum allowable relative displacement of the wind turbine and hub is minimal. A collision of the blade pin and the flange could very likely lead to unacceptable damage, which has been evaluated in several studies (Verma et al., 2019; Verma et al., 2020). Therefore, control systems are introduced, which should help to minimise the relative motion between the blade and the root. Some of those measurements could include an active predictive control system for the tugger lines (Ren et al., 2018), a constant tension tugger line control, a passive tuned mass damper that increases the damping behaviour of bottom-fixed turbines (Jiang, 2018), a hub motion estimator (Ren et al., 2018) or simply workers pulling in the blade with the use of ropes if the local safety standards allow it. Some of those control measurements are widely applied for the single blade installation of bottom-fixed turbines, but using a floating foundation drastically increases the hub motions and make the established methods less suitable.

2.5 WTIVs for the turbine integration of floating wind turbines

As it was described in chapter 2.3.2, it is expected that a large amount of all port-based wind turbine integrations will take place by utilizing a jack-up type wind turbine installation vessel for the integration as landslide cranes take very long to set up and have larger requirements for the quay in regards to load-carrying possibilities. From an operational perspective, the difference between using a WTIV and a landslide crane is not making much difference, as both cranes are fixed. Also, the floater motions are highly restricted in its motions by being fixed to the quay, while the waves acting on the floater are small as the port is sheltered.

However, as Table 1 highlighted, there are also substantial requirements that a port location would need to fulfil to be a suitable assembly port. Chapter 2.2 highlighted that floating wind opens the potential for new markets with little to no offshore wind or offshore engineering experience. This means that the port infrastructure in many potential floating wind locations is not sufficiently built out yet. The initial investment which is required to upgrade an existing facility to an assembly port lie somewhere in the range of €0.5-1bn and completely new facilities are even more expensive (Torr, 2022, p.63). Those investments are only taken if it can be foreseen that a large volume of around 50 or more units is produced at the port every year for several years (Ramirez et al., 2020, p.31). However, floating wind is so far only in a pre-commercial stage, where it will be especially hard in new markets to find investors willing to invest this much money in infrastructure if there is no track record or if the port initially only integrates a few turbines.

Therefore, for floating wind projects up to 200MW, the wind turbine installation vessel could also be utilized in a sheltered area with sufficient draft to integrate the floating wind turbine. In this case, the deck space of the jack-up vessel would also be utilized to store the wind turbine components, which are delivered by feeder vessels or picked up by the jack-up in storage ports, which else wise don't have the facilities or properties to perform the wind turbine integration. The

floaters would be moored alongside the jack-up while ensuring minimal displacements. As long as the floater is not connected to the jack-up or fixed in some other way, for instance, by a mooring dolphin, the motion profile of the floater enhanced in the scenario, which could complicate the wind turbine integration. This integration concept is only focused on integrating a semi-submersible or barge-type floater, as spar-buoys have a too significant draft to be moored alongside a jack-up while the TLP could have some stability issues. Port authorities have mentioned the concept for different ports in the UK in Scotland and in the Celtic Sea and one version of the concept also has been already patented by the Norwegian company Fred Olsen 1848 (Fred Olsen 1848, 2023b; Associated British Ports, 2023; Cromarty Firth, 2022). However, it has seen no implementation yet and also no detailed study of the concept has been published. This thesis aims to understand better the concept, which can also be seen in Figure 14 and Figure 15. The figures show different setups in which the floater could be moored alongside the vessel. The concept in Figure 14 has the floater connected to some sort of mooring lines. In contrast, the patented solution of Fred Olsen 1848 in Figure 15 uses a permanently installed mooring dolphin, to which the floater is fixed and can also be utilized as further storage for components.



Figure 14: Concept art of a jack-up vessel used for the floating wind turbine integration (Associated British Ports, 2023)

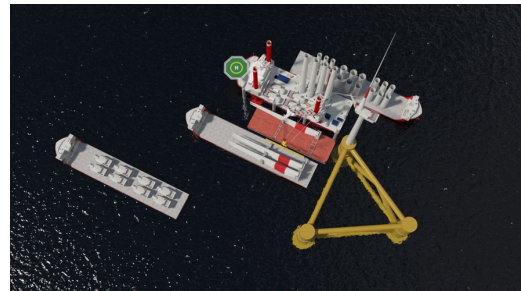


Figure 15: Mobile Port Solution of Fred Olsen 1848 (Fred Olsen 1848, 2023b)

Besides integrating the wind turbine, the concept could also be utilized if major components should be exchanged during the operation phase. For this procedure, it will be challenging to have an available port when major components should be exchanged. Also, exchanging the components on-site could become tricky as either a very expensive heavy lift vessel would need to be used for the very challenging floating-to-floating installation operation or a crane would need to be installed on the floater (Fred Olsen 1848, 2023a). Therefore, if possible with the draft, the jack-up could be either be placed besides the installed wind turbine for the exchange of components or the floater could be disconnected from the cable and mooring lines and towed to a shallower draft location with less demanding wave conditions where the jack-up is then used for the component exchange.

2.5.1 Wind turbine installation vessels

To better understand the characteristics of the proposed integration concept, this chapter should introduce the wind turbine installation vessel a bit more. During the increasing growth of offshore wind an increasing need for specialized installation vessels has been identified. Those vessels are usually either heavy lift vessels for the foundation installation or wind turbine installation vessels

for the turbine integration. Some WTIVs are also suited for the foundation installation, but the turbine integration usually requires the minimal displacement characteristics of the jack-up type WTIV (also called jack-up vessel or simply jack-up) (H-Blix, 2022, p.38). There is no clear definition of a WTIV, but it generally has those three characteristics: self-propelled and able to manoeuvre precisely, able to load and transport wind turbine components by itself and able to install the wind turbine components without other support vessels (Goh, 2022, p.2).

The number of specialized WTIVs has been growing while it is still relatively low as the initial upfront investment is very high and can only be justified with sufficient demand. Based on the confirmed fleet additions, by 2026, it is estimated that 28 WTIVs will exist worldwide. China is not included in these numbers as the Chinese vessels only operate in their own market. But also not of those 28 vessels can be utilized everywhere as Japan and the US have a legislation that prohibits foreign flagged vessels to enter their ports, thus also requiring their own vessel (H-Blix, 2022, p.38). While 28 vessels in 2026 seems to be a small number, when comparing it to the ten existing WTIVs in 2021, the increase of new vessels is very drastic. This increase is also displayed in Figure 16, where it also can be seen that mainly vessels of the new category three are being built. The capacities of the WTIVs has grown with the turbine size as the cranes needed to reach increasingly higher hub heights with larger component weights. Building a WTIV with a higher capacity than forecasted for the following years of operation is not economical. Instead, existing vessels are often upgraded in their crane capacity after some years of operation to be ready for the next generation of wind turbines. The required vessel upgrades are mainly related to the crane, while the rest of the vessel can remain the same, where fewer turbines can be stored on deck due to the decreased size. For instance, Van Oords Aeolus WTIV was delivered in 2014 with a 900t crane and was upgraded to a 1600t crane in 2018, which again got upgraded in 2023 to a crane with the same capacity but now a 133m long crane boom in order to install 15MW wind turbines (Buljan, 2023). Not all existing WTIVs will be upgraded as many have been built with the goals of the lowest cost and with limited ability to be upgraded, whereby they won't be able to install new turbines but still can be utilized for maintenance of existing wind farms (Goh, 2022, p.2).

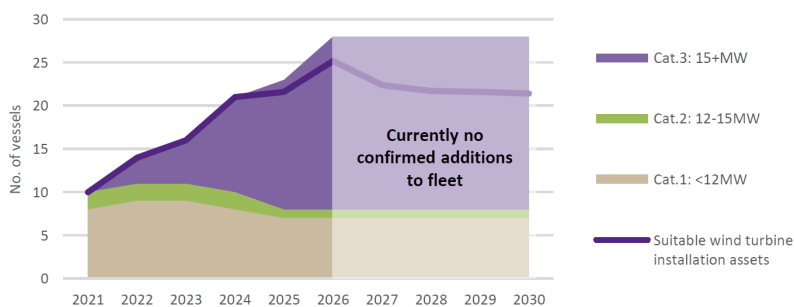


Figure 16: Global WTIV fleet up to 2030 (H-Blix, 2022, p.39)

Leg-encircling cranes are generally preferred for modern WTIV as they allow an increased deck utilization and, thus, the installation of more wind turbines in one go. Every project can have different working procedures. Therefore, the required equipment and lifts must be assessed in detail (Thomsen et al., 2014, p.192). One of the characteristic features of the WTIV is its jacking

mechanism. To have the vessel and especially the crane in a stable position, the four or six truss or closed legs are lowered to the seabed, penetrated into the ground and the vessel is lifted above the water. To do this lifting, which requires a lot of brute force, in the closed leg configuration, a pin and hole system driven by hydraulic cylinders is used (Vanderheggen et al., 2021, p.5). For the truss legs, either a rack-and-pinion system is utilized or a hydraulic hand-over-hand system, which is cheaper but slower (Thomsen et al., 2014, p.220).

To know the safety of the soil beneath the jack-up, it is important to do a detailed investigation of the soil conditions with a seabed scan, cone penetration tests and core drillings. This is essential as any soil failure could have severe consequences for the vessel. The worst failure is punch-through, which happens when a sand layer overlies a soft clay layer (Vanderheggen et al., 2021, p.6). In this case, the leg initially penetrates the high-density layer of sand, where the resistance will drastically drop once the leg enters the clay layer. Thus, the leg will experience an uncontrolled punch-through into the clay layer whereby the leg could buckle or the unit could even tip over (Lee et al., 2013, p.1). The exceedance of the bearing capacity won't be as problematic in other soils. For instance, the bearing capacity is very high in dense sand. A pure cohesive clay layer only increases penetration depth and settlement but with acceptable behaviour in extreme conditions (Vanderheggen et al., 2021, p.6).

One feature that should decrease the likeliness of punch-through are spudcans at the end of the legs as they increase the footprint of the leg and thus decrease the required ground pressure and penetration depth while protecting the leg from increased scour. However, despite the soil tests and the spudcans, it is still important to verify that the leg can sustain the operational loads by preloading each individual leg before jacking up (Y.-K. Kim et al., 2012, p.218). The leg is preloaded by carrying the hull weight on pairs of diagonally opposed legs, either by actively pushing those legs more into the ground or by reducing the loads on the other legs (Vanderheggen et al., 2021, p.6). The operational limits are based on the preloading results, where the preloading per leg can be in the range of 1000-2000t. At the same time, the preloading is kept as low as necessary for minimal wear and tear, to save time and avoid a deeper penetration than necessary (Vanderheggen et al., 2021, p.4).

If a jack-up should be positioned near a port, either to load the components on deck or utilize the crane for the wind turbine integration as previously described in chapter 2.3.2, it is essential to prepare the sea bed beforehand. Quays are usually secured by sheet piles where a penetrated jack-up leg could reduce the stability of the piles. Therefore, the jack-up is positioned at some distance to the quay, the sea bed is flattened and stone cushions are dumped on the location to create a hard, firm base for the leg (Thomsen et al., 2014, p.91).

2.6 Integration sequence

The complete installation of a floating offshore wind farm is complex and has many different operations involved, where besides the turbine integration, the floating wind turbine needs to be towed, the moorings need to be installed, the cables need to be laid and also a substation needs to be constructed either offshore or onshore. The operability analysis, which will be conducted in chapter 6, should purely focus on all installation activities during which the jack-up vessel would be involved for the wind turbine integration, which is further simply called the integration sequence.

When doing a operability analysis of this sequence, the outcomes can be evaluated in regards to the technical feasibility of the proposed concept and as a comparison to a port-based integration sequence. All other installation activities will need to be done regardless of the turbine integration concept.

The wind turbine integration has been described in detail in chapter 2.4 and can be broken down into the three core integration steps of tower installation, nacelle installation and rotor installation. As previously described, given sufficient crane capacities, modern wind turbine towers are usually still installed in one piece by an WTIV as it has roughly the weight of the RNA and minimizes the number of required lifts. The nacelle integration is also very sensitive due to the minimal allowed displacements, while the single blade operation is the most critical task.

Besides the wind turbine integration, the jack-up and the complete integration system are also occupied during other related tasks. First and foremost, the wind turbine components, which should be integrated, need to arrive somehow on the jack-up. For this, two alternative solutions exist: feeder barges and shuttling. For a feeder concept, the components are loaded in the port on simple barges, which are then towed with tugboats to the jack-up vessel and transferred onto the vessel. Compared to the jack-up, they are very cheap and allow a maximal utilization rate of the jack-up vessel. At the same time, they represent additional cost and marine operations as the barge needs to be moored along the jack-up and the components need to be transferred onto the vessel. Furthermore, they have a lower sailing speed than the WTIV and have a smaller operational range (Tjaberings et al., 2022, p.4). Especially for sites far offshore in harsh conditions, this could cause significant delays and require additional feeder vessels to ensure the high utilization of the jack-up, further increasing the cost. Therefore, many current bottom-fixed offshore wind projects use a shuttling approach where the jack-up vessel returns to the port, jacking up and loading the components without further restrictions on the vessel and then returning to the site. While saving the cost of additional vessels and operations, the utilization rate of the vessel for its main purpose, the wind turbine integration, decreases while the charter time increases.

The integration sequence also includes the arrival of the floater from the assembly port, which is either nearby or can be also a more distant specialized port. The floater will arrive using tug boats, it will be positioned in the designated location and connected to a station keeping system. Therefore, a crew also needs to be on the floater. After the wind turbine is successfully integrated, the complete floating wind turbine must be commissioned before it can be towed offshore to its designated location. Therefore, technicians need to check the electric and safety equipment, do paint touch-ups for corrosion protection, tension the bolts of all connections and eventually disconnect the floater from the temporary mooring system. After this step, the floater can be towed to the site, where it is connected to the mooring lines and cables. However, as the tow-to-site of the floater technically doesn't include the jack-up vessel system anymore, it is not regarded as part of the integration sequence. A visualisation of the complete installation sequence is given in the Figures 62 and 63 in chapter 6.

3 Case study

To better understand the feasibility of the investigated integration system, this chapter should highlight a location suitable for implementing the system introduced in chapter 2.5 and the environmental conditions of this location. Furthermore, it will be examined which detailed components the system could consist of and how those would be implemented in the exact location. The outcomes of this chapter will then be used as reference inputs for all further studies.

3.1 Site location

As described in chapter 2.3, the requirements for an assembly port of a floating wind farm are plenty and are different from the requirements of common shipyards or even bottom-fixed wind suited ports. This becomes even more problematic if a floating wind farm should be implemented in a region that has been so far not involved in offshore engineering and does not have any large port infrastructure. One of those regions is the Celtic Sea. So far, regions the dominant maritime industries, both in the UK and Ireland, are trade, like the large energy port port of Milford Haven, fishing and repairing ships like the port of Falmouth (Port of Milford Haven, 2023; A&P Group, 2023). In contrast to other locations in the region, the area has only seen very few offshore oil and gas activities on the Irish part, while no activities were performed in the UK (Irish Offshore Operators Association, 2023). At the same time, despite good wind resources, the water depth of more than 80m in most of the Celtic Sea hindered so far the implementation of bottom-fixed offshore wind (Pinnegar et al., 2004, p.9).

Floating wind turbines are therefore opening up a whole new industry for the region, where the Crown Estate is currently planning tenders for up to 4GW of floating offshore wind farms in the Celtic Sea by 2035 (The Crown Estate, 2023). However, given the previous activities in the region, the port infrastructure of the region is not ready to facilitate large floating wind projects. A further limitation for several of the local ports is the tidal range in the Bristol channel, which is the second highest in the world with a range of up to 12.3m (ABP South Wales, 2023a). Therefore, several of the adjacent ports, like Swansea, Cardiff and Bristol, have sea locks, which due to their width restriction, make them unsuitable for the manufacturing or assembly of floating wind turbines. This limits the number of potential floating wind ports substantially.

All UK ports adjacent to the Celtic Sea and the planned areas for floating wind projects can be seen in Figure 17. The pink areas are the Crown Estates development zones for commercial-scale FOWT projects, while the yellow areas are projects under development of up to 1GW. The red markers are ports, which, based on a personal assessment, are unsuitable for the manufacturing and assembly of FOWTs due to their size, location or sea locks. However, they could still be utilized for the production and storage of subcomponents. The orange markers are ports with some potential but limitations due to ongoing activities like the energy port in Milford Haven or space limitations. The single green marker close to Swansea represents the port of Port Talbot, which is the reference location of this case study.

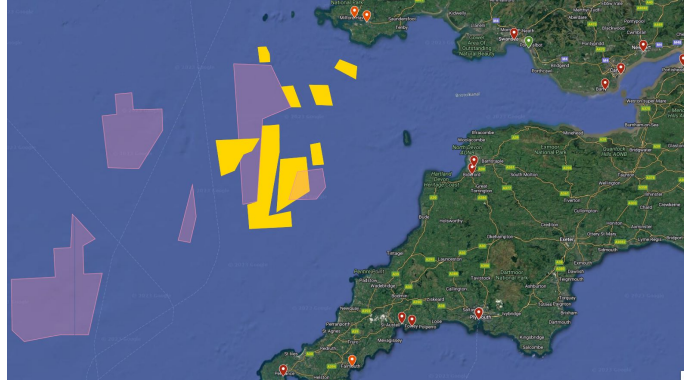


Figure 17: Map of the planned floating wind areas in the British Celtic Sea and adjacent ports (4C Offshore, 2023a; Celtic Sea Cluster, 2023)

The port was built in the 1970s as a tidal harbour 13.7km east of Swansea for the import of coking coal, minerals and ores for the steel production at Tata Steel (Associated British Ports, 2023; Welsh Ports Group, 2023). To handle even the biggest bulk carriers of up to 170000dwt, the port has one of the deepest berths in the UK, with a maximum allowable vessel draft of 17m. This deep water port also makes the port attractive for the manufacturing and assembly of floating wind turbines. As seen in Figure 18, the port currently still has plenty of development zones, which could fit well for the required port infrastructure. The port owner, ABP, envisions Port Talbot as a floating wind hub, where many of the port's development zones are upgraded to build and assemble floating wind turbines (Associated British Ports, 2021). A visual representation of the upgraded port can be seen in Figure 19.



Figure 18: Current picture of the port of Port Talbot (ABP SouthWales, 2023b)



Figure 19: Floating wind vision of the port Port Talbot (Associated British Ports, 2021, p.10)

The floating wind infrastructure in this port should include deep water quays (12m+ at all tides, 21m max) for the manufacturing and assembly of the FOWT, load-out barges for the assembled floaters and a manufacturing cluster for the whole FOWT supply chain with blade, cable and mooring manufacturing facilities (Associated British Ports, 2021, p.20). Those infrastructure upgrades of minor developed terrain require major financial investments, which are estimated at around £400-600m for the marshalling, assembly and integration facilities (Torr, 2022, p.43). Those investments predict an annual production of 25 units per year and integration capabilities of 40 units per year. Further investment will be required if the manufacturers should also be located at the facility, which

would cost further £150-250m (Torr, 2022, p.43). To attract more investors for the port, the British government also gave Port Talbot the freeport status in March 2023, which gives companies within the zone tax and duty reliefs with simplified custom processes (Thomas, 2023).

Those investments are not made out of the blue and are only done if the pipeline of projects foresees a large production of units over several years (Ramirez et al., 2020, p.31). Therefore, the current pre-commercial projects of 50-200MW are a critical phase for the investment in the port facilities as they are insufficient to trigger the large investments needed for the port upgrades (Associated British Ports, 2021, p.19). Therefore, ABP is planning an initial stage where a jack-up vessel would be deployed in the sheltered area of the port and used for the turbine integration, which can be seen in Figure 14. All components would be delivered to the location from other ports, or the jack-up would shuttle to a storage port. Utilising the concept in this location would help signal the market that the port will be a front runner in floating wind (Associated British Ports, 2021, p.19). Furthermore, it would cut the required tow distance from the port to the site as any other potential facility is significantly further away from the Celtic Sea. As previously described, the tow to site operation is very sensitive to the environmental conditions. Thus, having the assembly close to the site could increase the installation speed drastically.

3.1.1 Wind farm site

In this case study, the reference wind farm is the White Cross farm, a cooperation of the British developer Flotation Energy and the Spanish developer Cobra. The project has an area of 49km² where six to eight wind turbines with a total capacity of up to 100MW should be installed 52km off the coast of Barnstaple by 2026 (4C Offshore, 2023c; White Cross, 2023). Like the several other demonstration projects in the Celtic Sea (Llŷr 1 & 2, Erebus, Pembroke Demonstration Zone), this wind farm size is insufficient to trigger significant port infrastructure investments. Thus, it could be a suitable scenario for using a jack-up vessel to integrate the turbines. The project's turbine size and floater design are not published so far. Still, given the planned installation time in three years, turbines of 12-15MW are a realistic estimate, where eight 12MW turbines could reach the maximum capacity of 100MW, the closest with a total nameplate capacity of 96MW. The floater type will be a semi-submersible, which suits the water depth of 60-75m (4C Offshore, 2023c; 4C Offshore, 2023a). As seen in Figure 81 in Appendix C, the site is around 105km (56nm) away from Port Talbot, which is optimal for towing as a tow would only take around 19h.

3.2 Environmental conditions

The investigated system is subject to environmental loads, which induce the critical motions that determine the success or failure of the integration. To simulate those loads, environmental data is needed. As there is no publicly available data from a meteorological measurement station near the port site, hindcast data is used to determine the metocean environmental conditions. Hindcast data is based on numerical models in combination with historical data to provide localised information about waves, winds and other oceanographic conditions. In this case, the open access data from NORA3 waves are used, for which the Norwegian Meteorological Institute has provided the tools to access the data (Christakos, 2021). Based on this data, the load cases of the simulation are determined in chapter 4.5.5.

The location for the hindcast data can be seen in Figure 20. The reference point is not within the port, as the NORA3 model is designed for the North Sea and has reduced accuracy for other locations in Europe. As no other data is available, this data point is further used, while its implications will be discussed in this work. To increase the statistical accuracy of the data, 39 years of hindcast data from 1982 to 2021 were extracted from the database. The data is analysed based on the Metocean Procedure Guide from Goward Brown et al. (Goward Brown et al., 2018).

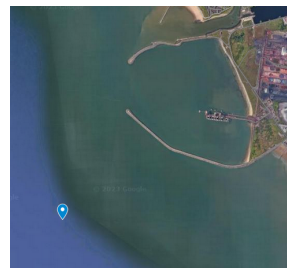


Figure 20: Location of the hindcast data

The scatter diagram of the significant wave height H_s and wave period T_p , displayed in Figure 21, shows that the site has very moderate wave conditions where 73.4% of the time the wave heights are lower than 0.9m. As the wave rose in Figure 22 shows, the waves are relatively unidirectional, coming on average from 255° . Considering the topography of the port, it means that the main breakwater is designed to protect the port from incoming waves. Therefore, the waves within the port are probably lower than the hindcasted data indicates. The breakwaters make it unlikely that the conditions within the port are harsher at any point than outside of it. Thus, at worst, the made investigations are overly conservative and represent an open water, nearshore integration. The impact of the insufficient environmental data on the results will be further discussed in chapter 5.8 and 6.5. Another important factor is the resolution of the predicted wave data. Numerical wave models are generally less accurate for near shore areas than offshore and in addition the forecasting of low significant wave heights of up to 1m is very challenging as the resolution becomes lower and thus the uncertainty is higher (Alday et al., 2022, p.1; DNV, 2011, p.32). Additionally, the metocean hindcast model is not designed for the Celtic Sea and has less accuracy in this area. The used wave data needs to be assessed under those limitations, especially when low significant wave heights are considered. When comparing Port Talbots open water, nearshore data to the conditions of the White Cross wind farm in Figures 82 to 84 in Appendix D, it becomes clear that the site is substantially harsher. This would most likely also make the on-site wind turbine integration much more challenging.

Regarding the wind, displayed in Figure 23, it has a much higher directional variation. The majority of the wind is coming from the west, mainly 250° to 260° , which coincides with the main wave direction, but there are also a substantial amount of winds coming from 100° , 110° and 340° . Only from the direction of the coast in the northeast there is hardly any wind. The average wind speed on the location is 6.4m/s while 99% of the wind speeds are below 15.6m/s. In contrast, this is 8.04m/s and 17.4m/s on the wind farm site.

Condition	Duration [h]	Jan	Feb	Mrz	Apr	Mai	Jun	Jul	Aug	Sep	Okt	Nov	Dez	Average
Hs<1.5	3	77,48%	82,58%	89,35%	95,79%	96,16%	96,85%	97,52%	96,01%	93,28%	86,24%	83,86%	77,26%	89,36%
Hs<1.5	6	74,96%	80,55%	87,63%	94,97%	95,34%	96,20%	96,93%	95,09%	91,83%	84,20%	81,38%	74,58%	87,80%
Hs<1.5	12	70,53%	76,90%	84,48%	93,48%	93,81%	94,94%	95,89%	93,36%	89,27%	80,42%	77,11%	69,96%	85,01%
Hs<1.5	24	63,69%	71,28%	79,48%	90,89%	91,11%	92,59%	93,98%	90,11%	84,90%	74,02%	70,23%	62,86%	80,43%
Hs<1.5	48	54,40%	63,31%	72,00%	86,26%	86,43%	88,36%	90,34%	84,42%	78,00%	64,32%	60,07%	52,50%	73,37%
Hs<1.5	72	47,80%	57,33%	65,95%	82,15%	82,34%	84,50%	86,83%	79,56%	72,36%	57,12%	52,12%	44,76%	67,74%

Figure 24: Monthly distribution of the significant wave height below the threshold of 1.5m at the data point, data from NORA3

The tidal range within the port can vary from 3.2m to 10.3m, depending on whether you have neap tides or spring tides (Welsh Ports Group, 2023). This indicates that there could also be significant currents within the port, especially in the entrance channel. Simulations have shown that in some regions of the Bristol channel the current speeds could reach up to 3m/s which would have drastic consequences on the ability to position the jack-up and the floater. However, for the Swansea bay only a maximum MST current speed of 0.5m/s was estimated (Uncles, 2010, p.9). There is no available measured long-term data on currents within the port. The only measurement that has been found is a single-day measurement from 1974 made by Collins et al., where they measured 0.3m/s of currents at the channel entrance during spring tide and 0.22m/s during ebb (Collins et al., 1979, p.53). Like the metocean data, this wouldn't be sufficient data if the operation were executed. For a preliminary assessment, it is deemed sufficient to assume currents of 0.3m/s as those fairly coincide with the simulated maximum current speed in the Swansea bay of 0.5m/s.

The bathymetry of the Swansea Bay can be seen in Figure 25. It is seen that the port of Port Talbot is already dredged deeper than the rest of the bay, whereby the mean sea level (MSL) within the port ranges from 11m to 12m. Additionally, a channel leading to the port was dredged. While the installation draft of most semi-submersible and barge concepts would be sufficient for this water depth, the large tidal range could lead to challenges, especially for low tides. Meanwhile high tides also increases the allowable draft in this port up to 17m (Welsh Ports Group, 2023). However, the floater needs to be accommodated longer than one high tide time and must be able to tolerate the full tidal range. The tidal range will also complicate the integration procedure as the crane constantly needs to be adjusted.

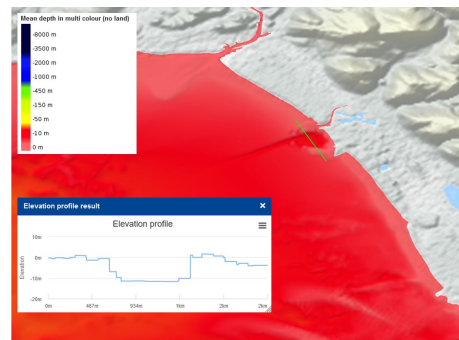


Figure 25: Multicolored bathymetry profile of the Swansea Bay with the elevation profile of the green line (EMODnet, 2023)

Regarding soil conditions, a study of the Swansea Bay has found a mix of different sands and some

clay beds (Thethys, 2022). As the mix of clay and sand bares the risk of punch-through of the jack-up legs, detailed geotechnical investigations should be held at the specific location to avoid a severe failure during the preloading. Furthermore, stone cushions should be dumped on the seafloor so that the jack-up legs have a hard, firm base (Thomsen et al., 2014, p.91).

3.3 Implemented components

This chapter will now highlight which components are assumed to be used in this case study. Many other vessels, turbines and floaters could be used, but the investigated components should be used as a further reference for the simulations.

3.3.1 Jack-up vessel

With the turbines being assumed to be 12MW turbines, the number of potential jack-up vessels is limited as only a few available vessels have cranes with sufficient lifting capacity and lift height. For this thesis, it is assumed that the integration is done with the Bold Tern vessel of Fred Olsen Windcarrier as the crane was upgraded in 2022 to a 1600t leg-encircling crane that is suited for turbines up to 15MW with detailed available vessel data (Buljan, 2022a; Fred. Olsen Windcarrier, 2023b). A picture of the vessel can be seen in Figure 26.



Figure 26: Bold Tern jack-up vessel with the upgraded crane (Fred. Olsen Windcarrier, 2022)

3.3.2 Floater

There are a vast amount of semi-submersible and barge concepts on the market. The large tidal range within the port emphasise using foundations with a shallow draft or an adaptable draft, whereby steel floaters are preferred as they can have an active ballasting system.

The focus on steel floaters limits the number of potential floaters only to a certain extent, as a floater database list 41 different concepts for steel semi-submersibles and barges (QuestFWE, 2022). Some concepts like the steel Damping Pool of Ideol, the TetraSub of Stiesdal or the OCG Wind Floater from Ocergy are interesting solutions from a manufacturing and assembly perspective as they are lightweight, have a shallow draft and are made out of standardised components (Ideol, 2023; Stiesdal, 2023; Ocergy, 2023). The detailed investigation of the integration process requires a sufficient



Figure 27: INO Windmoor 12MW concept (Silva de Souza et al., 2021, p.9)

model where all hydrodynamic properties need to be known. As those parameters are essential components of every floater design and critical intellectual property of the developers, this thesis focuses on designs with available data. In this regard, for 12MW steel floaters, only the design of the INO Windmoor 12MW floater is available for the modelling software SIMA as it was developed during a research project of SINTEF (Silva de Souza et al., 2021). Therefore, this floater is also the chosen concept for this scenario.

As seen in Figure 27, the floater is a three-column steel semi-submersible connected by pontoons at the upper and lower end of each column. The operational draft of the floater in the model is 15.5m, which contradicts the low draft target for the installation to address the large tidal range in the port. However, most steel floaters can vary their ballast based on the requirements. Therefore, during the wind turbine integration, the ballast tanks are as empty as possible so that the draft is minimal while also maintaining the required stability. Also, during the tow-out, the draft is kept moderately low so that the floater is not interfering with the seabed in shallower regions. Only when the floating wind turbine arrives on site are the tanks filled with permanent water ballast to increase the stability of the floater (Principle Power, 2023b). However, the draft of the floater is kept in this work at 15.5m as changing the draft would require the determination of new hydrodynamic properties of the floater, which exceeds the scope of this thesis.

The INO Windmoor 12MW floater is a good example for other floater designs as it is pretty similar to the floater design of Principle Power, which is the most used semi-submersible design (Principle Power, 2023a), while Equinor is collaborating with Technip Energies to apply the INO Windmoor design in its upscaled 15MW version for projects in France and Korea (Equinor, 2022).

3.3.3 Wind turbine

Based on the current wind turbine market, in an actual application, the used wind turbine could be, for instance, the 12MW version of GEs Haliade-X design (GE Renewable Energy, 2023). Regarding the numerical model, there is a lack of reference turbines for 12MW offshore wind turbines, therefore, for the INO model, SINTEF has upscaled the IEA 10MW wind turbine (Bortolotti et al., 2019). The airfoil shapes are kept the same while they upscaled the blade dimensions and structural properties based on common upscaling laws (Silva de Souza et al., 2021, p.15).

3.3.4 Moorings

The setup of the wind turbine integration with a jack-up vessel has unique requirements for the mooring system, as the floater is in very shallow waters. At the same time, the floater displacements also have to be minimal for the integration. Research has so far focused on the operational shallow water moorings for depths beyond 50m as bottom-fixed foundations are expected to always be cheaper in any lower water depth (Xu et al., 2018, p.1). Even for the range of 50-100m, catenary mooring lines can get quite challenging as the angle change rate increases, whereby the catenary shape could get lost, which risks vertical forces acting on the anchor. To overcome the high angle change rate, the footprint of the catenary mooring system has to get very large with a lot of chain on the seabed (Xu et al., 2018, p.5). When sites below 50m are considered, the catenary mooring system will become even more expensive. Thus, this solution is not feasible for integration moorings at this location. Taut moorings generally have a much lower footprint and lower offsets. However, it would be very challenging from an operational perspective to set them up in the shallow draft

area. At the same time, the tidal variation can largely impact the system’s functionality.

An alternative use case where shallow water moorings will be required is the temporary storage of the floaters. Those temporary moorings will be needed when the manufactured floater has to wait for the transport to the assembly port or when the assembled FOWT is waiting for the tow-out to the site. Those storage spaces with temporary moorings are expected to be required for many floating wind ports and are also included in the Port Talbot vision as seen on the left side in Figure 19. The research on those mooring systems has been very limited, with one joint industry project founded in September 2022 to investigate this issue, but it hasn’t published results so far (Buljan, 2022c). The optimal temporary mooring solution will be very site-specific and depends on the storage period, the number of floaters to be stored, and the storage site’s water depth. Furthermore, a regulatory framework of the local authority is required for the storage site (Torr, 2022, p.24). Regarding displacement, the allowable offset for storage moorings can be very high, as only a collision with surrounding structures needs to be avoided.

The only time a semi-submersible wind turbine was temporarily stored, was during the Kincardine project, as seen in Figure 28. For this mooring solution, the floater was connected via horizontal mooring to bollards which are piled into the ground. This solution is appealing from an operational perspective, as the mooring lines are much easier to access and the footprint can be kept moderately low. Therefore, this mooring solution has been chosen for Port Talbot. As the temporary storage system allows higher displacements, it can use softer fibre ropes like Nylon. In contrast, stiffer ropes made out of HMPE/Dyneema will be used for the installation moorings so that the floater movement is minimal. The much stiffer mooring is anticipated to substantially change the system’s response compared to the operational state, where the allowable offset is relatively high. This will be further investigated in chapter 4.3.4.



Figure 28: Storage of the Kin04 floater with horizontal mooring lines and bollards (Buljan, 2022b)

3.4 Setup

A visualisation of entire assumed setup of the wind turbine integration during the single blade installation is shown in Figure 29 with the true-to-size sketches of the Bold Tern jack-up vessel, the INO Windmoor 12MW floater, the scaled 12MW blade and the horizontal mooring configuration.

The direction of the installation process is designed so that both frontal mooring lines are aligned symmetrically to the incoming waves from 255° . This also means that the blade is most likely perpendicular to the incoming wind during the single blade installation, but, the tugger lines are particularly designed to minimize the perpendicular movement of the blade. The impact of the wind direction on the blade motions will be assessed in chapter 5.6.

The overall dimensions of the system are a 132x39m large jack-up vessel with a floater of the footprint of 74x64m if considered as a rectangle. The hub height is at 131.7m. The detailed properties of all components will be presented in chapter 4.3. The distance between the crane base and the hub is at 49.3m, based on a reference work for a bottom-fixed installation (Zhao, 2019, p.23). From a practical perspective, it is probably more favourable to have a bit smaller clearance between the vessel and the turbine as this would increase the carrying capabilities of the crane and improve the ability to monitor the integration process visually. However, a certain clearance between the vessel and the floater must be kept so that any collision between them during the transport of the floater or even during installation can be avoided.

This work focuses on the single blade installation, where the optimal orientation of the crane would be a perpendicular alignment to the blade and the hull orientation. However, in practice, this setup could change, as it would mean that the lifts of the much heavier tower and nacelle would require a much larger outreach to access the wind turbine column of the floater. Potentially, this could lead to an exceedance of the maximum crane capacity and certainly increase the complexity of the operation. Therefore, in practice, it is advisable that the setup is chosen to favour an optimal tower and nacelle integration where the crane would need to slew for the blade installation. Nevertheless, this work assumes a perpendicular crane setup during the installation as a slewed crane complicates the numerical model, especially the tugger line system. It would be interesting to consider the impact of other installation setups but to limit the scope of the thesis only the proposed setup of Figure 29 is investigated.



Figure 29: Visualisation of the investigated integration operation in Port Talbot

3.5 Implementation of the integration sequence

When the integration sequence of chapter 2.6 should be implemented in Port Talbot, it is important to evaluate the local conditions, especially how the jack-up can be supplied with components for the wind turbine integration. Both shuttling and feeder concepts will be evaluated to better understand the impact of choosing one or the other. It is assumed that besides the mooring bollards, no floating wind infrastructure has been built in the port. Thus, the port could not provide sufficient infrastructure for storing and loading the components. As seen in Figure 30, the closest port to Port Talbot is the port in Swansea, which is 12km away. Due to the high tidal range, this port has a sea lock which keeps a stable water level with no waves within the port, which is favourable for transferring the components onto a vessel. The maximal theoretical acceptance of the sea lock is a vessel with a length of 200m, a beam of 26.2m and a draught of 9.9m (ABP, 2023). While this is small enough for the vessels which are delivering the components, like the nacelle roll on/roll off vessel of Siemens Gamesa (Ship Technology, 2016) or a simple feeder barge with tug boats, the jack-up vessels beam it too large to fit into this port. Therefore, for the the shuttling scenario, the jack-up vessel would travel 120km to the port in Pembroke Dock, the nearest open water port with sufficient access. In this port, a sufficient storage area for wind turbine components is currently in the planning (RWE, 2022). The jack-up would then arrive and load components for up to three 12MW turbines (Fred. Olsen Windcarrier, 2023b). Then the jack-up would return to Port Talbot.

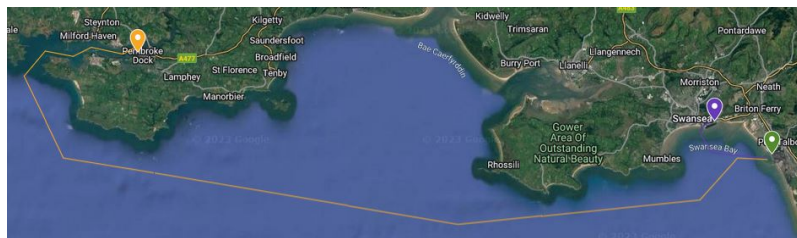


Figure 30: Routes between Port Talbot (green), Swansea (purple) and Pembroke Dock (yellow)

4 Modelling of the system

A model of the fixed-to-floating operation has been created to understand the general system behaviour when a jack-up vessel is being used to integrate a wind turbine. Based on this model, loads and response analyses are conducted based on the local environmental conditions to understand the system's performance, its limitations and the technical feasibility of the concept. While the integration procedure consists of several different steps, which were examined in chapter 2.4, to limit the scope, the model has been only designed for the single blade installation as this is regarded as one of the most critical operations due to the minimal displacements allowed during the mating phase. Doing the response analysis of this integration system can help decrease the operation's uncertainty as it can provide a deeper understanding of the floater and blade motions during the installation when both are subject to environmental loads. This chapter explains the methods which are being used to create the model. Then it will be explained how the different components are modelled in detail and how this model is integrated numerically. Chapter 5 will then focus on the outcomes of the response analysis.

4.1 Literature review

As previously mentioned, the proposed system has not been investigated so far, but some studies on somewhat similar systems either related to floating wind in general or the installation of bottom-fixed turbines can be utilized have references for this work and not create the entire model and procedures from scratch.

Regarding the single blade installation with a WTIV, Zhao has developed a detailed numerical model of the vessel and the blade lifted by the crane while being subject to wind loads with a tailored Aero code (Zhao, 2019). Over several papers and her doctoral thesis she investigated both a jack-up vessel and a floating vessel, while gradually advancing the model by also regarding soil-structure interaction and the tugger line tension (Zhao, 2019, p.13). Rognstad and Nakstad as well as Kim have then validated the performance of those models in deeper water depths (Rognstad & Nakstad, 2020; T. Kim, 2021). Furthermore, in a very recent work, Bhaskaran developed the same jack-up model for the single blade installation in ORCAFLEX and compared it to the SIMA model of Zhao (Bhaskaran et al., 2023). Jack-up vessels need to lift very heavy loads for the wind turbine integration, therefore, Vanderheggen investigated the crane load induced foundation failure (Vanderheggen et al., 2021). In regards to transporting wind turbine components with a jack-up vessel, Gucma determined maximum safe parameters (Gucma et al., 2022).

Several studies have been also conducted for the single blade installation of bottom-fixed wind turbines, where Gaunaa investigated the aerodynamic behavior of the blade (Gaunaa et al., 2014), while Jiang looked in detail at the success and failure criteria for the alignment phase and the mating phase (Jiang et al., 2018b). The alignment phase of the single blade installation has also been investigated in detail by de Leuw (de Leuw, 2019). Sander published measurement from studies conducted during the single blade installation in the North Sea (Sander et al., 2020) and Skrzypinski has modelled the vortex-induced loads on the single hanging blade at various inflow angles (Skrzypinski et al., 2016).

While many publications have so far tackled the dynamics and other operational characteristics

of a floating wind turbine, only very little have regarded the installation and integration of the FOWT. Some studies focused on the installation of spar type FOWTs, which due to their large draft have specific installation restrictions and characteristics. Therefore, Jiang, Ren, Hong and Liu investigated the installation of spar-FOWTs with a tailored floating dock or different types of installation vessels (Jiang, 2018; Ren et al., 2021; Hong et al., 2022; Liu et al., 2023). In a recent work, van der Kaaij investigated the on-site single blade installation of a semi-submersible with a floating crane vessel (van der Kaaij, 2023). Other works focused on the marine operations of floating wind (Ramachandran et al., 2021), but the combination of a jack-up vessel and a floating wind turbine has not been investigated as of June 2023.

This work will utilize the SIMA model of the jack-up vessel from Zhao, while the model will be modified to address the requirements of the 12MW floating wind turbine and the site. The used floating wind turbine has been modelled in SIMA in a research project by SINTEF (Silva de Souza et al., 2021) and is also modified to represent the installation phase and not the operational phase. This work will combine both existing models, while the mooring system has been newly designed for the integration model. The assessment of the single blade installation will then be done in the same methodology as with the work of Jiang.

4.2 Modelling method

The goal of the load and response analysis of the system is to solve the equations of the system's rigid motions when subject to different load scenarios during the single blade installation. This analysis is done by implementing the system in the numerical simulation software SIMA, which can be used to analyse complex multi-body systems. Load cases are defined based on environmental data of the location, which then can be implemented in SIMA. Those load cases are then run as time-domain simulations in SIMA, which gives the time series of the system's components as an outcome. Those outcomes are then post-processed in MATLAB by statistically analysing the motions, determining outcrossing criteria and performing Fourier transforms of the time-series to obtain the power spectral density function of the motion. The results of those analyses are then used to evaluate the behaviour of the individual components and the whole system based on an exemplary rough load case and the outcomes of all investigated load cases are used to determine the system's operational limits.

To create the model of the integration system, it is first important to identify the key components of the system, which are important for the single blade installation. First up is the jack-up vessel, combined with the crane installed on its deck, where the jack-up positioned itself in operational condition with the hull elevated above the sea (Zhao, 2019, p.22). The second important component is the blade which is lifted to the hub height of the wind turbine and connected to the crane by lift and tug wires without a connection to the wind turbine. The third component is the floating wind turbine, where the floater is positioned close to the jack-up vessel and the tower and the nacelle are already installed on the platform. The fourth key component is the mooring system, which enables the floater to stay in its destined installation location. The general setup of all components can be seen in Figure 32.

Figure 31 and Figure 32 are also showing the coordinate systems of the different components, which is based on the jack-up description by Zhao and extended with the floater (Zhao, 2019,

p.20). The global reference point is the centre of the floater and the blade is initially aligned with the global y coordinate. The floater coordinate system is rotated as the turbine carrying column is defined in positive x-direction in the numerical floater model (Silva de Souza et al., 2021, p.8).

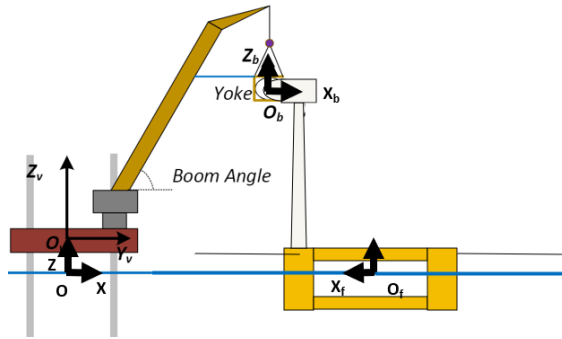


Figure 31: System and its coordinates from a side view (Zhao, 2019, p.20)

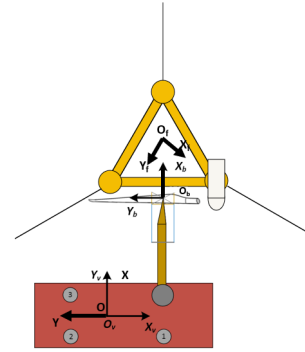


Figure 32: System and its coordinates from a top view (Zhao, 2019, p.20)

4.2.1 Assumptions

The numerical modelling of a procedure always underlies a certain range of assumptions which have been made to simplify the model, reduce the scope of the work, adapt to the available tools or are generalisations due to the lack of sufficient data. Those main modelling assumptions should be examined in this chapter to create a better understanding of the scope that this study has been made in and its limitations. Their impact on the outcomes of the modelling will be then discussed later on in chapter 5.8. Further assumptions will be stated within the coming chapters, but they are not regarded as major factors on the outcome of this work.

This study is only focusing on one vessel and one floating wind turbine to limit the scope of the work. A comparison of different floater concepts and turbine sizes would be certainly interesting to understand the impact on the dynamics of the system. It would help to understand how much it would be universally applicable or how much it would need to be adapted for every design. However, there is only a limited amount of other floater data available and another detailed investigation would exceed the time limitations of this thesis. Regarding the vessel, it is not expected that a different of jack-up model would largely effect the motion characteristics of the vessel as it is fixed to the ground regardless. An investigation of heavy lift vessels would be interesting but is extending the scope of this work.

The computational effort is further reduced by only investigating a limited amount of load cases. To determine the exact allowable sea states, the simulations would need to be run for all probable sea states which would drastically increase the simulation time. Instead a few selected load cases are investigated.

Even though the site is subject to a very large tide regime, the simulation is only done in one water depth, which is also deeper than the actual site to work with the given hydrodynamic data

of the floater. The simulation software is not capable to model a change of water depth during the time-domain simulations and running the simulation for multiple water depths would extend the scope of the work. In context of the large tidal range of Port Talbot, this could mean that the results of the simulation can be no longer applied to the investigated location. In theory, the draft of the floater could also be changed to a draft that is more likely during the installation phase, in contrast to the operational draft of 15.5m. However, this would require a recalculation of all hydrodynamic properties in WAMIT, which would exceed the scope of this thesis. The outcomes of the simulation with this draft can be used as a reference to future works with adjusted draft.

As the tides can't be included in the model, it is also deemed as sufficient to use the high-tension, high-stiffness horizontal mooring lines. They are not applicable for large vertical variations but are the only mooring solution that is found to sufficiently reduce the floater motions in a shallow water depth. Bottom-fixed station-keeping-systems would be an alternative but are undermining the research goal of understanding the fixed-to-floating operation.

The mating procedure can only be done if some sort of control mechanism is restricting the relative motions between the blade and the hub. While some sort of control measurements do exist for bottom-founded wind turbines, they are not adapted for floating wind. Those measurements would require advanced motion prediction tools for both the blade root and hub motion and potentially some control mechanism for the floater motions, for instance, by controlling the mooring tension. However, developing those advanced control systems and implementing them in the numerical model exceeds the scope of this thesis but should certainly be of interest to future research. Therefore, in this work the controller is simplified as a restrictive highpass filter.

Based on those assumptions it can be concluded that the outcomes of the conducted response analysis won't be able to accurately represent the local site conditions, give detailed operational limits or give a conclusion about the performance of other setups. However, the outcomes will be still sufficient to create a general understanding of the concepts behaviour in regards to the sensitivity to different environmental loads, understand which components are generally governing the system motion and to understand which general technical challenges exist when the concept should be implemented.

4.2.2 Environmental loads

The external loads that lead to the system's movement are the environmental loadings from wind, waves and currents. One goal of the simulations is to better understand which environmental loads impact the individual components of the system and the system as a whole.

The environmental loads acting on a real system are complex and can only be modelled under significant computational efforts. Therefore, it is important to simplify them to a certain extent while maintaining sufficient accuracy. For the waves, this is done by modelling them as long-crested, irregular waves based on the JONSWAP spectrum, which is defined as

$$S(\omega) = \frac{\alpha g^2}{\omega^5} \exp\left[-\beta\left(\frac{\omega_p}{\omega}\right)^4\right] \gamma^{\exp\left[\frac{(\frac{\omega}{\omega_p}-1)^2}{2\sigma^2}\right]} \quad (2)$$

with ω_p as the wave peak frequency, α as the spectral parameter, β as the form parameter and γ as the peakedness parameter (Zhao, 2019, p.40). The JONSWAP spectrum has been developed

for sea states in the North Sea, while this case study will focus on a site in the Celtic Sea where the wave regime could slightly differ. Some studies have investigated those wave regimes in the Celtic Sea (Palmer et al., 2015; Wyatt, 1995; Pingree & Mardell, 1985), but for simplicity, the most commonly used JONSWAP spectrum is still deemed as sufficient.

The wind loads are modelled as a three-dimensional turbulent wind field. The turbulence is based on the Kaimal model and also wind shear is regarded with the mean wind speed calculated based on the power law principle as a function of the height above mean sea level z :

$$U(z) = U_{ref} (z/z_{ref})^\alpha \quad (3)$$

In this equation, U_{ref} represents the mean wind speed at the reference height z_{ref} and α as the power law exponent (Zhao, 2019, p.40).

The currents are modelled as constant loads acting on all submerged elements in one constant direction. As the tides mainly induce the currents in this scenario, this might be an oversimplification and should be evaluated based on the impact of the currents on the system behaviour.

To implement the environmental loads into the model, load cases are defined based on the given hindcast data. The load cases are defined in chapter 4.5.5.

4.2.3 Equations of motion

The environmental loads are acting on the integration system, leading to the components' movement. The response of every component is different based on its properties and coupled effects, which can be described as an equation of motion of the body, as long as the body is assumed as rigid. The corresponding body motions can be obtained by solving those equations for the defined load cases.

For the single blade installation, two body motions are particularly interesting: the blade root and the hub motions. Knowing the relative motions between those points is the key parameter for determining the success of the installation and therefore, their equations of motion are examined in detail here.

As the wind turbine blade is assumed to be rigid, the blade root motions can be calculated based on the blade equations of motion and the distance between the blade root and the blade centre. The equation of motion of the blade can be formulated as

$$M\ddot{x} + D\dot{x} + Kx = q(t, x, \dot{x}) \quad (4)$$

with M as the mass of the combined blade-yoke system, D as the damping matrix, K as the stiffness matrix and q as the external load vector. The tugger lines connected to the blade play an important role in the stiffness and the damping of the blade motions, while both are only working unidirectional as a slack wire can't provide stiffness to the system. The external loads on the blade are mainly due to the wind loads acting on the blade but also due to the motions induced by the crane. The resulting forces of the wind force acting on a 2D-wind turbine blade can be seen in Figure 86 in Appendix E. The resulting force can be split into the lift force, perpendicular to the direction of

inflow velocity, and the drag force, parallel to the velocity (Hansen, 2015, p.8). Their coefficients can be calculated with

$$C_l = \frac{L}{\frac{1}{2}\rho V_\infty^2 c} \quad (5)$$

and

$$C_d = \frac{D}{\frac{1}{2}\rho V_\infty^2 c} \quad (6)$$

The aerodynamics of an actual 3D wind turbine blade are much more complex during the turbine operation but for the installation the 2D approximation of the cross-flow principle is sufficient.

The nacelle's rigid body motion governs the hub motions. Those motions are closely linked to the floater motions as it is connected to the substructure by the tower. Under operational conditions, this assumption can not be directly made as the thrust forces acting on the wind turbine result in the tower's bending. In comparison, the wind forces acting on the nacelle and the tower in non operating conditions are much smaller, therefore, it is deemed sufficient to assume that the hub motions are governed by the floater motions. The floater equation of motion can be formulated as follows:

$$(m + A_\infty)\ddot{x} + D_1\dot{x} + Kx + \int_0^t h(t-\tau)\dot{x}(\tau)d\tau = q(t, x, \dot{x}) \quad (7)$$

with m being the rigid-body inertia matrix, A_∞ the infinity-frequency added-mass matrix, D_1 the linear external damping matrix, K the hydrostatic restoring matrix, h being a matrix for retardation functions. The external loads are represented by the vector q , which can be formulated as:

$$q = -mg\hat{k} \times r_g + \rho g V \hat{k} \times r_b + q_{1st} + q_{2nd} + q_{vis,q} + q_{FE} \quad (8)$$

where m is the total mass of the floating wind turbine without accounting for the buoyancy, which is regarded as a vertical specified force, ρ being the water density, g the acceleration of gravity, V the displaced volume, r_g and r_b the position vectors from the centres of gravity and buoyancy to the origin, q_{1st} being a vector for the first order wave loads, q_{2nd} accordingly representing the second order wave loads, $q_{vis,q}$ containing the viscous contributions from the columns and pontoons for the quadratic term of the Morison formulation and q_{FE} including the loads which the connected RIFLEX elements (tower and usually moorings) impose to the platform (Silva de Souza et al., 2021, p.27).

The mentioned first order wave loads consist of two problems. The first is the diffraction problem, which regards the oscillation-restraint floater subject to incident waves, consisting of the Froude-Kriloff and diffraction forces and moments. The second one are the forces and moments when the body is oscillating at the wave frequency without incident waves, the so called radiation problem. Those loads are the added mass, damping and restoring terms (Faltinsen, 1993, p.39). The Morison formula can not be applied here as the floater can't be regarded as a slender structure. Second-order wave loads are accounting for the non-linear effects of the wave-structure interaction. Those wave loads include effects when the structure is oscillating with a frequency other than the waves, such as drift effects, and the interaction among the components. The amplitude of the second order wave loads is usually 1/10th of the first order (Gao, 2022, p.20).

As weight and buoyancy are in equilibrium, the hydrostatic restoring matrix K has only contributions from volume variation caused by small motions around the equilibrium. Thus this matrix is

$$K = \begin{bmatrix} 0 & 0 & 0 & 0 & 0 & 0 \\ 0 & 0 & 0 & 0 & 0 & 0 \\ 0 & 0 & C'_{33} & 0 & 0 & 0 \\ 0 & 0 & 0 & C'_{44} & 0 & 0 \\ 0 & 0 & 0 & 0 & C'_{55} & 0 \\ 0 & 0 & 0 & 0 & 0 & 0 \end{bmatrix} \quad (9)$$

with the coefficients calculated in $C'_{33} = \rho g A_{wp}$, $C'_{44} = \rho g \int \int_{A_{wp}} y^2 ds$ and $C'_{55} = \rho g \int \int_{A_{wp}} x^2 ds$ with A_{wp} as the waterplane area and under the assumption of small roll and pitch angles.

4.2.4 Single blade installation criteria

The conducted studies of this thesis focus on the single blade installation. To better understand whether or not the operation has been successful, Jiang has established a methodology to define operational limits on which basis the motions of the system can be assessed (Jiang et al., 2018b).

Alignment

The alignment phase is initiated once the blade has been brought into position at hub height and a sufficient distance from the hub. The relative motions between the blade root and the hub in the xz -plane are of special interest for the alignment. Here it is deemed that the alignment can't be done if the distance D between the centre of the blade root and the centre of the hub exceeds the criterion $D < R_b + R_h$. R_b is the blade root radius and R_h is the hub radius. The limit can also be expressed as the circular safe boundary $R_{sb1} = R_b + R_h$. The alignment is usually rated as successful if the motion radius in the xz -plane is not exceeding this boundary at a given outcrossing rate. Once this criterion is fulfilled and if the clearance in the y -direction is also sufficient, the blade and hub can be aligned with visual or manual assistance (Jiang, 2021, p.1043). As the alignment can not use any further guidance mechanisms, it is important to restrict the blade motions with the tugger lines. The impact of the tugger line tension will be further discussed in chapter 5.1.

Mating

Once the alignment is successfully done, the distance between the hub and the blade in the y -direction is minimized and the mating phase is initiated. As previously discussed, the collision of the guide pin with the flange hole could lead to very problematic damage. Therefore, the safe boundary R_{sb2} is also much lower. According to Jiang, it is only the difference between the flange hole radius and the guide-pin radius, also written as $R_{sb2} = R_{fh} - R_p$ (Jiang et al., 2018a, p.12). As the bolts usually have a diameter of a few centimetres and as also the flange holes are just a bit wider to have a sufficient bolt-flange connection, this safe boundary is usually just in the area of a few mm. Once the critical relative motions, determined by a defined outcrossing rate, are below this boundary, the mating and, therefore, the complete single blade installation is deemed successful.

To perform the mating process, some controller which can filter out the large motions of the blade and the hub needs to be applied. In theory, this controller would need to predict the incoming wind and wave loads and the response of the blade and the floater and adjust their movement in some way. There are control measurements for the bottom-fixed integration which try to keep the tugger line forces constant and some also use an active feedback control, but so far, those have not been adapted for floating wind turbines. To minimize the relative motions, the floater motions would also need to get controlled in some way, for instance, by controlling the mooring tension. As mentioned in chapter 4.2.1, due to the novelty of integrating wind turbines on floating foundations with a jack-up vessel nearshore, research on specialised installation control measurements has not yet been published. To limit the scope of this thesis, only a very simplified controller is introduced for the mating phase and a larger focus is set on the alignment phase and the general behaviour of the system.

4.3 Integration system

This chapter should now focus on the detailed parameters for all key components included in the model. The properties of the features are based on the systems assumed for the case study in Port Talbot, which were discussed in chapter 3.3.

4.3.1 Jack-up vessel

The jack-up vessel used in this model is assumed to be the Bold Tern vessel from Fred Olsen Windcarrier. The numerical SIMA model of this four-legged vessel with the single blade lifted by the crane has been developed by Zhao (Zhao, 2019). The properties of the vessel are presented in Table 2. Compared to the work of Zhao, the only modification that has been made is that the water depth is changed from 39.1m to 20m to represent the shallower conditions of the site. As previously discussed, the water depth in the actual area in Port Talbot lies at around 11m, but to have a running model with the floater model of 15.5m draft, the modelled water depth is 20m.

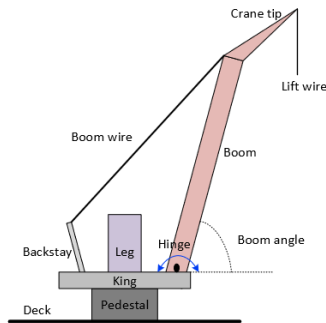
Parameters	Unit	Values
Hull length, breadth, depth	[m]	132, 39, 9
Displacement during transportation	[m ³]	2.20×10^4
Total elevated load	[t]	1.69×10^4
Leg length and diameter	[m]	92.4, 4.5
Long. and trans. leg spacing	[m]	68.3, 30.6
Airgap	[m]	7.2
Leg below hull	[m]	29.9
Soil type		Dense sand
K_x, K_y, K_z	[kN/m]	$1.35 \times 10^6, 1.35 \times 10^6, 1.47 \times 10^6$
K_ϕ, K_θ, K_ψ	[kNm/deg]	$6.4 \times 10^5, 6.4 \times 10^5, 8.3 \times 10^5$

Table 2: Main parameters of the jack-up vessel, soil values representing the equivalent linear spring stiffness (Zhao, 2019, p.23; Fred. Olsen Windcarrier, 2023b)

There is no detailed information on the soil on site. Thus, the given properties are kept. Nevertheless, the assumption of dense sands matches the previously mentioned geotechnical study in

the Swansea Bay, which found a mix of different sands in the area (Thethys, 2022). Thus, this assumption is deemed sufficient. Based on the soil conditions, the penetration depth of the jack-up legs can drastically change, in this case, it is assumed to be 2.7m.

The vessel is equipped with a leg-encircling crane, as seen in Figure 33. In 2022, the Bold Tern vessel got an upgrade to a 1600t crane, making it suitable for installing wind turbines from 10MW to 15MW. Previously, the vessel could only install turbines up to 8MW like its sister ship Blue Tern, which hasn't gotten the upgrade yet (Fred. Olsen Windcarrier, 2023a). As the vessel should be suitable for integrating the 12MW wind turbine, the upgraded crane is assumed. The parameters of the new crane in Table 3 are not published, but they are estimated based on pictures and previous work by Zhao (Zhao, 2019, p.23). To coincide with Bold Terns' new crane design, in contrast to Figure 33, it is now assumed that the main hook of the crane is very close to the upper end of the main boom instead of the tip of an inclined top section as the figure suggests (Dalley, 2023).



Parameters	Unit	Values
Boom length	[m]	128.2
Crane boom angle	[deg]	70
No. of equivalent boom wires	[-]	2
Equivalent boom wire stiffness	[kN/m]	8560.9
Equivalent boom wire damping	[kNs/m]	90.5

Table 3: Main parameters of the modified crane (Zhao, 2019, p.23)

Figure 33: Illustration of a leg-encircling crane (Zhao, 2019, p.22)

4.3.2 Wind turbine blade

The wind turbine blade which will be installed is the 12MW wind turbine blade, which Silva de Souza et al. had developed by upscaling the DTU 10MW blade (Silva de Souza et al., 2021). The blade should be installed at a hub height of 131.7m and is assumed to be straight and rigid. The blade mass was given from the airfoil data and the blade centre of gravity (COG) is calculated to be 22.6m from the blade root along the blade span.

In the model of Zhao, the 10MW blade and the yoke had a combined mass of 88.6t, with the DTU 10MW blade having a weight of 44t, which meant the yoke weights 44.6t. For the increased blade of the 12MW turbine, the properties which are not given in the report of the 12MW wind turbine are upscaled using the scaling procedure with the scaling factor s and the scaling rules presented in Table 4:

$$s = \sqrt{12/10} \approx 1.095 \quad (10)$$

Property	Scaling rule
Power	s^2
Mass	s^3
Length	s^1
First mass moment of inertia	s^4
Second mass moment of inertia	s^5
Axial stiffness	s^2
Bending stiffness	s^4

Table 4: Rotor scaling procedure with scaling factor s (Sieros et al., 2012; Bak et al., 2013, p.11)

The yoke holds the blade around its centre of gravity and is lifted by four slings connected to the crane's main hook. Furthermore, the yoke is connected to the crane by two horizontal tugger lines, which are pre-tensioned to prevent the lines from being slack (Zhao, 2019, p.21). An illustration of the blade system, where the leading edge is aligned horizontally, can be seen in Figure 34 while Table 5 presents the properties of the upscaled lifting system. The dimensions of the yoke system in Figure 34 are assumed to remain the same for both the 10MW and 12MW blade, while only the mass is upscaled.

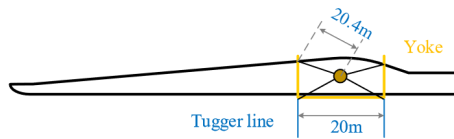


Figure 34: Illustration of the yoke system (Zhao, 2019, p.22)

Parameters	Unit	Values
Yoke mass	[t]	58.7
Blade mass	[t]	63
Total mass	[t]	121.7
Blade length	[m]	105.4
Blade COG	[m]	22.6
Installation height	[m]	131.7
Tugger line arm length	[m]	10

Table 5: Main parameters of the upscaled blade lifting system (Silva de Souza et al., 2021, p.16)

The blade root diameter of the 12MW blade is 5.04m. As the pins and guide pins are always positioned at the outside of the blade root, the guide pin and flange hole is thought to be 2.4m away from the centre of the blade root.

4.3.3 Floating wind turbine

The considered floating wind turbine is the INO Windmoor 12MW, developed by Technip and implemented in a numerical model in a research project of SINTEF. The floater is a three-column steel semi-submersible whose properties can be seen in Table 6 and Table 7.

Parameters	Unit	Values
Column diameter	[m]	15
Column height	[m]	31.0
Pontoon width	[t]	10.0
Pontoon height	[m]	4.0
Center-center distance	[m]	61
Total substructure mass	[t]	11974
Total substructure COG _x	[m]	-5.91
Total substructure COG _z	[m]	-9.7

Table 6: Main parameters of the floater (Silva de Souza et al., 2021, p.10)

Parameters	Unit	Values
Draft	[m]	15.5
Displacement	[t]	14176.1
Hub height	[m]	131.7
Tower length	[m]	110.2
Nacelle dimensions	[m]	6x12x6
Tower weight	[t]	1165
Nacelle weight	[t]	600

Table 7: Main parameters of the assembled FOWT (Silva de Souza et al., 2021, p.10)

The hydrodynamic coefficients of the substructure were also obtained in the work of SINTEF, where a diffraction-radiation analysis of the floater has been done in WAMIT (Silva de Souza et al., 2021, p.12). This analysis obtained the added mass terms, wave radiation damping, wave force, and drift force coefficients for the numerical model. If the draft of the floater changed due to reduced ballasting during the integration phase and to cope with the site’s local water depth, this diffraction-radiation analysis would need to be repeated. This would exceed the scope of this thesis, and thus, the draft is kept at 15.5m, despite the previously discussed limitations of this assumption.

When modelling the single blade installation, it is assumed that the integration of the first wind turbine blade is investigated. This means that all wind turbine blades are removed from the model while the tower and nacelle are kept as they need to be integrated beforehand. The dynamics of the floating wind turbine are likely to change depending on how many blades are already installed, as those blades mean an increased weight with a large lever arm and an increased area susceptible to wind loads, despite not operating. The change of dynamics with the number of installed blades is worth investigating but exceeds the scope of this thesis. During the modelling, it was noted that the floating wind turbine without blades has a fairly high mean roll and pitch displacement of 1.5° and 1.9° , which leads to unfavourable mean displacements of the hub, given the high hub height. It was found that those rotational motions can be alleviated once a ballast is applied to the turbine column, which is equivalent to the weight of the removed wind turbine blades. In a real application, this displacement should also be possible to handle either with the ballasting system of the floater or external ballast as the added ballast of 185t is equivalent to 188m^3 water, which is around 3.4% of the volume of one floater column.

4.3.4 Moorings

The moorings for the installation are set up as a high tension, high stiffness mooring system where two of the mooring lines are connected to piled bollards above sea level and one connected to a tug boat as it can be seen in Figure 28. One factor which significantly impacts the mooring system’s response is the direction of the mooring lines. During the modelling process, it was found that an asymmetric mooring setup quickly can lead to the exceedance of the maximum loads for one of the mooring lines and has a significant impact on the system’s dynamic response. Figure 35 displays some decay tests of the floater with different mooring line directions, shown in Figure 36, where 120° is the case with the highest symmetry in all directions. Only then angles of the left

and top mooring line are varied (line 2 and 3) as the floater is assumed to be towed in position like in Figure 28. Figure 35 shows clearly that the line direction of line 2 and 3 especially impacts the system's surge, sway and yaw responses, while heave, roll and pitch are not affected by it. The spectral density distribution of surge and sway shows that the peak period changes with an increasing mooring angle and the intensity of the response changes dramatically. The 150° setup has much higher energy at its natural period for the surge PSD than the 140° setup, even though their natural period is fairly similar, meaning that there are also higher loads on the mooring lines. Therefore, the 120° mooring setup has been chosen.

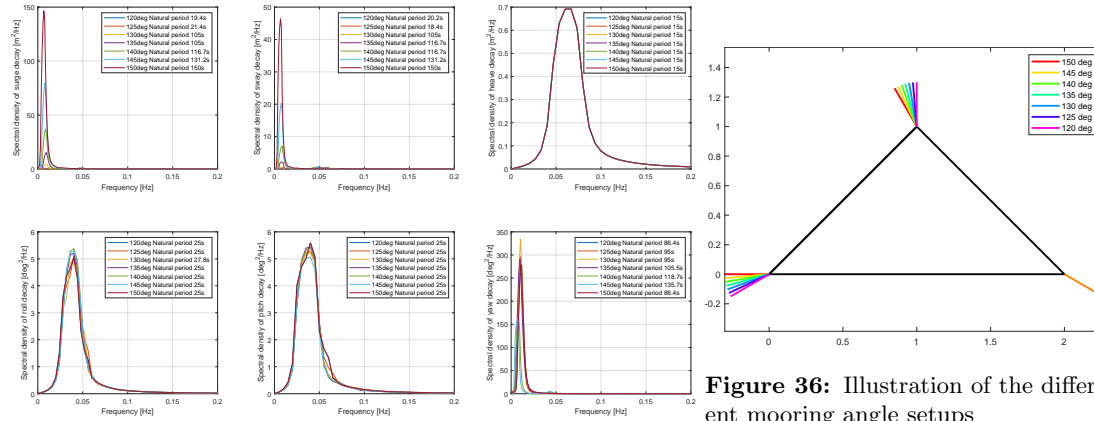


Figure 35: Results of decay tests for different mooring setups

The moorings are designed to be out of fibre rope as neither chain nor steel wire can realize the chosen mooring setup. The moorings need to be very stiff to ensure minimal displacement of the floater and especially the hub. Therefore, HMPE (High-modulus polyethylene) was chosen because other fibre ropes like Nylon won't be able to provide the needed stiffness. Multiple simulations have been done to find the suiting rope thickness for this scenario based on the MAGNARO[®] datasheet published by the Singaporean rope manufacturer TEHO (TEHO, 2023). Ropes with smaller diameters were found to not sufficiently reduce the floater motions, while large-diameter moorings were found to have a too-high stiffness which led to an exceedance of the maximum allowable tension in the line during several load cases. Therefore, ultimately HMPE rope with a 48mm thickness has been chosen for the mooring lines as the displacements are small enough without exceeding the maximum tensions. The properties of the mooring line are presented in Table 8. The line length has been set to a reasonable length based on other SIMA models with a somewhat similar setup. However, for a detailed model, further investigations would need to be taken to find the optimal ratio of minimal displacements and minimal line length to reduce the cost of the system.

Figure 36: Illustration of the different mooring angle setups

Parameters	Unit	Values
Diameter	[mm]	48
Weight	[kg/100m]	121
MBL (Unspliced)	[t]	179
MBL (Unspliced)	[kN]	1756
Pretension (15% MBL)	[kN]	263
Max tension (2×MBL)	[kN]	3512
Weight in air	[N/m]	11.87
E Modulus	[GPa]	132
Length	[m]	118

Table 8: Main parameters of mooring line (TEHO, 2023; Amaral Jr & Moravia, 2020, p.33)

A measurement that could help reduce the peak loads within the stiff mooring line might be a load reduction device (Strivens et al., 2021, p.55). However, implementing this device in the model would complicate it significantly and thus is not considered in this work but could be included in future research.

The moorings are considered to be connected to bollards, where the mooring connection point/anchor for each mooring is considered 3m above above MSL while the floater connection point is 6m above MSL. This anchor height allows easy access to the mooring lines, which are also buoyant and thus are favourable from an operational point of view. Nevertheless, the mooring hook-up operation is still expected to be fairly time-consuming as pre-tensioning the high-stiffness moorings is complicated. An advantage of installing the bollards for the temporary mooring setup for the installation is that they could also be utilised later on. Once the port is further developed as a floating wind hub for larger-scale projects, they could be used with a simpler mooring line setup for the temporary storage of already assembled floaters, which are stored until the integration of the wind turbine takes place.

Within the model and during the simulations, a constant water depth of 20m is assumed for the site. However, as mentioned in chapter 3.2, the tidal range within the Celtic Sea and also Port Talbot is very high. Figure 37 shows a one-year time series of the hourly mean sea level in Port Talbot, which was extrapolated based on low tide and high tide data from a location right next to the port with the MSL of 5.46m, which was then adjusted to the assumed water depth within the port of 11m (TideTimes, 2023). As seen, the tides can range from as low as 6m up to 16m, which significantly impacts the mooring system. As the connection point of the bollard must be fixed, the mooring lines would need to allow significant vertical displacements of the floater as the integration procedure of the entire turbine takes longer than one tidal cycle. Furthermore, the connection point to the bollard would be submerged during some high tides, significantly changing the properties of the system. Those factors would make it extremely challenging to implement the assumed high stiffness, high tension mooring system to the extent that it is unlikely to be implemented in this scenario as it would be deemed not technically feasible. As discussed in chapter 3.3.4, other mooring configurations like catenary moorings or taut moorings are also very unlikely to be implemented and would struggle to cope with the high tidal range. Therefore, an optimal station keeping system would be one where the floater is lowered onto the seabed, which was previously

prepared to be flat, where then the floater is ballasted and anchored so that it stays in place no matter the tidal range. This would largely benefit the integration procedure as the floater and the hub would stay in one location without any larger displacements, essentially like a bottom-fixed wind turbine. However, the floater would need to be designed to carry its own weight under all conditions. Even though this mooring setup is promising for this site, it would essentially undermine the research goal of this thesis, where the performance of a jack-up vessel for the integration of a floating wind turbine should be investigated as this system lacks the floating characteristics. Therefore, the assumption of the high tension, high stiffness, horizontal mooring system is kept as it might be applicable for other sites with large tidal range. The exact impacts of the tides on the mooring system can't be evaluated as the modelling software is not capable of including tides into the time-domain simulations.

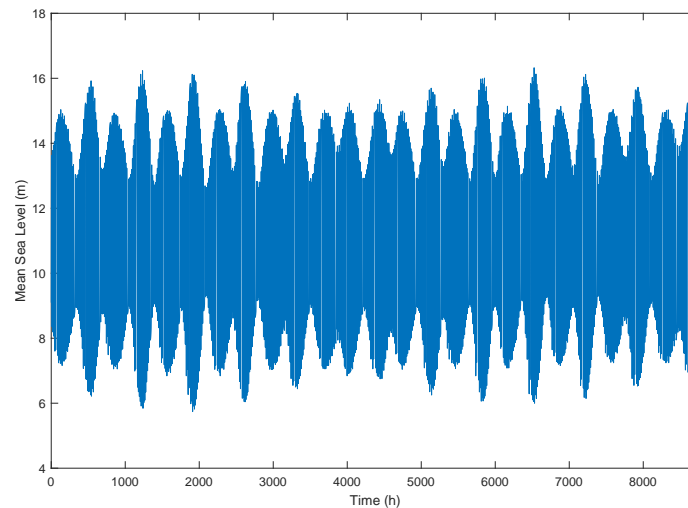


Figure 37: Hourly time series of the extrapolated MSL on site in 2015, data extrapolated from tidetimes.co.uk

4.4 Applying the integration criteria

In this integration system, the blade root radius is assumed to be 2.52m, while the hub is slightly wider at 2.54m. Applying those numbers to the alignment criteria, which has been defined in chapter 4.2.4, results in the safe boundary for the maximum distance in the xz -plane in $R_{sb1} = R_b + R_h = 5.06m$. The alignment procedure is deemed unsuccessful if this safe boundary is exceeded during the alignment phase by defined outcrossing criteria. This outcrossing criterion for the alignment phase is assessed based on the critical motion radius in the xz -plane η_{cr1} , which is defined as the motion radius that is being exceeded at the critical outcrossing rate ν_{cr1} . Based on the work from Jiang, ν_{cr1} has been defined for the alignment as one outcrossing per three minutes, which is equivalent to $\nu_{cr1} = 5.5 \times 10^{-3}$ (Jiang et al., 2018a, p.8). This means that if the frequency of the motions getting as big as 3m were once every three minutes, the critical motion radius would be $\eta_{cr1} = 3m$.

For the mating procedure, the safe boundary has been defined as $R_{sb2} = R_{fh} - R_p$ with R_{fh}

as the radius of the flange hole and R_p as the guide pin diameter. In the model, the pins of the blade are assumed to have an M42 thread size: This assumption is based on a work on blade root connections for an 84m long blade, so roughly for a 10MW turbine (Ha, 2020, p.2). The guide pin can be slightly smaller than the bolted pin, as it will be replaced after a successful mating. Therefore, the guide pin radius is estimated at $R_p = 20mm$. According to EN 20273:1991, the through hole diameter for an M42 screw would be 43 to 48mm (CEN, 1991). Assuming the maximum diameter for the flange hole for an easier mating connection results in a mating safe boundary of $R_{sb2} = 4mm$. The critical outcrossing rate of the relative guide pin-flange motion during mating is one per minute, which can be also expressed $\nu_{cr2} = 1.67 \times 10^{-2} Hz$ (Jiang et al., 2018a, p.12). Based on this critical outcrossing rate, the critical motion radius η_{cr2} is determined and if $\eta_{cr2} \leq R_{sb2}$, the mating process is deemed as successful.

As mentioned in chapter 4.2.4, the motions of the system must be restricted in some way during the mating phase to have a critical motion radius below 4mm. Therefore, in this work it is assumed that an unknown control mechanism can control all low-frequency components of both motions below 0.5Hz (Jiang et al., 2018a, p.3). Thus, in the post-processing, a highpass filter is applied to the guide pin and flange motions. It is very questionable if a real controller would be capable of controlling the motions to this extent, especially given that most of the system's motions are governed by motions below 0.3Hz. Nevertheless, this type of controller is still being applied as it represents in some way a best-case scenario, where actual solutions are expected to filter out only a smaller amount of motions. To better understand the controller's effects, a filter rate of 0.3Hz will also be tested. Some other control mechanisms which could be applied for the mating are less technical from a control perspective but would involve workers pulling in the blade with the use of ropes, if the local safety standards allow is operation. This manual pull in would increase the safe boundary of the mating operation.

4.5 Numerical model

A response analysis of the described system is done to determine its operational limits. Therefore, the system is implemented in SIMA, an advanced numerical simulation toolbox developed by SINTEF to analyse complex multi-body systems. SIMA combines several toolboxes, such as SIMO, used to simulate motions of bodies and RIFLEX, which can analyse slender structures. The complete implemented numerical model in SIMA can be seen in Figure 38, while the practical implementation of the different system components and the load scenarios will now be further discussed.

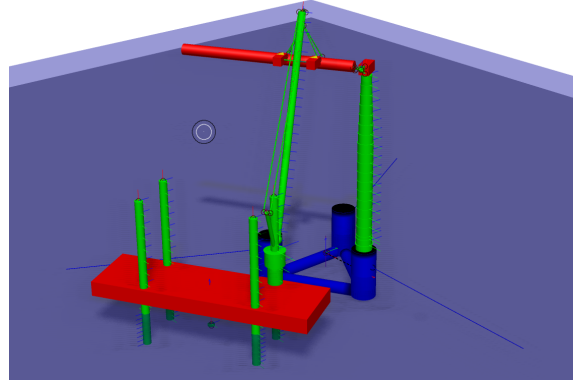


Figure 38: Numerical SIMA model of the integration system, red and blue elements are SIMO elements and green elements are modelled in RIFLEX

4.5.1 Jack-up vessel

The SIMA model of the jack-up vessel, including the crane and the blade, is mainly based on the work made by Zhao (Zhao et al., 2018), while modifications have only been made to the model as it was described in the previous chapters.

The jack-up hull is modelled as a rigid body, while the legs are beams to also account for their flexibility and their connection point is assumed to be rigid as the jacking mechanism of modern jack-up vessels is very stiff (Zhao et al., 2018, p.355). The motions of the jack-up vessel are mainly caused by wave loads acting on the leg, the structural flexibility of the leg, and the rigidity of the soil. As the ratio between the leg diameter and the wavelength is less than 1/5, the Morison equation for fixed structures in waves shown in equation 11 can be used to calculate the wave force on each section of the submerged leg. ρ represents the density of water, A the cross-sectional area of the leg, D the diameter of the leg, u the water particle velocity, C_D the non-dimensional drag coefficient and C_A the non-dimensional added mass coefficient. The wave force from the seabed to the surface is then integrated using the strip theory to calculate the total force on the leg.

$$f_N(t) = \rho(1 + C_A)A\dot{u} + \frac{1}{2}\rho C_D D u |u| \quad (11)$$

To account for the soil-structure interaction, linear elastic springs, combined with dampers, are assumed to act on the spudcans, which are modelled as a point mass at the end of each leg. This simplified model is feasible if the significant wave height H_s stays below 2.5-3m. Given the environmental conditions in Figure 21 this limit is not exceeded 99.6% of the time and thus the assumption is acceptable. Only in scenarios with higher H_s the loads acting on the spudcans are much lower than the required ones to reach the soil yield surface. The linear springs are set up in 6 degrees of freedom, where the values are presented in Table 2. The corresponding soil reaction force can then be expressed as a function of the spudcan displacement.

For the crane, the assumption is made that the crane deformation is mainly due to the boom and the wires. The crane boom is modelled with beam elements, with the lower end being hinged

onto the crane base while the crane wires are modelled as bars. The bending of the crane has some notable contribution to the blade position within the model. Therefore, the blade starting position is 1.4m above the hub height so that the blade root and hub are aligned during the installation.

The lift wires connected to the blade from the crane tip are modelled as bar elements with equivalent stiffness, as they are permanently tensioned due to the weight of the blade. The tugger lines are connected between a trolley on the crane boom and the yoke, where they are modelled as bi-linear springs as they are non-compressive, meaning they can't provide stiffness if the blade is pushed towards the crane. Furthermore, they are set under pretension to avoid slack lines (Zhao, 2019, p.22). The slender structures like the crane boom and the jack-up legs also account for structural damping, which is implemented in the model using the Rayleigh damping model.

4.5.2 Wind turbine blade

The yoke and the blade are modelled combined as one rigid body. This is sufficient as the structural flexibility of the blade only has a minor contribution to the blade's rigid body motions during installation. To account for the aerodynamic forces and moments which are acting on the blade, Zhao has implemented an aero code in SIMA, whose interaction with the system can be seen in Figure 39 (Zhao, 2019, p.27). The code is based on the cross-flow principle and should also account for the effects of wind shear, turbulence and dynamic stall. The cross-flow principle calculates aerodynamic forces on a wind turbine blade, given that the local blade element can be approximated in 2D. The inflow velocity in this principle is always normal to the cross-section, while the inflow in the y direction is neglected. Furthermore, the wake-induced velocities are also neglected, as the blade motions are very small during the installation compared to the operational state. The blade's changing lift and drag coefficients are in the Aero code calculated using the Beddoes-Leishmanns dynamic stall model, which was initially established for helicopters but can also be used for wind turbine blades. According to the Kaimal turbulence model, the incoming wind is calculated with TurbSim as a three-dimensional turbulent wind field.

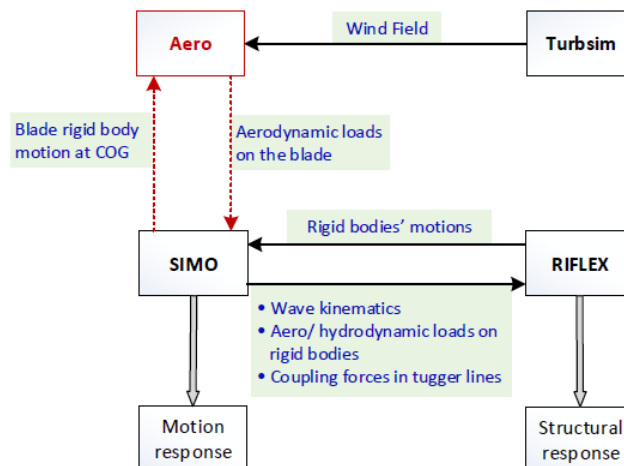


Figure 39: Coupled simulation method for blade loads (Zhao, 2019, p.27)

The Aero code also accounts for wind loads on the area above the hull baseline. However, as the complexity of all the equipment on the vessel's deck would require a detailed analysis for getting the coefficients of the vessel, the wind loads are simply assumed as a block with equivalent area. This is also sufficient as the motions of the jack-up vessel are mainly wave induced. Furthermore, the code is also calculating the wind loads on the tower.

A complete description of how Zhao structurally models the different component of the jack-up vessel, including the blade, in SIMA can also be seen in Figure 40.

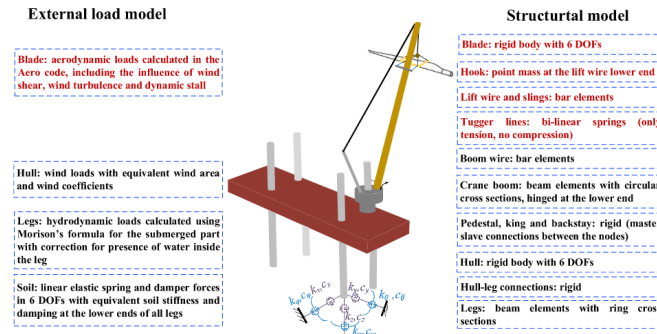


Figure 40: Overview of the structural model of the jack-up crane vessel (Zhao et al., 2018, p.354)

4.5.3 Floating wind turbine

The SIMA model has been developed by SINTEF in the INO Windmoor research project (Silva de Souza et al., 2021, p.26). The floater is modelled in SIMO as a rigid body, coupled to a flexible tower modelled in RIFLEX, while the nacelle is a rigid body in SIMO. In the simulation, the platform is then subject to the wave loads and the loads coming from the finite element structures in RIFLEX.

The second-order wave loads in q_{2nd} are accounted for by having the drift coefficients from the calculation in WAMIT and using Newman's approximation. The tower is modelled in RIFLEX with 20 steel tower sections as beam elements with decreasing diameters. The floater is positioned within the SIMA model so that the hub connection point is in the y-direction 1m away from the blade root (according to Figure 32) in the model to simulate the alignment phase. The results from the same distance in the y-direction are also used to evaluate the mating phase, as the connection in the y-direction has already happened and is less relevant, while only the motion in the xz-plane is of interest.

4.5.4 Moorings

As the mooring lines are not submerged at any point in the model but only are supposed to be taut above the waterline, they are not modelled as separate RIFLEX elements but as a catenary system within the SIMO body of the floater. Each line is segmented into 40 elements to describe the line behaviour sufficiently. Those methods are a large simplification of the system. If it should be modelled in detail, modelling the moorings in RIFLEX is advisable, but as this is not the focus of this work, the catenary system is deemed sufficient.

4.5.5 Load cases

The goal of the study is to understand the limiting responses of the single installation when using a jack-up vessel to install a floating wind turbine in the port of Port Talbot. Therefore, different load cases are defined based on the given hindcast data for the location examined in chapter 3.2. All examined load cases are summarized in Table 10. U_w describes the mean wind speed at the reference hub height of 131.7m, where wind speeds from 6m/s up to 14m/s were investigated as 14m/s is regarded as the maximum upper limit for the blade installation (Jiang et al., 2018b, p.1045). The turbulence of the wind speed is set to the IEC turbulence class C for lower turbulence cases (TI=0.12), the impact of this decision will be further discussed in chapter 5.2. For each wind speed, three cases were defined. While the load cases for the operational state of the offshore wind turbine are widely adapted (Natarajan et al., 2016), there is very little literature which can be used as a reference for installing offshore wind turbines, let alone floating wind turbines.

For the installation of bottom-fixed wind turbines, Jiang has defined load cases with different sea states. One has the highest probability of occurrence, one has the largest H_s and two are close to the first fore-aft frequency of the tower (Jiang et al., 2018a, p.7). The first fore-aft frequency is not applicable to floating wind turbines and also the highest H_s is not sensible when basing the load cases on 39 years of data, as this would result in very severe load cases. Instead, one mean load case, Case A, has been defined, which represents the mean significant wave height H_s and the mean wave period T_p at those five wind speeds, based on the hindcast data set from NORA3. To represent a more severe load case, which is still statistically likely, Case B is a scenario where H_s is 35% higher than the mean and T_p is the mean wave period at that H_s . By applying this method at least 52% up to 98% of all probable sea states are covered. However, this method is not efficiently calculating severe sea states, especially not for the smaller wind speeds as the percentage increase in wind speed only lead to slightly absolute increase in H_s (compare LC 1 and 2), while at higher H_s the absolute increase is much larger (compare LC 13 and 14). This insufficiency has only been noted late on into the thesis, where a redefinition of the load cases would require a complete recalculation of all numerical simulations. Therefore, those load cases are kept this way in this work. The goal of defining load cases is to have reference scenarios on which basis operational limits can be defined. Calculating those limits on the basis of only a few load cases always will lead to inaccurate results, therefore those statistically not well proven load cases are not assumed to largely worsen the outcomes of the study. If the operation fails at those less severe harsh sea states, this finding would actually be helpful as a properly harsh sea state would overestimate the operational limit. A methodically better proven severe H_s limit would be a limit that would always represent the upper 90% of the probable sea states at the corresponding wind speed.

To find an corresponding peak period to the increased Case B, the average of the subset of T_p 's at H_s 20% higher or lower the increased H_s is taken. This is also a very broad assumption, a range of 5% seems more sensible. Case C should investigate whether a large peak period or a large significant wave height has a larger impact on the system response. This load case has been also calculated with the insufficient methodology of Case B, now just increasing T_p by 35% and finding the corresponding mean H_s .

As it has been discussed, those simplified load cases won't be sufficient to determine the exact operational limits of a marine operation, as detailed operational investigations would test a lot larger set of combinations of H_s and T_p for every wind speed while also regarding the probability

of the sea state. The sea states with the highest probability for every wind speed can be seen in Table 9. In general, it can be said that those values are fairly close to the mean sea states of case A and, therefore, should be covered by those cases. A detailed investigation of all sea states with a higher probability would drastically increase the number of required simulations. If not all probable sea states should be investigated, it could be an alternative assess load cases based on 20%, 40%, 60% and 80% of probable sea states per wind speed. Another interesting load case would be to investigate a T_p close to the natural periods of the floater if those are somewhat close the possible T_p values. However, given the limited scope of the thesis, it is deemed sufficient to use the limited number of methodically not well defined load cases in Table 10 to have a first estimate the operational limits of the single blade installation.

U_w [m/s]	H_s [m]	T_p [m]	Probability [%]
6	0.3	6.3	8.1
8	0.9	9	7.6
10	1.2	9	11.4
12	1.5	9	14.3
14	1.8	7.5	22.6

Table 9: Sea states with the highest probability for every wind speed

LC	Case	U_w [m/s]	H_s [m]	T_p [m]	β_{wind} [deg]
1	A	6	0.529	8.669	0, 90, -140
2	B	6	0.7	7.436	0, 90, -140
3	C	6	0.569	11.7	0, 90, -140
4	A	8	0.793	7.545	0, 90, -140
5	B	8	1.1	8.862	0, 90, -140
6	C	8	1.018	10.2	0, 90, -140
7	A	10	1.187	7.863	0, 90, -140
8	B	10	1.6	9.136	0, 90, -140
9	C	10	1.411	10.6	0, 90, -140
10	A	12	1.602	8.597	0, 90, -140
11	B	12	2.2	10.041	0, 90, -140
12	C	12	1.939	11.6	0, 90, -140
13	A	14	2.028	9.117	0, 90, -140
14	B	14	2.7	10.313	0, 90, -140
15	C	14	2.290	12.3	0, 90, -140

Table 10: Examined load cases, Case A: Mean H_s & T_p , Case B: +35% H_s , Case C: +35% T_p

As seen in Figure 22, the waves are approaching the location very unidirectional, so the integration system also aligns with this direction. However, as Figure 23 has shown, the wind can come from several directions. Therefore, it is also investigated how much the wind-wave misalignment β_{wind} has an impact on the installation procedure, which is done with the misalignment angles of 90° and -140° as those represent misalignment scenarios with higher probability, based on Figure 23. The

different heading angles regarding the system are described in Figure 41. All cases are run with a constant current speed of 0.3m/s, according to (Collins et al., 1979, p.53).

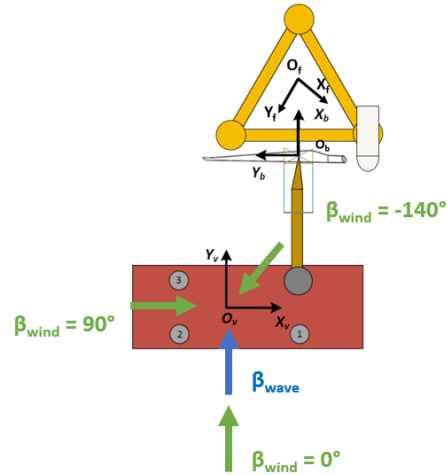


Figure 41: Investigated wind and wave heading angles

4.5.6 Time-domain simulations

With the given load cases, steady-state time-domain simulations are now carried out to study the dynamic responses of the blade integration system during mating. Therefore for each case, six 30-minute simulations were conducted, with each having a random wave seed and a random TurbSim wind field to reduce the statistical uncertainty. The waves are simulated as long-crested irregular waves based on the JONSWAP spectrum. Each simulation lasted 2400s with the start-up transient of 600s discarded during the post-processing. Given the 15 load cases with three alignment angles and six simulations for each case, this totals 270 carried-out simulations in SIMA.

5 Simulation results

All load cases have been simulated in SIMA, which gave the time series of the rigid body motions and the investigated body points as a result of the response analysis. This chapter will present the results of those simulations and investigate them to understand the governing motion characteristics of the individual components and the whole system. Furthermore, the simulation outcomes will be assessed to determine the critical motions of the components and the total system and if those exceed the integration criteria defined in chapter 4.4.

5.1 Blade motion

The results should be investigated to ultimately determine the success or failure of the alignment and mating procedure. For this purpose, mainly the motions of the blade root are investigated. However, those are directly linked to the motions of the entire blade. Thus it is worth assessing these at first. For this purpose, decay tests of the blade were conducted, which results can be seen in Figure 87 and Figure 88 in Appendix F. Those decay tests have shown that the tugger lines are very effective at reducing the surge and pitch motions of the blade, while the heave decay motion is minimal due to the weight of the yoke-blade-system. However, it can also be seen that the crane system cannot restrict the sway, roll and yaw motions. The natural period in both sway and roll is 17s and in yaw it is 80.3s.

To better understand the motion characteristics of the blade, it is worth looking at the spectral density functions (PSD) of the blade during load case 14 ($\beta_{wind} = 0^\circ$), as this is among the roughest load cases investigated in this study. The PSDs are displayed in Figure 42. As the surge and yaw functions show their peaks at very small frequencies which coincide with the frequencies of the wind loads, it can be concluded that the wind loads dominate those motions.

When Zhao did an eigenvalue analysis of the blade with a fixed crane tip, she found that the most dominant response was the in-phase pendulum motion of the blade around the hook, which is equivalent to the blade roll motion (Zhao et al., 2018, p.360). This can also be seen in the spectral density functions, where a significant amount of energy close to the natural period of the pendulum motion can be found both in surge and yaw. Furthermore, a small peak can be seen in the surge PSD around 0.225Hz or 4.4s. Based on the work of Zhao, this could be the dominant double pendulum motion of the blade and the hook when they are out of phase in the $Y_b Z_b$ plane (Zhao et al., 2018, p.360). The wind loading does not impact the sway motion of the blade and only shows a clear peak close to the natural period in sway/roll, which can also be related to the pendulum motion. Zhao found the yaw period to be the second highest dominant response, but in contrast to the conducted blade decay test, her yaw resonance period was only at 5.11s compared to the 80.3s of this model. Furthermore, in this model, the blade natural yaw period doesn't seem to impact the blade PSDs, where the blade yaw is also dominated purely by the wind loads and the dominant pendulum motion.

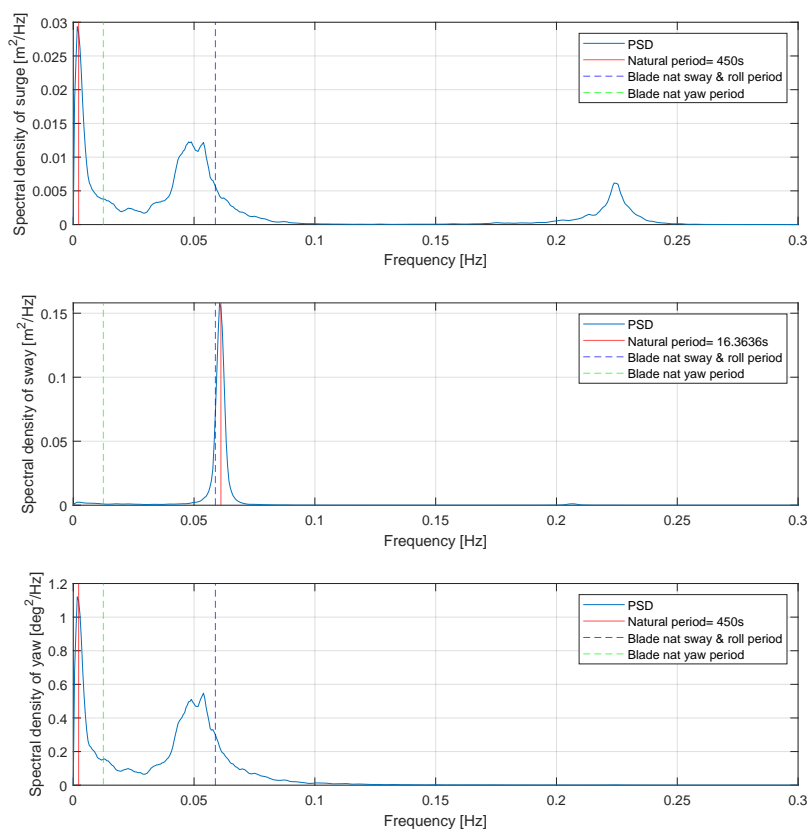


Figure 42: Spectral density functions of the blade motion for load case 14, $\beta_{wind} = 0^\circ$

5.1.1 Crane motion

As the blade is connected to the crane through the lift wires, the crane motions should be investigated to understand the impact of those motions on the blade motion. The crane is subject to the wind loads acting on the jack-up vessel and the wave loads acting on the jack-up legs. For the blade motions, the crane tip motions are of particular interest as this is the connection point of the lift wire.

The motions of the crane tip for LC 14 and the PSD of the relative motion in the xz-plane can be seen in Figure 89 and Figure 90 in Appendix G. It becomes clear that despite the very strong environmental loads, the crane tip displacements are only in the range of a few centimetres. The PSD of the relative crane tip motion shows that the crane motions are majorly influenced by the wind loads, where only the small peaks around 0.2Hz could be attributed to the waves. However, in general, the crane tip motions are very small.

5.2 Blade root motion

For the installation of the blade, the blade root motions in the xz-plane are of particular interest as they are the critical parameter for the alignment and mating procedure. In the spectral density

function of the blade root motion during LC 14, presented in Figure 43, it can be seen that, like the blade centre also, the blade root motions in the x-direction are dominated by the wind with another significant peak in the around the pendulum motion. The motion in the z-direction is only dominated by the blade pendulum motion. As the yaw motion of the blade is only governed by the wind and the pendulum motion in this case, the impact of the yaw on the blade root motion can't be determined in detail.

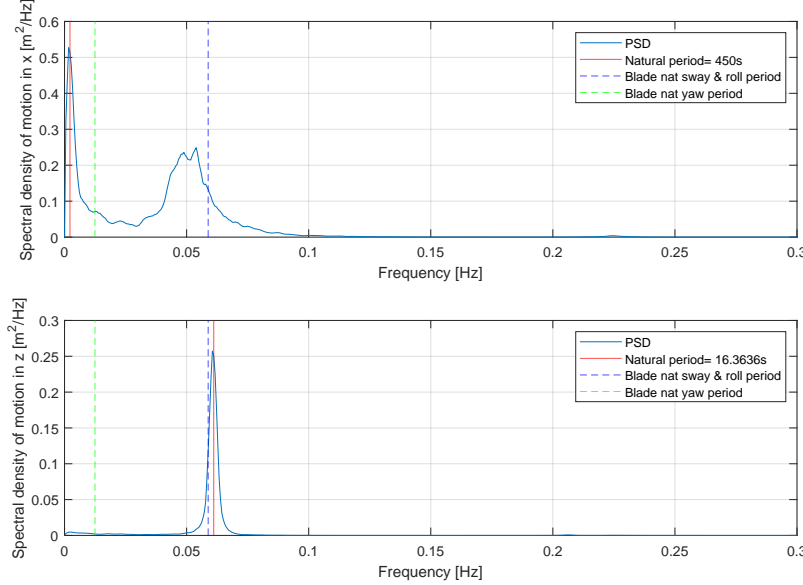


Figure 43: Spectral density functions of the blade root motion for load case 14, $\beta_{wind} = 0^\circ$

For an improved understanding of the blade motion, the motions in the xz-plane are combined to one motion radius defined as $\sqrt{x^2 + z^2}$. This radius can also be examined statistically, which is displayed in Table 11. The mean describes here the actual mean position of the blade root compared to the model's theoretical mean blade root position. As the blade root motion is only marginally impacted by the waves, the statistics are grouped per wind speed and without regarding wind misalignment. It can be seen that the blade root mean position is decreasing with increasing wind speed, which can be related to the increase of the mean yaw of the blade as it was -0.024° at LC 1 while increasing to -0.3° at LC 14. The maximum value and the standard deviation (std) both increase quadratically with increasing wind speed since the aerodynamic forcing of the blade is proportional to U_w^2 , which also the following equation indicates:

$$dF_y = \frac{1}{2} \rho U_w^2 c C_d dx \quad (12)$$

where ρ is the air density, c the chord and C_d the drag coefficient (Jiang et al., 2018a, p.8). The skewness indicates the symmetry of the underlying data, where values smaller than zero indicate a negative skewness. This means that most of the data is more distributed on the right side with a longer tail to the left. The kurtosis indicates how tailed the data is, where values around 3 indicate a normal distribution, values lower than 3 indicate thin tails and thicker tails have a kurtosis higher

than 3. Given the skewness and kurtosis values, it can be said that the blade root motions are non-Gaussian.

LC	U_w [m/s]	Mean [m]	Max [m]	Std [m]	Skewness	Kurtosis
1,2,3	6	1.08	0.06	0.03	-0.03	2.38
4,5,6	8	1.07	0.08	0.03	-0.11	2.72
7,8,9	10	1.05	0.13	0.05	-0.11	2.69
10,11,12	12	1.02	0.18	0.07	-0.29	3.17
13,14,15	14	0.94	0.28	0.12	-0.62	3.45

Table 11: Statistics of the blade root motion radius

Figure 44 gives an example of how the time series of the motion radius of the blade root can look like at LC 14. On the right side of the figure, the time series is also displayed as a displacement compared to the mean position to better understand the motion characteristics in the xz-plane, where the motions in the x-direction dominate. When looking at the corresponding spectral density function in Figure 45, it becomes very clear that the wind loads and the blade's pendulum motions dominate the blade's motions. The motions of the blade root in the y-direction are comparably low, where they have at LC14 an average std of 0.055m across all six simulations.

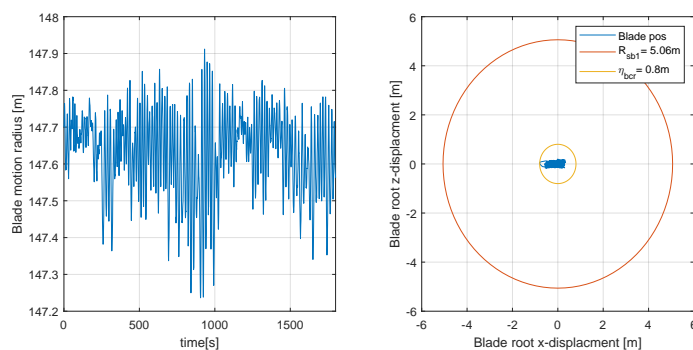


Figure 44: Time series of the blade root motion radius and tracking of the blade root centre compared to its mean position at LC14

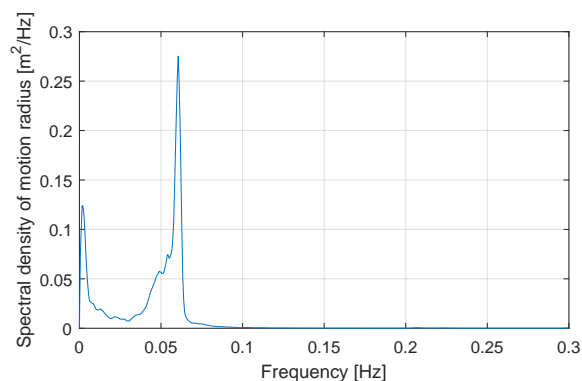


Figure 45: PSD of the motion radius of the blade root at LC14

The critical outcrossing rate of the blade root η_{bcr} can be determined based on the time series where the frequency of each motion radius is calculated and η_{bcr} is the motion radius that is the closest to the critical alignment outcrossing rate of one in three minutes ($= 5.5 \times 10^{-3}$ Hz). Figure 46 displays how the blade root's critical motion is determined based on the time series from Figure 44. It can be seen that the data for the motions at this outcrossing is already getting fairly sparse. If the critical outcrossing rate is even lower, it will become necessary to extrapolate the data with Monte Carlo methods to estimate the values better (Naess & Gaidai, 2008). However, for this work with the given outcrossing rate, the data is still deemed sufficient and thus, no extrapolation methods have been applied.

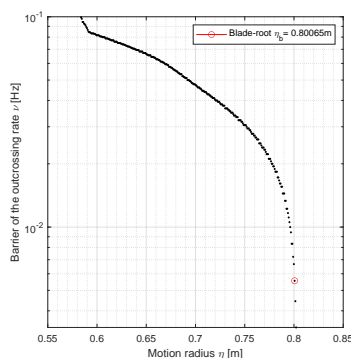


Figure 46: Determination of the critical motion of the blade root motion

To better understand the impact of the modelling assumption which have been made, it is valuable to assess the sensitivity of the critical blade root motions to some of them. For the turbulence, the IEC class C (TI=0.12) has been used as the flat, offshore environments generally have a lower turbulence intensity. However, the site is nearshore and sometimes the wind can also come from the land direction as Figure 23 showed. Therefore it is worth investigating the impact of different turbulence classes. The IEC classes A and B are for higher turbulence environments with TIs of 0.14 and 0.16 (Zhang, 2015, Appendix II). Figure 91 in Appendix H shows the critical motion radius of the blade when those different IEC classes are used at LC14 with the same seeds. It can

be seen that both turbulence intensities have more or less the same critical motion radius, which is around 32% higher than the default turbulence intensity of class C. This shows that the blade root motions are very sensitive to larger turbulence but is not scaling linearly with increased TI. For more sheltered locations like a fjord, this sensitivity has to be regarded, for the site of Port Talbot, the wind approaches the site more undisturbed and thus the turbulence class C is valued as sufficient. In the alignment phase, the blade motions are largely restricted by the tugger lines. The tugger line pretension could have a larger impact on the blade motion characteristics. Therefore, Figure 92 in Appendix H presents the critical blade root motions when the pretension is increased and decreased by 33%. A decrease in the pretension has found the critical blade motion to increase by 13.6%, while increasing the tension led to a decrease of the critical motion be 32.4%. Therefore, it can be concluded that an increased pretension of the tugger line can lead to a substantial reduction of the blade motions. The outcomes of those two minor sensitivity studies showed, that the careful selection of the systems parameter has a large impact on the outcomes of the study.

5.3 Floater

Compared to a bottom-fixed offshore wind turbine, the motions of the hub will be much more significant as the floater has an increased motion profile which governs the motions of the hub. Therefore, decay tests of the floater have been carried out to understand the motion profile of the floater better and, consequentially, the hub. The results can be seen in Figure 93 in Appendix I, where it is especially worth noting the differences to the SIMA model developed by Silva de Souza, which are displayed in Table 12. While the natural periods in heave, roll, pitch and yaw remained more or less the same, there was a drastic change in the surge and sway periods. This change is due to the different mooring system, which has very different characteristics than the catenary system with which the model was initially designed. When comparing the natural periods to the probable sea states in Figure 21, only a small share of all wave periods ($\approx 3\%$) could come in the range of the natural heave period and even less in the range of the surge and sway period.

	Surge	Sway	Heave	Roll	Pitch	Yaw
SINTEF	97.3s	98s	16.3s	29.5s	31.4s	88s
Decay tests	19.4s	20.2s	15s	25s	25s	86.4s

Table 12: Comparison of the natural periods from the SINTEF project and the conducted decay test (Silva de Souza et al., 2021, p.11)

The characteristics of the floater motions can be further investigated based on the spectral density functions in Figure 47. It can be seen that the surge, sway, roll and pitch motions have a very characteristic peak at the natural frequency of the respective motion. The incoming waves are modelled as an irregular wave spectrum, thus, in the PSDs, they are also seen as a broader spectrum. The best example of their impact is the heave PSD, where they are clearly governing the motion profile. Furthermore, the impact of the waves can be seen in the surge and the roll motion. The sway and surge are only governed by their natural frequencies, while a very wide spectrum of motions governs the yaw motion. It is assumed that this very unconventional motion spectrum is due to the high tension and stiffness mooring system.

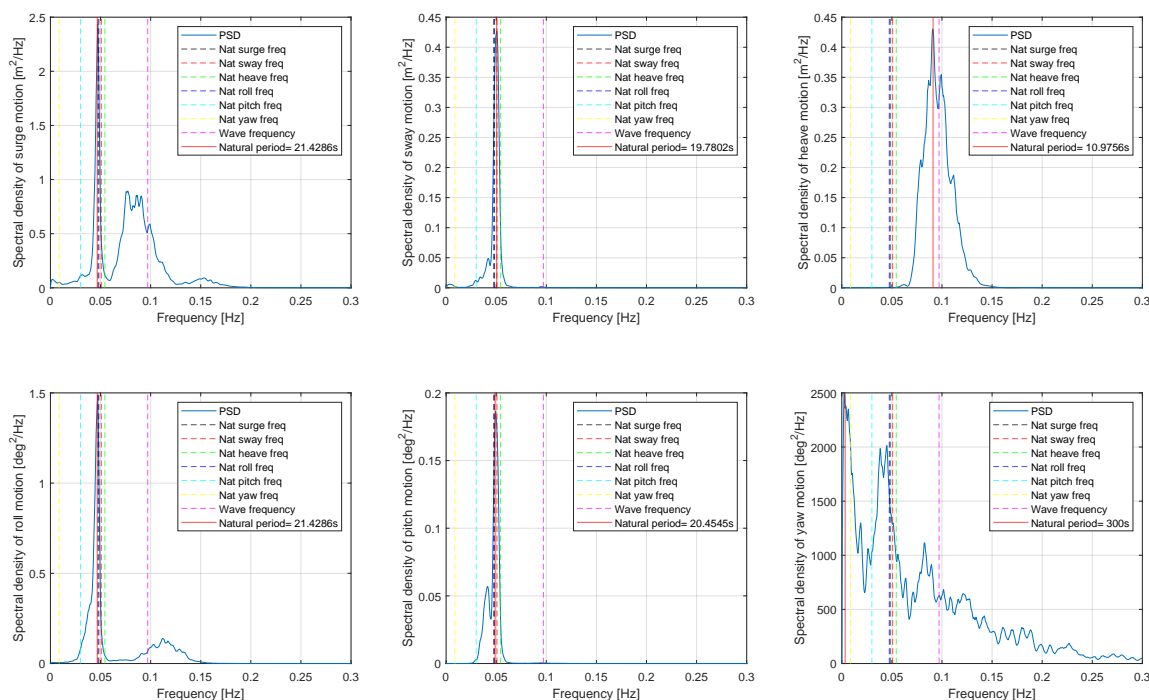


Figure 47: Spectral density functions of the floater motions at LC 14

5.3.1 Mooring forces

Regarding the floater motions, it is also of interest to evaluate the assumed high stiffness, high tension mooring systems' performance. Therefore, the statistics of the mooring line forces for the rougher Case B are presented for all five wind speeds in Figure 48. The figure presents the mean value, the standard deviation and the maximum value of each mooring line, where the average of the six simulations is taken. Line 1 is the mooring line connected to the column with the tower, line 2 is the mooring line of the rear column and line 3 is the line connected to the last remaining column.

When looking at the statistics, it becomes clear that none of the values exceeds the maximum allowable tension of $2 \times MBL = 3512kN$, introduced in Table 8. Generally, the system has a high symmetry as the mean and std values of lines 1 and 3 are basically identical, while the mean of line 2 is smaller and the std a bit higher. The main difference can only be seen when looking at the maximum values of each line. Here it becomes clear that, despite lower stds and means, the maximum mooring line forces in line 2 are larger than the other two lines across all load cases. Even though the mooring lines 1 and 3 are symmetrical, the maximum forces in line 1 are always slightly larger than in line 3. This could be related to the asymmetrical weight distribution of the floater with the turbine not being installed centrally. However, the ballasting system of the semi-submersible should counteract this asymmetry and the difference in the max values of lines 1 and 3 is only minor.

To better understand the phenomenon of the substantially larger maximum forces in line 2, the time series of the six simulations for load case 14 is displayed in Figure 94 in Appendix L. The

results show that the maximum excitation is largely on the wave seed. While in four of the six simulations, the maximum line forces are more in the range of the other line forces, a sudden peak can be observed only in the other two simulations. This means that the randomized wave seed induced resonance into this particular mooring line, which does not seem to occur in any other mooring lines. However, the maximum mooring force is still below the maximum tension limit. Based on those results, it can be concluded that the mooring system can be implemented. However, the mooring system also will need to sustain harsher conditions, where the operational limits are exceeded and the integration is halted for better weather windows. In those very harsh conditions, the mooring system would still need to sufficiently keep the turbine in place without breaking. Therefore, for an actual implementation, the performance should also be evaluated for extreme environmental conditions.

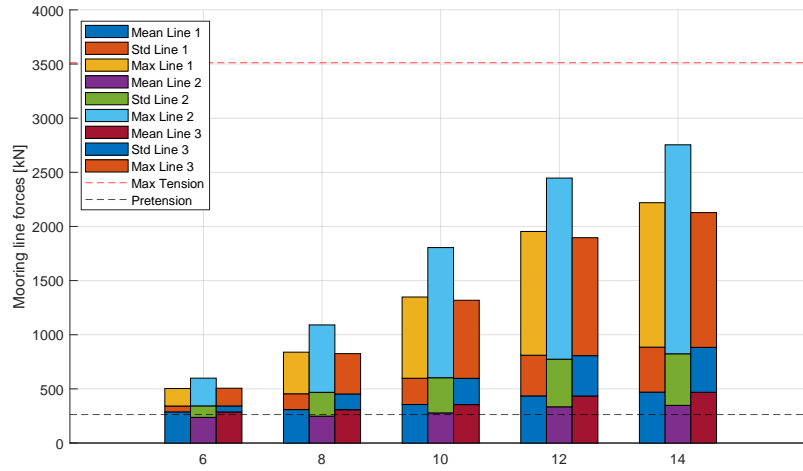


Figure 48: Statistics of the mooring forces

5.4 Hub

The movement of the hub is directly related to the wave-induced motions of the floater. The hub PSDs are displayed in Figure 49. Even though the hub motions are also impacted by the floater surge and sway motions, which are comparably small, they are mainly induced by the floater's rotational resonant motions in pitch and roll, as also very small angle rotational motions can lead to large displacements of the hub at 131.7m height. This can be seen in the figure, where the translational hub motions in x-direction are governed by the natural roll/surge period, while the motions in this direction are much larger (as seen by the higher energy) than the translational motions in y- and z-direction. In relation to the floater, the impact of the wave spectrum on the hub motions in x-direction is also relatively smaller. Also, the motions in the y-direction are very similar to the rotational motion of the floater, aside from the small peak at very low frequencies, which most likely is the impact from the wind loads onto the tower and nacelle. The hub motions in z-direction are still largely influenced by the waves. However, the roll and pitch motions of the floater also play an essential role in the hub's global z-position, which can be seen from the peak with the same natural period as the floater roll motion.

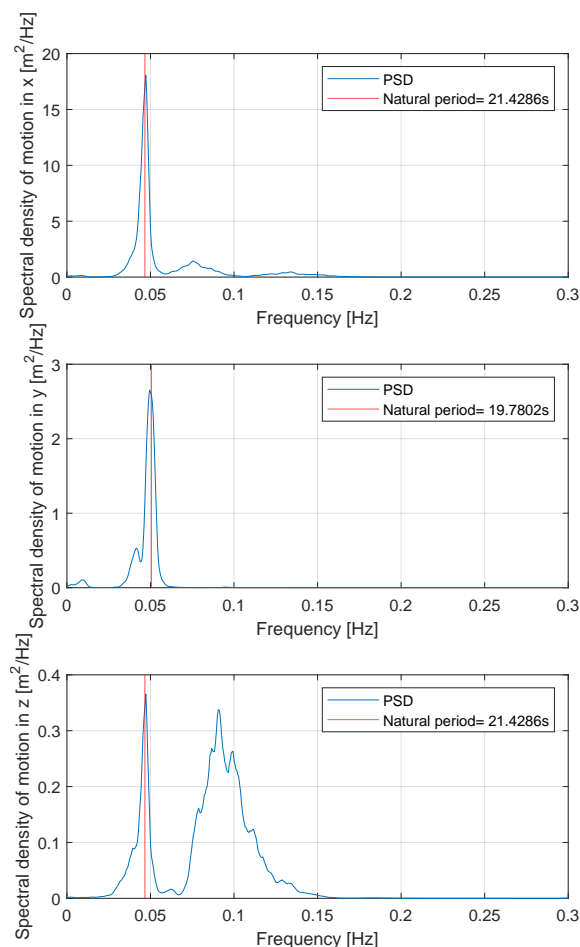


Figure 49: PSDs of the hub motions in x- and z-direction at LC14

When looking at the motion radius of the hub in the xz -plane, it is worth investigating at first the statistical characteristics of the motions. As the wave motions govern the motions, the statistics now have to be assessed for every load case separately, which is done in Table 21 in Appendix M. Generally, the mean, maximum and standard deviation increase with the increased wave height and wave period. In most of the load cases, Case C, with the increased wave period, has the highest statistical values, where especially the max and std are often more than double the values of Case A. The hub motions mainly have a positive skewness and a kurtosis higher than 3, showing that the motions are also non-Gaussian.

Figure 50 shows the time series of the hub motion in the xz -plane for one simulation at LC 14 and the tracking of the hub motions. It can be seen that the motion radius of the hub is significantly larger than the one of the blade root, while the motions in x -direction still dominate, but also, the z -motion got substantially bigger. Figure 51 presents the spectral density function of this motion. It can be seen that the characteristic peak of the rotational rigid body motions of the

floaters governs the motions of the hub with minor impact from the wave spectrum.

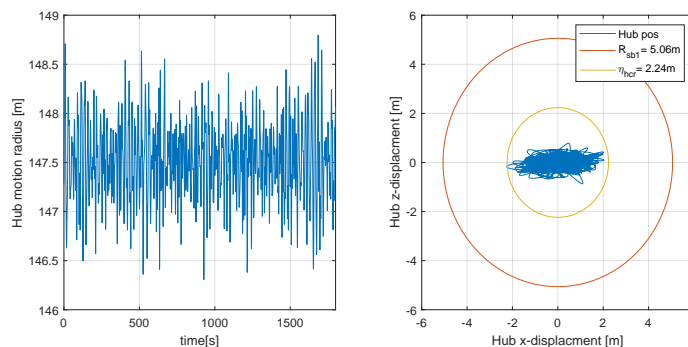


Figure 50: Time series of the hub motion radius and tracking of the hub centre compared to its mean position at LC14

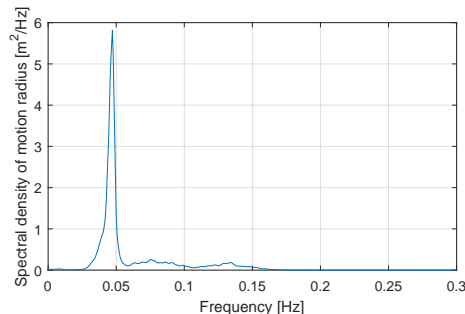


Figure 51: PSD of the motion radius of the hub at LC14

5.5 Relative motion

The relative motion between the blade root and the hub is the motion of highest interest for the single blade installation as it decides the success or failure of the single blade installation. Like the motion radius of the hub and the blade root, the relative motion between the two in the xz -plane is assessed for the rough load condition of load case 14 for one simulation with the initial focus on the alignment phase. Figure 52 shows the time series of the distance D between the hub and the blade root's centre. The displacements are fairly high and exceed the previous critical motion radius of the individual components, as seen on the right side of the figure. At the same time, the critical motion radius is still far below the safe boundary of R_{sb1} . The spectral density function of the relative motion at LC14 is presented in Figure 53. It becomes clear, that in contrast to the PSDs of the individual components in Figures 45 and 51, the wind and the wave forces now play a much more important role. The waves, which marginally had an impact on the hub, have now a much larger proportion of the motion profile and also the wind, which was only a small share of the motion profile of the blade root is now much more important. The characteristic peak of the floater rotational motions can be still seen while the peak due to the pendulum motions of the blade is not observable anymore.

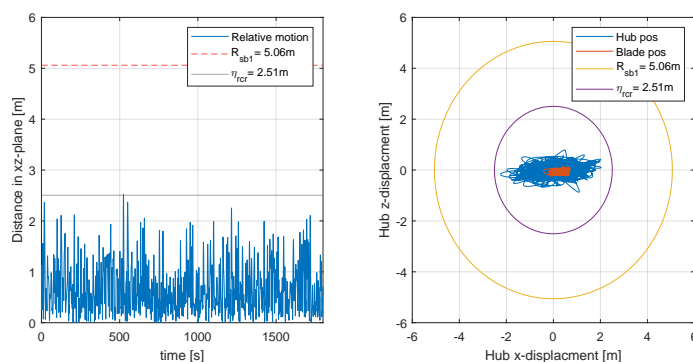


Figure 52: Time series and tracking of the relative motion between the hub and the blade root in the xz -plane at LC14

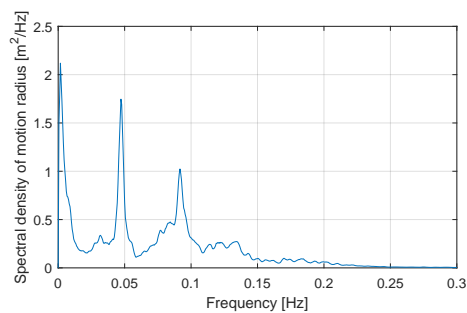


Figure 53: PSD of the relative motion in the xz -plane at LC14

For a better understanding of the impact of environmental loads on the system, Figures 95 to 97 in Appendix O are also displaying the PSD of the relative motion between the blade root and the hub when only wind loads, only wave loads and only currents are simulated in LC14 as environmental loads. It can be seen that the wave loads have the largest impact on the relative motions, where besides the governing roll/pitch period and the wave spectrum, a high peak can also be observed at very low frequencies. This could potentially be the excitation at the natural yaw period, which previously was not observed and could have been restrained by the currents. The wind-only-case in Figure 96 shows a very characteristic peak at the low frequencies, which is the wind load, but also some minor peaks around the characteristic roll/pitch period, which might indicate that the wind loads acting on the floater are also leading to a rotational excitation of it. However, in this case, the relative motions have much lower energy than the wave motions, showing that the wind is less impactful. The currents result only in a peak at the characteristic floater roll period, however, the total energy is substantially lower than for the other two cases, which means that the currents barely influence the relative motions between the blade root and the hub.

Figure 54 shows how the critical motion radii for the blade η_{bcr} , the hub η_{hcr} and the relative motion η_{rcr} are determined for the alignment process. It becomes clear that the hub contributes much more to the critical motion radius of the relative motion than the blade. However, the blade

motion still has some impact and in some load cases even leads to a critical motion radius lower than the one of the hub as the combined motion is smaller.

Jiang et al. had conducted fairly similar studies of a single blade installation of a 5MW blade of a bottom-fixed wind turbine in HAWC2, with the crane and jack-up as one rigid fixed body (Jiang et al., 2018b, p.1044). However, when looking at the critical motion radii also at 14m/s, his study has found the critical motions of the blade to be much higher with $\eta_{bcr} = 4.33m$, $\eta_{hcr} = 2.02m$ and $\eta_{rcr} = 5.2m$ (Jiang et al., 2018b, p.1052). The motions of the blade are much larger as he investigated a bottom-fixed turbine, while for this study the hub motions dominate. However, even the hub motions in this model are only merely larger than in the one of Jiang, while the blade motions of Figure 54 are substantially lower. As a large proportion of the used numerical model is based on previous, verified numerical models and the modelling assumptions stated in section 4 are deemed adequate, the simulation results are still deemed sufficient. However, Jiang's much larger, bottom-fixed motion radii indicate that further verification of the results in another software like HAWC2 should be conducted. However, this would exceed the scope of this thesis, but it is a good suggestion for future work.

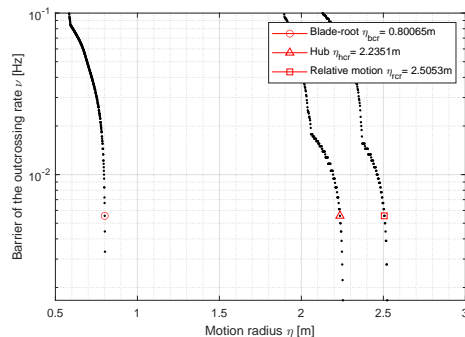


Figure 54: PSD of the motion radius of the blade root at LC14

Given the calculated critical motions, the alignment procedure would have been rated as successful as $\eta_{rcr} < R_{sb1}$. However, the distance in the y-direction is another important factor during the alignment process. A too-short distance or even a collision of both components would impose a too-high risk for the single blade installation. Therefore, for the alignment, a limit is set that the hub and blade root should not come closer to than 0.1m (initial distance 1m) throughout the simulation as both of them are not flat plains but could have several components reaching out as it can be seen in Figure 13. As Figure 55 shows, this limit is exceeded in several of the simulations runs at LC 14. The large difference in the simulations time series stem from the different irregular wind and wave regimes as every simulation has a different seed. The combination of the irregular environmental loads can in some cases lead to an high excitation of the system like in simulation 2 and 4 or no significant excitation like in the simulations 3, 5 and 6. Therefore, it must be concluded that the alignment would not be possible for this load case as the risk imposed by a collision of the blade root and the hub is too high, while the assumed installation equipment would also not be capable of restricting this movement.

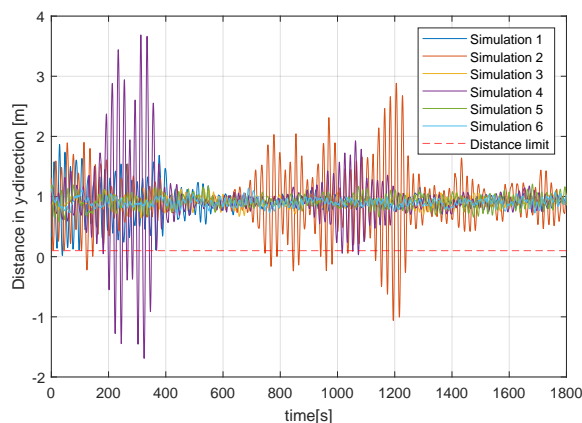


Figure 55: Distance in y-direction between the hub and the blade root

5.6 Alignment results

The critical motion radii are now determined for every simulation run. The mean of the η_{cr} of the six simulations has been calculated to find one critical alignment motion radius for every load case. Those results can be seen in Figure 56, where the critical motion radii for every load case with $\beta_{wind} = 0^\circ$ are displayed.

It can be seen that the critical blade motion is only marginally impacted by the wave regime and only scales with the wind speed. In contrast, the waves have a very significant impact on the hub motions and thus also on the total critical motion radius. In some scenarios like LC8 or 11, Case B leads to the higher motions, while in others, Case C was larger. This is due to this thesis insufficient methodology of load case definition. For instance at 6m/s, the proportional Case B increase H_s from 0.53m to 0.7m was not as impactful as the proportional Case C increase T_p from 8.7s to 11.7s, where the H_s remained more or less the same. In regards to the relative motion radius η_{rcr} , it can be said that for the wind speeds of 6 and 8 m/s, it is substantially larger than the individual critical motion of both the hub and the blade root, which is most likely due to a slight mean misalignment of both components whereby the relative motions radius also becomes higher. With increasing wind speeds, this difference reduces where in several cases, the critical hub motions are actually higher than the relative critical motions, which means that the blade root is moving more with the hub. Thus the distance between the two of them is smaller than compared to the mean position of the hub.

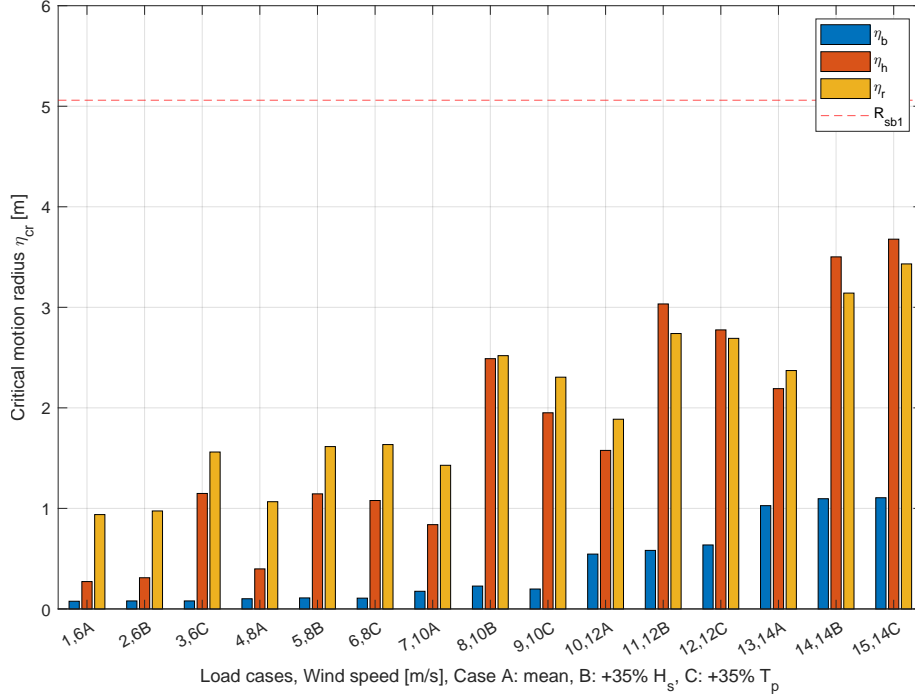


Figure 56: Critical motion radii for all considered load cases with $\beta_{wind} = 0^\circ$ and the safe boundary of $R_{sb1} = 5.06m$

While the critical motion radius increases with the wind speed and differs from case to case, all the critical motions remain below the safe boundary of 5.06m. Therefore every case, in theory, has fulfilled this alignment criterion in the investigated model. However, it is worth discussing the safe boundary itself as it was introduced by Jiang in his work for a 5MW wind turbine blade with $R_{sb} = 3.54m$ (Jiang et al., 2018b, p.1048). With the increasing size of the wind turbines and their blades, this safe boundary would always gradually increase. At the same time, from a purely operational perspective, a relative displacement of 5m would be very large. This is especially the case, given that in the next phase of the blade installation, the maximum displacements of the components are in the region of a few mm to mate the guide pin and the flange. Therefore, an alignment safety boundary of 75% of $R_{sb}(= 3.8m)$ could make more sense, but also this is not reached by any load case, even the 5MW safe boundary of $R_{sb} = 3.54m$ would only be exceeded by η_{hcr} in LC 15, where the relative motions are already below it again.

To assess the impact of the wind heading angle, the relative increase and decrease of the relative critical motion radius $\eta_{r,cr}$ is plotted for both alternative heading angles in Figure 57. No clear trend can be observed when comparing the angles to the default heading angle, where a small majority of the cases lead to a decrease in the critical motion radius. Most were only minor changes in the range of $\pm 5\%$. One large difference can be seen for load case 8, where one randomized wave seed in the default led to very high excitations of the systems, where the critical motions were 30% higher than the average of the other five cases. Thereby, the other heading angles were significantly smaller than the default direction.

No wind direction seems to bring an apparent increase or decrease across all load cases, where the impact of $\beta_{wind} = 140^\circ$ seems to be a bit higher than $\beta_{wind} = 90^\circ$ but without clear tendency. Therefore, it can be concluded that the wind heading angle doesn't seem to have a tremendous influence on the system, where most of the difference can be attributed to the different wind and wave seeds for every simulation. However, a detailed study of all wind heading angles would be needed to verify this assumption.

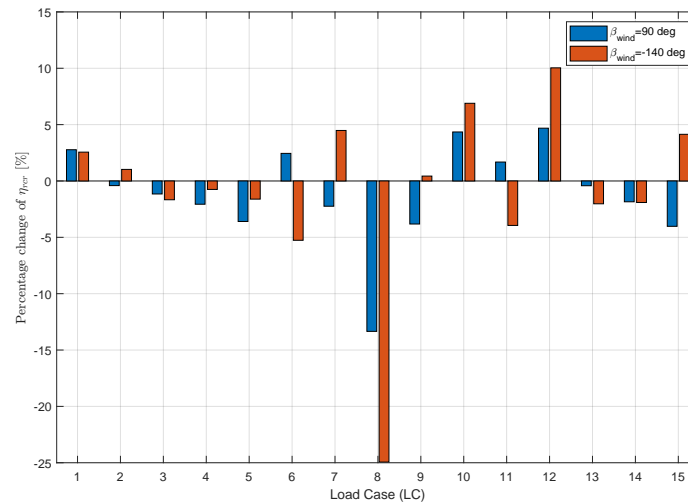


Figure 57: Impact of the alignment angle of the incoming wind on the critical outcrossing motion

To better assess the impact of the wind speed on the installation procedure, Figure 58 displays the critical motions of case A for every wind speed. It can be seen that the critical motion of the blade is scaling quadratically with the wind speed while the hub motions are increasing even more for every wind speed. As discussed in chapter 5.4, this increase does not stem from the higher wind speed, which has only very little contribution to the hub motion but is much more influenced by the increased mean sea state, which correlates with the stronger winds. The relative motion radius is also increasing more quadratically with the wind speed. The figure also represents quite clearly for the lower wind speeds that the relative critical motion is much larger than the one of the individual components.

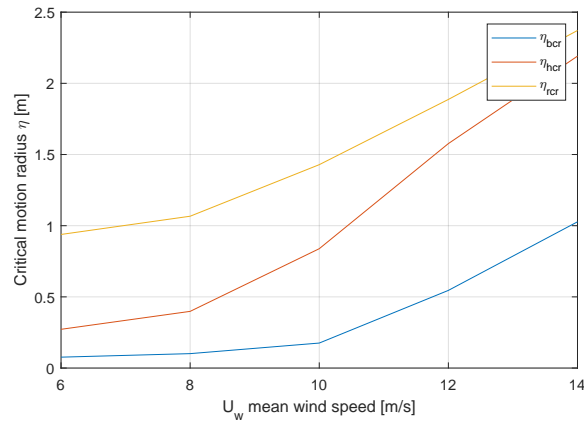


Figure 58: Critical motions at different wind speeds for Case A, $\beta_{wind} = 0^\circ$

Besides the relative motions in the xz -plane, it is also important to check if the hub and the blade root are coming too close in y -direction or even collide. The wave regime plays a significant role in this criterion as the floater/hub mainly governs the exceedance of this limit. It was found that there is a clear tendency for increasing wind speeds to exceed the limit, but not every wave seed leads to the exceedance as Figure 59 shows. The figure displays the number of simulations where the limit of a minimum y -distance of 0.1m has been exceeded. Besides one critical seed at load case 8 (wind 10m/s), the limit is only exceeded at wind speeds of 12m/s or higher. It can be seen that Case B for both 12m/s and 14m/s leads to more cases where the minimal distance between both components is too small. Case C also shows the exceedance of this limit, even though for fewer seeds. Case A shows no exceedance for 12m/s and only a few for 14m/s.

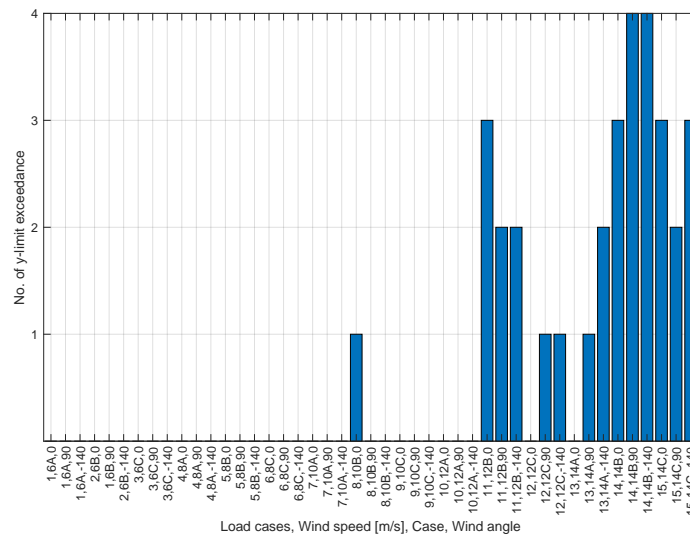


Figure 59: Number of simulations which have exceeded the y -limit out of six simulations

Based on those results, it can be concluded which load cases can be deemed acceptable environmental conditions for the alignment process. Table 13 displays those outcomes. As the results have shown, the system is only marginally susceptible to the wind direction without a clear pattern. Still, the table determines the success or failure of the alignment operation for every direction. The very rough wave seed for LC8 is estimated as a unique scenario. Therefore, it was determined that the alignment still can be successful. For the load cases where two or more simulations have exceeded the y-limitation, it was determined that the risk of collision is too high, making the alignment impossible. For LC12 and 13, there was a single exceedance in some directions, but as it also occurred in other directions, it has been decided that the alignment would not be possible in this case.

If operational limits should be determined, it can be said that the alignment procedure can be safely executed for all conditions up to LC10. If detailed conditions of the incoming wind are known, LC12 and LC13 can still be safely executed. However, as winds from multiple other directions have shown to not comply with the y-distance limit, this operation would become riskier as the wind could change direction quickly. Therefore, the operational limits of the alignment procedure are estimated to be H_s 1.6m, T_p 11s and winds of 12m/s.

LC	U_w [m/s]	H_s [m]	T_p [m]	β_{wind} [deg]	η_{rcr}	y-distance	Alignment
1	6	0.529	8.669	0, 90, -140	y/y/y	y/y/y	y/y/y
2	6	0.7	7.436	0, 90, -140	y/y/y	y/y/y	y/y/y
3	6	0.569	11.7	0, 90, -140	y/y/y	y/y/y	y/y/y
4	8	0.793	7.545	0, 90, -140	y/y/y	y/y/y	y/y/y
5	8	1.1	8.862	0, 90, -140	y/y/y	y/y/y	y/y/y
6	8	1.018	10.2	0, 90, -140	y/y/y	y/y/y	y/y/y
7	10	1.187	7.863	0, 90, -140	y/y/y	y/y/y	y/y/y
8	10	1.6	9.136	0, 90, -140	y/y/y	n/y/y	y/y/y
9	10	1.411	10.6	0, 90, -140	y/y/y	y/y/y	y/y/y
10	12	1.602	8.597	0, 90, -140	y/y/y	y/y/y	y/y/y
11	12	2.2	10.041	0, 90, -140	y/y/y	n/n/n	n/n/n
12	12	1.939	11.6	0, 90, -140	y/y/y	y/n/n	y/n/n
13	14	2.028	9.117	0, 90, -140	y/y/y	y/n/n	y/n/n
14	14	2.7	10.313	0, 90, -140	y/y/y	n/n/n	n/n/n
15	14	2.290	12.3	0, 90, -140	y/y/y	n/n/n	n/n/n

Table 13: Outcomes of the alignment modelling, y: yes operation is possible, n: no operation is not possible

5.7 Mating phase

Both the guide pin and the flange hole are modelled with a rigid connection to the blade and hub, respectively. Therefore, the motions of both points are very similar to the ones discussed in chapters 5.1 to 5.5, except that the points are 2.4m moved in negative x-direction so that the position of the pin and flange are represented adequately. As previously discussed, a high pass filter is applied to the motion series as it is assumed that a control system would be able to filter out all low-frequency components of the blade and hub motions by adjusting the tugger line forces. As it can be seen in

Figure 60, the unfiltered relative motions between the guide pin and the flange hole are dominated by frequencies below 0.2 Hz and thus applying high pass filters of 0.3Hz or even 0.5Hz like in the plots below would mean that it is assumed that the controller could filter out the vast majority of motions.

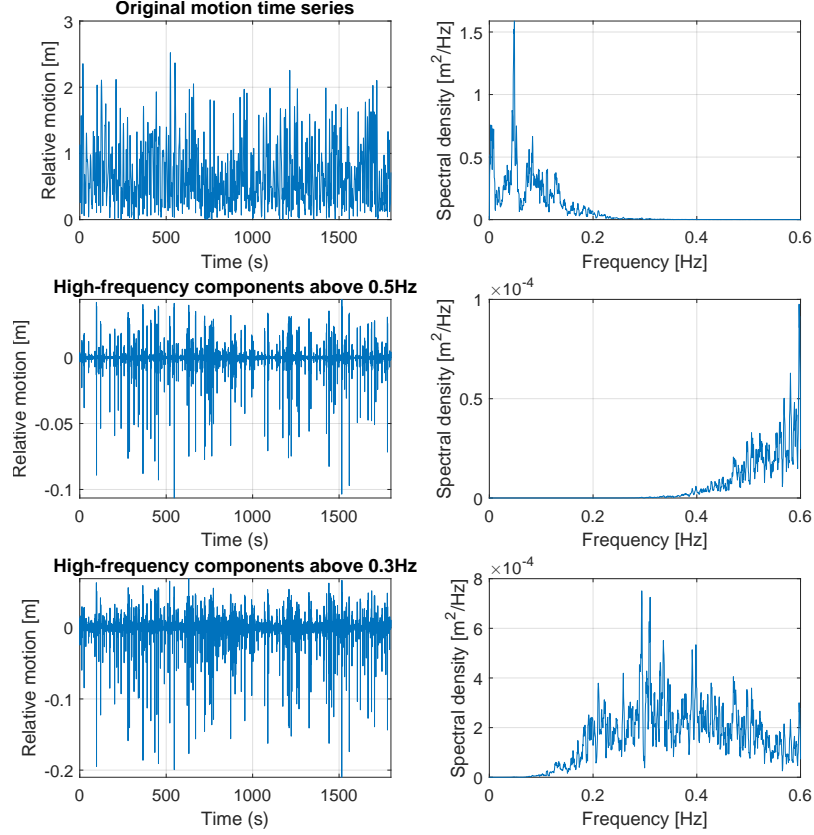


Figure 60: Time series and PSDs of the relative motion of LC14 when applying high pass filters of 0.5Hz and 0.3Hz

Like the alignment operation, the simulation of the mating operation has been carried out for all load cases and all wind directions. After applying the high pass filter, the critical motions of the pin, flange and relative motion are determined for the critical outcrossing rate of one outcrossing per minute, equal to $\nu_{cr2} = 1.67 \times 10^{-2} Hz$ is determined. The safe boundary of the mating procedure is the difference between the pin diameter and the flange diameter, which is $R_{sb2} = 4mm$.

Figure 61 is presenting the results for all load cases with no wind misalignment and a high pass filter of 0.5Hz. The safe boundary is exceeded by η_{rcr} for most load cases, with motions only being acceptable for very low wind speeds of 6 or 8 m/s. This is only the case for the mean sea states for Case A, with a stronger sea state of increased H_s in Case B only being acceptable for 6m/s while the increased T_p of Case C already exceeds the safe boundary in both cases. The high-frequency components of the pin/blade motions are much smaller than the flange/hub motions, where the η_{bcr}

is below the safe boundary for most load cases up to 10m/s. The critical hub motion exceeds the boundary for all load cases. However, especially for low wind speeds, the relative motion between the two bodies compensates a lot of this movement whereby η_{rcr} falls below the boundary again.

As previously discussed, using a controller that can filter all motions below 0.5Hz would be very hard to implement. Therefore, a controller with a 0.3Hz filter could be favourable from a technical perspective as it would still filter out most of the motions with fewer technical difficulties. However, as Figure 98 in Appendix P shows, with this filter, the safe boundary would be exceeded by the relative motion for every single load case. Therefore this controller is deemed unsuitable for this mating operation. If manual guidance assistance with ropes can be used during the mating, the safe boundary of the procedure could be increased. Given the very limited amount of load cases that are successful for mating, this would be very favourable, either to use an less advanced control mechanism or to increase the operational limits of the mating procedure.

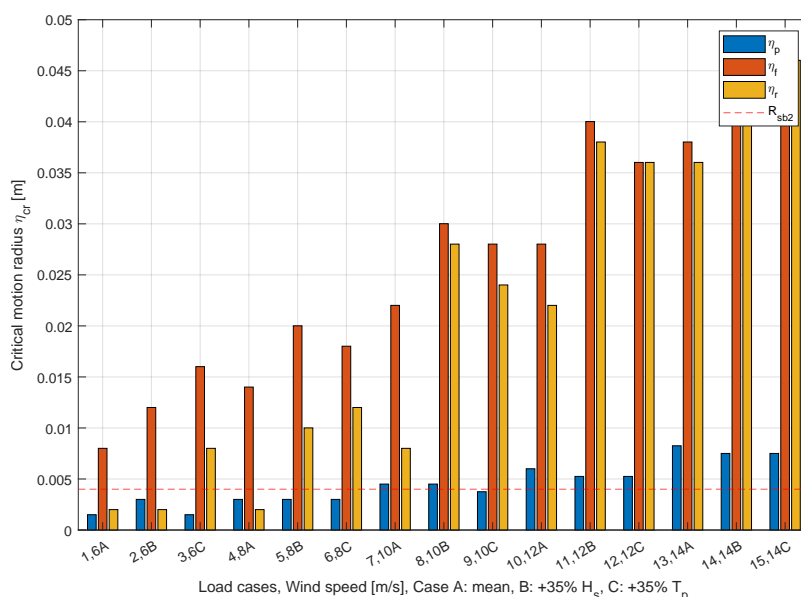


Figure 61: Critical pin-flange motion radii for all considered load cases with a filter of 0.5Hz, $\beta_{wind} = 0^\circ$ and the safe boundary of $R_{sb2} = 4mm$

Regarding the other wind alignment angles with a 0.5Hz controller, the mating process is only possible for the described load cases as seen in Table 14. One exception here is the mean sea state for 10m/s and $\beta_{wind} = 90^\circ$, where the mating is still possible, but given the fluctuation of the incoming wind, the risk of damaging the guide pin is still very high.

All in all, Table 14 shows that despite the very strong motion controller, most load cases are unsuitable for the high-precision mating process. The alignment is possible for more load cases. However, given that the mating phase is usually immediately initiated after successfully aligning the blade root and the hub, it can be said that the total single blade installation is only possible for load cases 1,2 and 4 for all wind directions. Based on those findings, the operational limits of

the mating procedure can be estimated at H_s 0.8m, T_p 8.7s and wind speeds of 8m/s.

LC	U_w [m/s]	H_s [m]	T_p [m]	Alignment	Mating
1	6	0.529	8.669	y/y/y	y/y/y
2	6	0.7	7.436	y/y/y	y/y/y
3	6	0.569	11.7	y/y/y	n/n/n
4	8	0.793	7.545	y/y/y	y/y/y
5	8	1.1	8.862	y/y/y	n/n/n
6	8	1.018	10.2	y/y/y	n/n/n
7	10	1.187	7.863	y/y/y	n/y/n
8	10	1.6	9.136	y/y/y	n/n/n
9	10	1.411	10.6	y/y/y	n/n/n
10	12	1.602	8.597	y/y/y	n/n/n
11	12	2.2	10.041	n/n/n	n/n/n
12	12	1.939	11.6	y/n/n	n/n/n
13	14	2.028	9.117	y/n/n	n/n/n
14	14	2.7	10.313	n/n/n	n/n/n
15	14	2.290	12.3	n/n/n	n/n/n

Table 14: Outcomes of the complete single blade installation, y: yes operation is possible, n: no operation is not possible

5.8 Discussion

The presented outcomes of the numerical simulations in Table 14 have shown, that the single blade installation with a jack-up vessel is successful if the wind and waves remain calm. However, this conclusion can only be made within the scope of the simplifications and assumptions which have been done in this thesis. The impact of the assumptions on the simulation outcome should be assessed in this chapter.

Figure 53 has shown that the motion characteristics of the floater do have a large impact on the relative motion between the blade root and the hub. The integration of a different floater concept would therefore largely impact the motion characteristics of the single blade installation as the hydrodynamic properties of the floater will change. Similarly, a change of the draft of the investigated floater would also change the relative motions between the blade and the hub as the hydrodynamic properties also change. A lower draft semi-submersible would have a reduced stability, which could result in more restrictive operational limits. However, without conducting detailed investigations of the models, this conjecture can't be verified.

The impact of the jack-up model and crane on the relative motions is extremely small and therefore it most likely doesn't make much of a difference if a different jack-up model were to be used with a similar crane model. However, using a heavy lift vessel certainly would change the motion characteristics as it then would be a floating-to-floating operation.

The load cases have been defined based on the extracted hindcast data for the location, how-

ever, this data does not stem from the area within the port area. Even though the load cases are thus not fully representative, it does not make much of a difference for the determination of the operational limits, as the limiting loads of the system remain the same regardless of the defined load cases. However, by only looking at three load cases per wind speed, which are also methodically not well proven, the actual operational limiting conditions can not be accurately represented. A detailed operational analysis of all probable sea states would be required to determine the actual operational limits, while the load case-based operational limits can be regarded as conservative as they are not accurate enough.

Not regarding tides within the simulations has a substantial impact on the outcomes of the simulation. First and foremost, the mooring system is very unlikely to work with a large vertical displacement of the floater as it is not designed to adapt with those variations. The large tidal variation would also impact crane operation as the crane would need to constantly adapt to the floater position, which could get especially challenging during the mating procedure. Lowering the floater to the seabed onto a prepared area might be more expensive than the proposed mooring system, even though the bollards and specialized mooring lines would certainly also cost a fair bit, but it could drastically improve the operability as the floater would be fixed in place. If the proposed horizontal mooring system would be implemented, a more detailed study of the mooring lines with more sophisticated simulation tools would be required to better understand the impact of the mooring system on the integration performance.

It is unlikely that any mating control system would be capable to reduce the relative motions between the blade and the hub so drastically as the assumed controller does. The highpass filter reduces the relative critical motions from a range of uncontrolled 1-3m to controlled 3-45mm. An actual tugger line control mechanism would need to be extremely advanced to even come close to this, as it would also need to predict the incoming environmental loads. At the same time, such a control mechanism would be required as the mating limits are only met with the restrictive controller.

Regarding the alignment process, the safe boundary R_{sb1} , which is close to equal to the blade root diameter, has been adapted from previous studies as a maximal displacement limit during the alignment process of a 5MW blade. Given the increase in blade root and hub diameter of larger wind turbines, it is questionable if this limit can still be applied for turbines of larger size as the larger allowable displacement will make the alignment procedure arguably much harder.

When comparing the results of the critical motions in the alignment phase with a similar study for bottom-fixed turbines by Jiang (Jiang et al., 2018b), it can be seen that the critical blade motions of this thesis are substantially lower, while also the hub motions are only marginally larger. Given the enhanced motion profile of a floating wind turbine, this is not intuitive, especially as the characteristics of the blade are supposed to be fairly similar. To eventually determine whether or not the operation is technically possible, further verification of the investigated system in a different simulation software would be required. However, as this thesis is the first known academic publication of the concept, no other studies can be used for verification. Verifying the system in a different code would exceed the limitations of this thesis, leaving it up to a task for future work.

The assumptions which have been made to simplify the numerical model of the system are deemed

as sufficient at the large majority of the systems motions are induced by the wind and wave loads while bending only play a minor role.

5.9 Technical feasibility

The technical feasibility study should determine whether it is possible to implement the system with the current technical resources (Kendall & Kendall, 2011, p.63). When conducting a feasibility study, among others, the following questions can be asked (APMG, 2023):

- Is the engineering of the project achievable?
- Can the technology be done with the given resources?
- Is the proposed technology proven?
- Which risk does the technology have?
- How is the performance of the technology?

A detailed technical feasibility study would answer those questions thoroughly, however, the limited scope of the thesis is only allowing a preliminary assessment of the technical feasibility based on the conducted study under the made assumptions. For instance, a detailed study would also regard the working procedures which are needed during the entire operation to assess whether the integration can take place in a safe and low-risk manner.

The outcomes of the response analysis and the assessment of the alignment and mating phases have shown that it is generally possible to execute the single blade installation of a FOWT with a jack-up vessel. To successfully conduct the installation, the environmental conditions need to be very calm as the mating has high environmental restrictions. Therefore, it would be preferable if the wind turbine integration would take place in a sheltered area. As even the installation of a component with a few millimetres of allowable displacement is deemed possible, it can be assumed that also the tower and nacelle integration would be successful. However, the characteristics of those lifts are substantially different as much heavier components need to be lifted with a very high hook height. To assess the technical feasibility of the whole wind turbine integration, further studies would need to be done.

Deeming the single blade installation as technically feasible underlies a vast range of assumptions which have been discussed in the previous chapter. The proposed mooring system is a novel design that has not been implemented so far for the integration of floating wind turbines, creating uncertainty for the technical feasibility. Even though in theory it can reduce the motions of the floater to a large extent, it is not capable of adapting to the large tidal range which is characterizing the port of Port Talbot. Therefore, this system would not be technically feasible for the investigated case study, but can be suitable for other sites which are not governed by a large tidal variation.

It is also questionable, if the engineering of the assumed controller for the mating procedure is actually possible to implement. The controller is extremely restrictive while the actual control system would need to predict and adapt to the environmental loads acting on the blade and also on the floater. With the current existing control mechanisms this can't be done while developing such a controller would take a lot of time and effort. Therefore, with the existing resources, the

technical feasibility of the controller is not given.

Besides the controller and the moorings, the system is utilizing existing components like a wind turbine installation vessel, that is bespoke for the integration of wind turbines, though usually for bottom-fixed turbines. Also the concept of a semi-submersible floating wind turbine is not new and has seen multiple implementations even though the particular concept has been not built so far. 12MW wind turbines are not new to the market, especially by 2026 when the integration of the White Cross wind farm should take place.

The risk of the proposed concept were not investigated in this study. However, the procedure involves multiple lifts nearshore, which is always a very risky operation, especially given the size and weight of the components. A further investigation of the risks and all the working procedures is needed. The performance of the system in regards to the speed of the turbine integration will be investigated in chapter 6.

In conclusion, it can be said that the technical feasibility of the concept is not given for the investigated case study as the tidal variation is making the station-keeping-system unsuitable. Furthermore, the mating control system is not possible with today's available, known technology. However, if further developments of the technology take place, the proposed system could be technically feasible in another location with smaller tidal range. An alternative is the integration of a FOWT when it is lowered to the ground to have much smaller variation in the floater motions and not be affected by the tides, but this system would need its own detailed investigation to know its technical feasibility.

6 Operability analysis

After some operational limits were determined in the previous chapter, it is beneficial to understand what those limitations imply from an operational point of view for the integration procedure when using a jack-up. This chapter aims to investigate this question in more detail to better understand the impact of the limits and which operation is the most sensitive one. Based on those findings, the economic feasibility of the concept can be estimated. Therefore, the simplified integration sequence, which has been introduced in chapter 2.4 is investigated for the described scenario in Port Talbot. The complete integration sequence considered in this operability analysis is displayed in Figure 62 and Figure 63. As the figures indicate, this operational analysis will also evaluate the different concepts of using either a feeder vessel or shuttle to the storage location as it was introduced in chapter 3.5. Those sequences are formulated for every turbine as a sequential process, where every task needs to be completed before the next one can start. To understand how the integration sequence would perform without delays, initially a calm weather model is considered. Then the effects of weather restrictions are considered to have a more accurate estimation of the time and cost of the procedure.

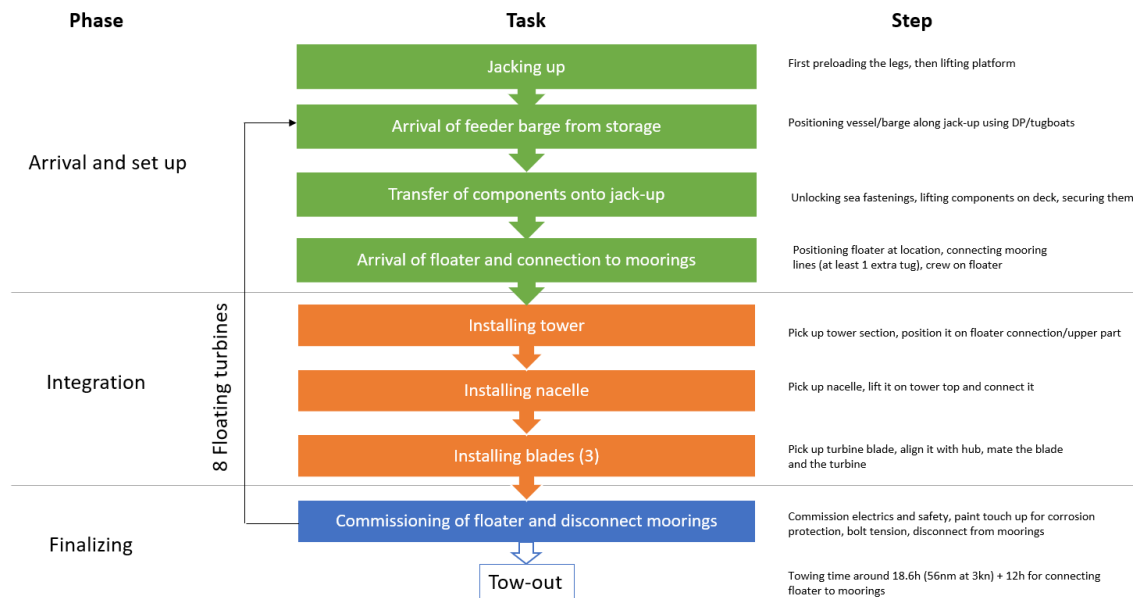


Figure 62: Integration sequence for the feeder concept

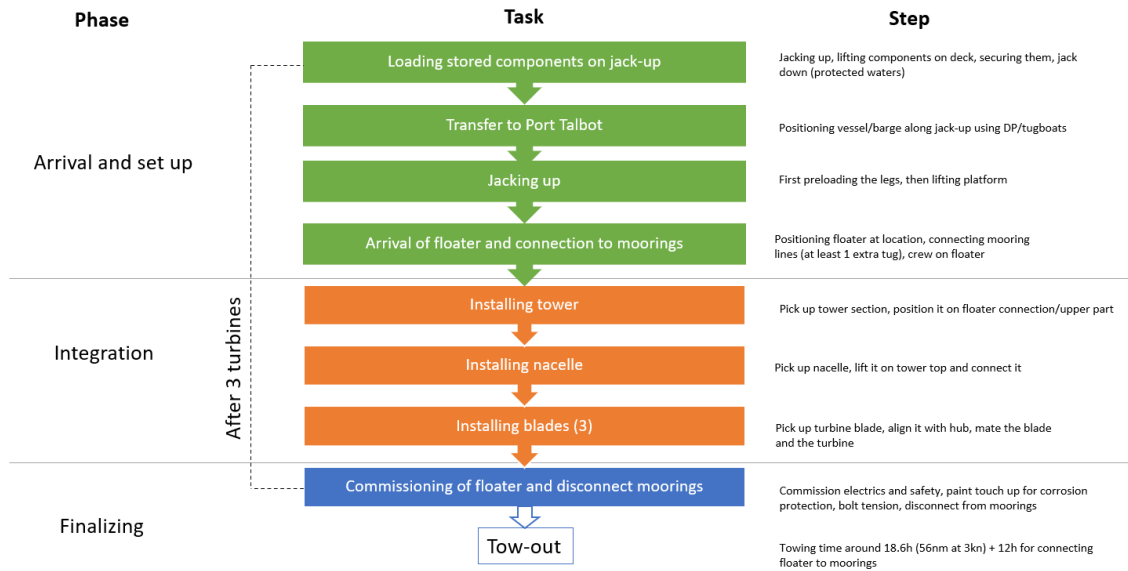


Figure 63: Integration sequence for the shuttling concept

6.1 Literature review

Instead of focusing on the operability analysis of the complete integration sequence of an offshore wind turbine, most research has so far focused on the operability of individual tasks of the integration sequence. This is logic as a practical implementation of the integration sequence requires the exact detailed operational limits of every individual operation to determine the total operability of the integration sequence. For example, Guachamin Acero and Gao introduced a methodology for the assessment of the operability of installation tasks and applied it on the installation of a monopile and transition piece (W. Guachamin Acero et al., 2016; Gao et al., 2016). The same methodology has been also applied to a new procedure of installing the assembled turbine with an upending system (W. I. Guachamin Acero et al., 2017). Furthermore, Sreenivasan investigated the operability of the transfer of the components from a specialized feeder vessel onto the jack-up vessel (Sreenivasan & Voogt, 2022). However, no operability analysis of any of the conventional wind turbine tasks has been published, neither in regard to floating wind or bottom-fixed offshore wind. The only work that regarded the full integration sequence of a bottom-fixed offshore wind turbine has been done by Boer, who investigated the duration and cost of the full sequence when subject to environmental loads (Boer, 2022).

Other research has focused on the optimization of modelling or implementing the integration sequence. Tekle Muhabie assessed the effects of the stochastic effects of the integration sequence with an discrete-event simulation, while Sarker investigated how to optimize the transportation and installation costs (Muhabie et al., 2018; Sarker & Faiz, 2017). Another work investigated how total installation time per turbine has dropped in the past years (Lacal-Arántegui et al., 2018).

This thesis will adapt the work and models of Boer to the proposed integration sequence of a

floating offshore wind turbine. The model will be extended to also account for the impact of each environmental condition on the waiting time, to evaluate different logistical approaches of supplying the concept with components and to perform a sensitivity analysis on the wind farm size and starting time.

6.2 Assumptions

Like in the numerical simulations of the single blade installation, multiple assumptions have to be made for the operability analysis to simplify the procedure or due to a lack of sufficient information. The focus of this operability analysis is on the weather-restricted wind turbine integration and the associated cost and time. Therefore, all other further delays are not regarded within this model. This means, for instance, that the operation takes place 24/7 without considering crew shifts or halted operations due to working hours. This assumption is deemed as realistic as the day rates of the jack-up vessel are very high, so the vessel should be maximally utilized. For the calm weather model, the starting date is also irrelevant as it is assumed that the operation can take place all the time without operational limitations. The starting time of the weather restricted integration sequence is initially assumed to be the first of May of the year at 10 am, as this starting date promises to utilize the favourable weather of the summer the best. The impact of a different starting date/month will be further discussed in chapter 6.4.4.

Other delays that could occur are the the delayed supply of components or waiting times due to failures. Generally, especially in a complex offshore wind environment, it can be very challenging to have the right components, tools and people are needed for every operation at the right location and time. Failures can occur in the equipment or components, which can have drastic consequences. Therefore, also regular maintenance might delay the operation to prevent even more severe delays due to failures. Some studies have tried to account for those stochastic failures and delays, however they are hard to account for in a planned, sequenced model like the one used in this study (Muhabie et al., 2018). Furthermore, their impact on the waiting time of the vessel is still comparably low (Boer, 2022, p.33). Thus, the assumption is made that any delays are not accounted for in the model.

Despite the previous study in chapter 5, where the alignment and mating phase were discussed in detail, the single blade installation is assumed as one task in this model. This is because the blade alignment usually wouldn't even be initiated if it is clear that the conditions are too rough for the mating. In practice, both steps of the single blade installation are fairly short in the range of a few minutes, with most of the single blade installation time accounted for by the lifting of the blade and the tensioning of the bolts.

As no detailed investigations have been made on the turbine and nacelle integration, it is assumed that their operational limits are the same as the ones from the the single blade installation. The operational limits in this study are fixed values which are not allowed to be exceeded. However, in a real application, the the allowable sea states are not only one operational limit but are a combination of T_p and H_s as it can be seen for example in Figure 99 in Appendix Q. Those limits could also vary for different factors like heading angles or in this case the wind speed. However, to obtain those detailed limits, extensive operational studies need to be executed for every task for the installation sequence, which exceeded the scope of this work. By applying the simplified operational limits, the complexity of the model is reduced significantly.

When the operational limits should be applied to the local site conditions, it is problematic that the used hindcast data stems from outside of the sheltered area of the port. While the wind loads might remain the same, the breakwater of Port Talbot will substantially reduce the wave height and period, whereby the operational limits due to waves are much less likely to be exceeded. Using hindcast data from outside the port will probably lead to significantly overestimating the waiting on weather due to waves. Due to the lack of other available data, while being aware of the issue, the assumption is made that using the hindcast data from outside the port is still acceptable.

As it has been discussed in detail, Port Talbot is a location where the tidal range is very high. This could lead to further issues for the integration sequence as the water depth could fall below the minimum draft requirement of the used vessels. Furthermore, as discussed in chapter 2.4, the tidal range makes the wind turbine integration very challenging as the floater constantly moves in the z-direction, whereby especially longer lifting operations become very difficult. Chapter 4.3.4 described that finding an actual mooring system that could work under those conditions is also extremely challenging. While some of those factors could be easily accounted for with a minimum draft requirement for some operations, the limitations of the mooring system and the constant displacement due to tides can't be factored in as easily. Therefore, the assumption is made that tides are not regarded as part of the operability analysis. The goal of this study is to better understand, in general, the feasibility of the proposed concept of using a jack-up vessel to integrate a floating wind turbine. Disregarding the unique local condition of the tides is deemed sufficient for a greater understanding of the system as it is unlikely to encounter those problems in other locations.

Using a sequential model to simulate the installation process brings its advantages regarding simplicity, but it also can lead to inefficiencies in the operational model. For instance, given that the feeder vessel would approach the jack-up vessel from a different side than the floater, the commissioning of the floater and the loading of the components onto the vessel can happen simultaneously as the jack-up cranes are not occupied during commissioning. The sequential model can not represent this, thereby the integration sequence takes longer than necessary.

A linear cost model is assumed for the charter rates of the vessels, which is probably not fully applicable for a real-case scenario where the charter rates would also depend on the rental duration, which could make a significant difference, especially for the very expensive jack-up vessel (Thomsen et al., 2014, p.215). Furthermore, the model only focuses on the charter costs of the vessels during the installation, while not all costs associated with the integration are vessel-related. Those costs include the installation of the mooring bollards, preparation of the area for the jack-up (e.g. with stone cushions), the storage cost of the wind turbine components in other ports as well as other port fees in Port Talbot or the storage ports. The model also does not include the charter cost of the vessels outside of the integration sequence as in a real installation scenario. In a real implementation, the vessels also need to be paid during the preparation of the vessel for the installation job and during the transfer of the vessel from the previous job to the new location. This is especially important for the jack-up vessel, while the other vessels are assumed to be available locally.

For the shuttling scenario, it is assumed to be sufficient that the jack-up vessel can position itself in the same position at the integration site several times. In practice, a detailed geotechnical

study would need to be pursued to know if this can be done in the location. It might also be advantageous to prepare the seabed beforehand with stone cushions. Those are already used in ports when a jack-up loads components to ensure the stability of the piles carrying the quay (Thomsen et al., 2014, p.91).

Based on those assumptions, it will not be possible to determine the exact cost or time of the integration sequence as neither all associated cost or waiting times are accurately represented. Furthermore, the outcomes of the weather restricted operability analysis will be only applicable to a very limited extent for the site in Port Talbot as the environmental conditions of the site are not represented accurately nor are the operational limits detailed enough to determine the exact operability of the concept in this site. Nevertheless, the outcomes of the simulation can be used as a first estimate how the system would perform in general regarding time and cost. Furthermore, an understanding can be established which tasks generally are resulting in the longest waiting times, how the system would perform during different times of the year and with different wind farm sizes. Those outcomes can be used to determine if the system in general could be economically feasible at all or if would be unfeasible even under all those assumptions.

6.3 Calm weather model

To have an initial reference for the cost and installation time of a integration sequence, Boer has developed a calm weather model as an initial reference, where it is assumed that the operation could occur at all times without any restrictions (Boer, 2022, p.21). The model's outcomes can be considered a best-case scenario for the installation. This model is now applied and modified to the integration sequences of Figures 62 and 63. In this scenario, the total calm weather integration time might also be regarded as a reference for a port-based integration if the port infrastructure had been built out and the floater is fixed to the quay, though some tasks in the integration sequence would certainly differ. In this setup, the operability of the integration is in theory much higher, as the floater motions are largely constrained. However, regarding cost, the calm weather model can't be a reference as the port infrastructure has a different cost structure, where a majority of the cost also comes from building the infrastructure.

The calm weather model is mathematically determining the duration of each of the individual installation tasks (not including tow-out) in Figure 62 and Figure 63. The model works sequentially, meaning that each task must be completed before the next task can be started. The model loops through the integration sequence of every turbine and is finished when the integration sequence of the last turbine is completed. The cost will then be calculated by multiplying the duration of the integration sequence with a fixed hourly charter rate for the used vessels. For this, a linear cost model is used, assuming that all involved vessels are rented for the entire installation time. The calculations can also be done for different vessels with different properties. However, as the vessel is set for the given case study, the model is varied instead for different installation times for every task and evaluates the different scenarios for shuttling and feeder vessels. The feeder vessel is assumed to be able to carry the turbine components of one turbine. The travelling time of the feeder barge is not represented within the model as it happens simultaneously with the other procedures while also being only marginally affected by the environmental conditions.

6.3.1 Parameters and input

The calm weather model includes many input parameters regarding the farm, vessel and operation characteristics. As described in chapter 3.1.1, in this case study, the jack-up vessel is being used for the White Cross wind farm which is assumed to consist out of eight 12MW turbines, totalling a farm capacity of 96MW. Some later discussions in chapter 6.4.4 will also discuss how the integration system would perform when larger or several smaller wind farms should be installed with it. Still, the eight-turbine wind farm will be the focus of the work. The used farm and vessel parameters are displayed in Table 15. As the Bold Tern crane has a maximum capacity of 1600t, while the tower weighs 1165t, it is assumed that the tower can be installed in one lift.

As the feeder barge travelling to storage is not regarded in the sequential model, the distance to the port is also no input parameter. The vessel's maximum speed is 12kn (Fred. Olsen Wind-carrier, 2023b), due to the loaded components, an average speed of 10kn is assumed. This would mean that it would take the feeder only around 2-2.5h to travel between Port Talbot and Swansea, therefore, only one feeder barge is needed. The day rates of a jack-up vessel can vary largely between the vessel types and the duration of the charter. Ahn estimated day rates in the range of 150000-250000\$, while in a recent study, Simons estimated 240000\$ for a non-US-flagged WTIV (Ahn et al., 2017, p.47; Simons, 2022, p.18). As the charter period for integrating eight turbines will be rather short and as a modern WTIV is required to install a 12MW turbine, the charter rate of 220000€/day is assumed. The tug boat charter rate depends on the power of the tug boat. As the floating structure is fairly large, a bigger tug boat is needed, while a smaller tug is also required to handle the floater during the positioning and for the feeder case to align the feeder barge with the jack-up. The feeder scenario also needs another tug boat to tow the barge that has no propulsion. According to Ahn, the feeder vessel cost ranges between 1000-5000\$/day, therefore, an average day rate of 3000€ is assumed (Ahn et al., 2017, p.47). Besides the vessels, also a crew of at least four well-trained technicians is required on the floater for all integration activities, which can be estimated at €1000/day/person, according to one industry expert from Moreld Ocean Wind (Armstrong, 2023). Furthermore, a simple crew transfer vessel is needed to get them on and off the floater. The cost of a specialized feeder vessel in the US market are assumed around \$24000-48000/day, a simpler barge without propulsion in the European market would be much cheaper, therefore, the barge is assumed to have charter rates of €8000/day (Simons, 2022, p.17).

Description	Parameter	Value	Unit
Number of turbines to be installed	N_{Wtb}	8	-
Number of tower pieces per turbine	N_{Tow}	1	-
Number of nacelle components per turbine	N_{Nac}	1	-
Number of blades per turbine	$N_{Blđ}$	3	-
Number of temporary moorings to be connected	N_{Moor}	3	-
Distance between storage port and Port Talbot	$PORT_{Dis}$	65	nm
Transit velocity jack-up	$TRANS_{Vel}$	10	kn
Vessel capacity turbines	CAP_{Vel}	3	-
Charter cost jack-up	CHT_J	220	k€/day
Charter cost barge	CHT_B	8	k€/day
Charter cost tug boat	CHT_T	3	k€/day
Charter cost crew on floater	CHT_C	1	k€/day
Charter cost crew transfer vessel	CHT_{Ctv}	1.75	k€/day

Table 15: Wind farm and vessel parameters (Simons, 2022, p.18; Ahn et al., 2017, p.47; Armstrong, 2023)

In regards to numbers which can quantify the duration of the total installation time per turbine, the literature states a very wide range of potential installation times, where Ahn stated a total integration time for the tower, nacelle and blades of 34-58h for a 7MW turbine while Boer assumed in his work only 12h (Ahn et al., 2017, p.51; Boer, 2022, p.29). A wide range of time estimates can also be observed for each task in the wind turbine integration. At the same time, it is hard to find any numbers for several of the individual tasks, like the floater connection to the high-tension moorings, due to the novelty of the tasks. To have a better understanding of the durations, it was very helpful to have discussions with industry experts from Havfram and Moreld Ocean Wind, who both gave some guidance on what numbers can be regarded as fairly realistic (Solis Boado, 2023; Armstrong, 2023). The novelty of the integration system and the floating foundation still brings considerable uncertainty with them. Therefore, a range of installation times is being tested within the model to better understand the effects on the total integration sequence. The operational time estimates are presented in Table 16. The estimate of the commissioning time comes from literature (ORE Catapult, 2020, p.22), the rest of the numbers are based on the discussions with the industry experts. The more complex weather-restricted model works on an hourly basis. Therefore, the operation times are also provided in full hours. The mean operational time will be regarded as the base scenario. According to the expert from Havfram, the current industry rule of thumb is to integrate one turbine on a fixed foundation in 24h. As the total turbine integration time estimates in the table show, this rule of thumb is roughly fulfilled.

Description	Parameter	Value			Unit
		Mean	Min	Max	
Positioning and jacking up	T_{Pos}	4	3	5	h
Transfer of components	T_{Load}	2	1	3	h/component
Connecting the floater	T_{Con}	4	3	5	h/mooring
Installing the tower	T_{Tow}	6	5	7	h
Installing the nacelle	T_{Nac}	8	7	9	h
Single blade installation	T_{Bld}	4	3	5	h/blade
Commissioning the floater	T_{Com}	6	5	7	h
Total turbine integration time		26	21	31	h/turbine

Table 16: Operation task times (Solis Boado, 2023; Armstrong, 2023)

6.3.2 Mathematical model

To calculate the duration of each task, simple equations are formulated based on the introduced parameters in chapter subsection 6.3.1. Those equations are then implemented in the Python model to calculate the total installation time in a calm weather model.

While most of the equations are the same between the feeder scenario and the shuttling scenario, some equations differ regarding loading and transit. When using a feeder barge, the components of only one turbine at a time can be loaded. The blades are transported in a rack of three and thus can be lifted simultaneously. Therefore, the unloading of the barge can be formulated as follows:

$$DUR_{Load} = T_{Load}(N_{Tow} + N_{Nac} + N_{Bld}/3) \quad (13)$$

while for the shuttling scenario, several turbines can be loaded onto the vessel. As not always three turbines need to be loaded, the eight-turbine project would need 3,3,2 loads. The parameter $WTB_{Onboard}$ is used, which determines how many turbines need to be on the vessel. Thereby, for the shuttling, the loading duration can be formulated with:

$$DUR_{Load} = WTB_{Onboard}T_{Load}(N_{Tow} + N_{Nac} + N_{Bld}/3) \quad (14)$$

Furthermore, the shuttling has the additional task of shuttling between the storage port and Port Talbot, which can be formulated with:

$$DUR_{Trans} = \frac{PORT_{Dis}}{TRANS_{Vel}} \quad (15)$$

All other equations are the same for both scenarios. First up, the vessel needs to be positioned in the port, which can be formulated with:

$$DUR_{Pos} = T_{Pos} \quad (16)$$

The jack-up time depends on the soil conditions, where preloading and jacking could take much longer in unfavourable conditions, but for this study, the soil conditions are assumed to be normal. When the floater arrives in its position, it is hooked up to the moorings, which in total can be formulated with:

$$DUR_{Con} = N_{Moor}T_{Con} \quad (17)$$

The turbine integration can be formulated with the following formulas:

$$DUR_{Tow} = N_{Tow}T_{Tow} \quad (18)$$

$$DUR_{Nac} = N_{Nac}T_{Nac} \quad (19)$$

$$DUR_{Bld} = N_{Bld}T_{Bld} \quad (20)$$

As previously described, the tower is assumed to be lifted and installed in one piece. In most cases, the nacelle is installed in one piece, but if the integration sequence plans to integrate the hub separately, N_{Nac} could be 2. The commissioning can be simply formulated as follows:

$$DUR_{Com} = T_{Com} \quad (21)$$

For the shuttling scenario, the vessel must also jack down when it runs out of components. As this procedure requires no preloading, the jacking-down duration is described in this model with:

$$DUR_{Jd} = \frac{T_{Pos}}{2} \quad (22)$$

After it is jacked down, it must return to the storage port with DUR_{Trans} .

Applying the introduced values to those parameters returns the total installation time, which for the feeder scenario can be formulated with:

$$T_{Tot} = DUR_{Pos} + N_{Wtb}(DUR_{Load} + DUR_{Con} + DUR_{Tow} + DUR_{Nac} + DUR_{Bld} + DUR_{Com}) \quad (23)$$

The formulation becomes a bit more complicated for the shuttling due to the loading of components every three turbines and the transit, but generally, it is quite similar. The total cost can be calculated based on this total time, which for the feeder scenario can be formulated with:

$$COST_{Tot} = T_{Tot} \frac{(CHT_J + CHT_B + 3CHT_T + 4CHT_C + CHT_{Ctv})}{24} \quad (24)$$

For the shuttling case, the cost differs slightly, as no barge and one less tug boat are needed:

$$COST_{Tot} = T_{Tot} \frac{(CHT_J + 2CHT_T + 4CHT_C + CHT_{Ctv})}{24} \quad (25)$$

6.3.3 Results

The calm weather Python model has now been run for the 96MW White Cross wind farm with the examined input parameters, assumptions and mathematical formulations. The outcomes of the calm weather model are represented in the total installation time and the total installation cost, which can be seen in Figure 64 and Figure 65. The model has been run for both the shuttling and feeder scenarios and the different operation time estimates of Table 16. As can be seen, the utilization of the feeder barge reduces the total installation time by around 65 to 82h or, on average, three days. Generally, due to the low number of turbines which need to be integrated, the total installation time is fairly low, with only 14 to 23 days, depending on the assumed scenario. Therefore, the daily charter rate of the vessel could be fairly high as usually the vessel owners aim for a charter time of at least 30 days (Thomsen et al., 2014, p.215). The difference in the installation

times between both scenarios is the smallest for the long-duration operation case and the largest for the quicker operation case. This is because the additional shuttling time has a larger effect on the operation time if the operation is executed faster, while its contribution to the total time is relatively lower if the integration sequence takes longer.

The difference between the feeder and the shuttling scenario becomes smaller when looking at the cost of the integration sequence. While the installation time was around 17.8-19.6% higher than the feeder, the calculated cost increase is only 12.3-14.1% due to the reduced amount of vessels that need to be chartered for the integration sequence. Still, the chartering of the extra vessels pays off for the feeder scenario as the wind turbine integration can be executed faster and cheaper than the shuttling scenario. The cost of the mean feeder scenario is calculated to be around €4 million, which, assuming the wind farm CAPEX of £3.52 million (\approx €4.12 million/MW) = €395.5 million (BVG Associates et al., 2023d), would make up around 1.01% of the total project CAPEX.

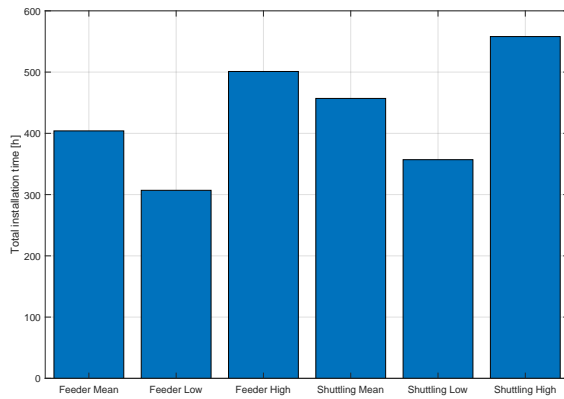


Figure 64: Total installation time in the calm weather model

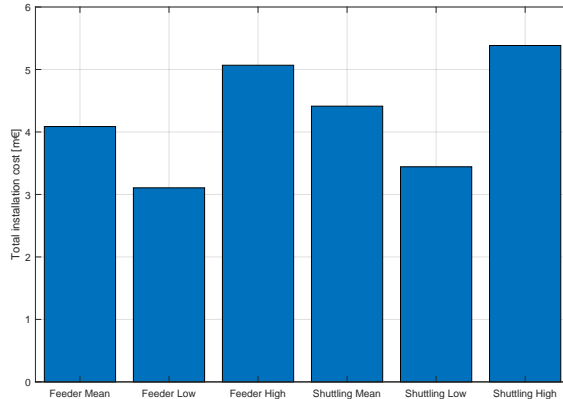


Figure 65: Total installation cost in the calm weather model

6.4 Weather restricted model

Now, based on Boer’s work, the calm weather model is being extended to include the operational limits of each task in the integration sequence and model the operation under the influence of the weather data (Boer, 2022, p.33). The operational limits are determined based on the operation’s physical limits, which would exceed the critical boundary if the environmental conditions get harsher. If the environmental conditions are below the operational limits throughout the operation time, the conditions can be regarded as an allowable sea state. However, if the weather exceeds the operational limits, the model will wait on suitable weather conditions. Those wait-on-weather (WoW) times will increase the installation time and cost as the vessel will be rented throughout the entire time, regardless of whether the vessel can operate.

The operational limits can vary a lot from operation to operation and the used vessel. Some operations are more sensitive to wind loads, while others are mainly restricted by waves. The goal of this analysis is also to understand which environmental condition has the larger influence on the waiting time and which task of the integration sequence is causing the longest waiting times.

Boer has previously verified the used model. As only the integration sequence and some tweaks like additional counters or conditions have been changed without differing the core structure of the model, it is assumed to be sufficient that no further verification is needed (Boer, 2022, p.49).

6.4.1 Weather windows

In the model, the weather conditions are assessed based on the historical hindcast data of Port Talbot, which was already discussed previously in chapter 3.2. When in the weather data the operational limits of H_s , T_p and U are not exceeded for the entire duration of the operation, it is a favourable weather window. If this weather window is long enough, several operations can be completed within the window. If the weather window is bad, the operation needs to wait (wait on weather), which increases the duration of the operation and cost. The model is run ten times for the weather data from 2011 to 2020 to cover scenarios with harsher and calmer conditions. Subsequently, the average of those ten years of data is taken to have a sufficient estimate for the times and cost.

The model is working hourly, with the historical data provided accordingly. If the operational limits are exceeded during the proposed time frame, the model will wait one hour to see if the operational conditions are acceptable. An example of one complete turbine integration sequence can be seen in Figure 66. The sequence shows that after the connection of the floater, the integration activity must halt for 17 hours, as the wind and wave conditions, which were still sufficient for the connection/preparation, are both exceeded. After the tower has been integrated, the operation must wait ten more hours as the wind speed exceeds the limitation of the nacelle integration. As seen in the figure, the blade installation of all three blades has been regarded so far as one task. However, when considering the weather-restricted model, it makes more sense to split the single blade installation into three separate steps for every blade, as the good weather window can be substantially shorter than waiting on a weather window where all three blades can be installed simultaneously. This separation in parts only makes sense for the single blade installation where the operational procedure is fully completed after the first component is installed and afterwards, it is simply repeated. It can not be done to transfer the components onto the deck or the mooring hook-up of the floater, as those are complete tasks where only a partial completion could endanger the system's safety or cause other problems.

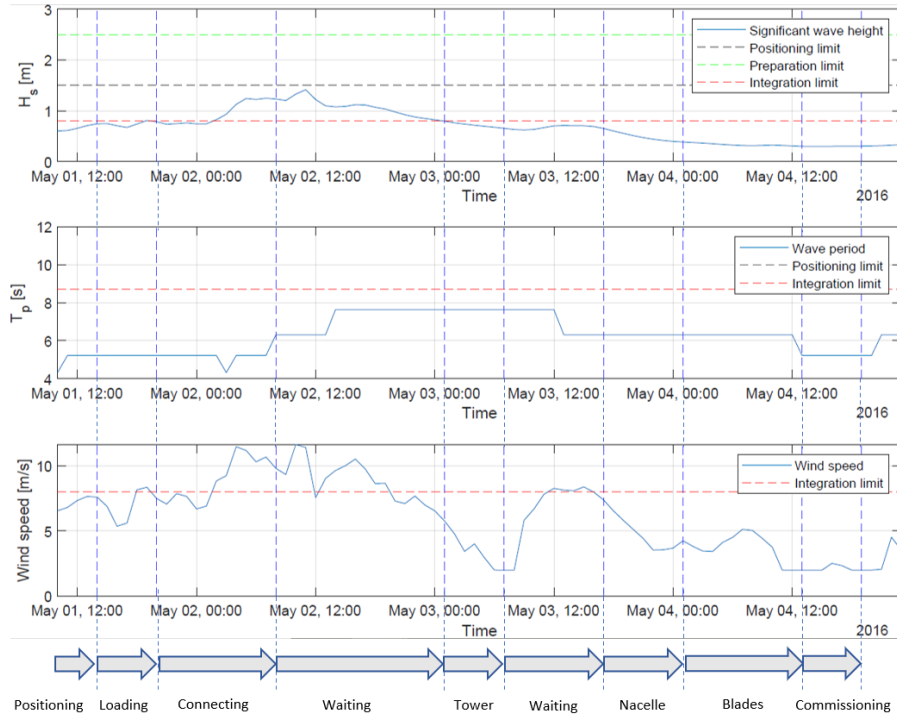


Figure 66: Exemplary integration sequence of a turbine for the weather data of 2016

6.4.2 Operational limits

The operational limits used in this simulation are assumed based on the conducted study in chapter 5 and publicly available values. The estimated limits for the significant wave height, peak period and wind speed are displayed in Table 17. The operational limits for the single blade installation are based on the accepted load cases for the procedure in Table 14. The mating is only a minor part of the total single blade installation time. However, as previously discussed, the entire alignment procedure is unlikely to be initiated when the conditions are too rough for mating. Therefore, the mating limit is assumed to be the operational limit of the entire single blade installation. Furthermore, the nacelle integration is also known to be fairly critical, as only displacements of a few centimetres are allowed without suitable guidance systems. For a better estimation of the operational limit of the nacelle integration, it should be studied in detail like the single blade installation has been, but for this operability analysis, it is assumed to have the same limitation as the single blade installation. The same goes for the tower installation, which in theory, is a bit simpler than the nacelle installation, as the rotational motion of the floater just above the water line is not as impactful. But as the lift of the fully assembled tower is the heaviest and as the bolt mating of the tower base is also most likely quite sensitive, the operational limit of the blade installation is also applied for the tower integration.

The limit of the transit comes from the spec sheet of the vessel (Fred. Olsen Windcarrier, 2023b) while for this case, not the local environmental data from Port Talbot is assessed, but the hindcast

data of a location in between Port Talbot and the storage port (51.51634°N, -4.611618°W) which was also retrieved from the NORA3 model. The positioning limit stems from the limitation of the jacking operation, where longer or higher waves would induce a very high overturning moment on the jack-up and especially high loads on the leg that is initially stabbed into the ground (Thomsen et al., 2014, p.232). Based on the limits of a purpose build feeder vessel, the limits of the transfer of the components are assumed to be possible for significant wave heights up to 2.5m, even though a simple barge has most likely lower limitations, but no detailed info on this operation was found (C-Job, 2021). This limit only applies to the feeder scenario. In the shuttling scenario, the jack-up is assumed to go to a sheltered port area where it loads the components onto its deck in a jacked-up state, thus unaffected by environmental conditions. The mooring connection and disconnection can generally happen in fairly rough wave conditions. However, the crew must also get on and off the floater during those operations. The most common limit for the transfer of crew offshore is 2.5m.

As it has been discussed in chapter 6.2, it is generally a large simplification to assess the operational limits based on fixed values for H_s and T_p , where proper limits should be determined as a combination of both values for different wind speeds like in Figure 99 in Appendix Q. However, due to the lack of those detailed limits for the operation, the simplified limits are used.

Operation task	H_s limit	T_p limit	Wind limit
Transit	3.5m	-	-
Positioning	1.5m	12s	-
Component transfer	2.5m	-	-
Floater connection	2.5m	-	-
Tower integration	0.8m	8.7s	8m/s
Nacelle integration	0.8m	8.7s	8m/s
Blade integration	0.8m	8.7s	8m/s
Commissioning	2.5m	-	-

Table 17: Operational limits of the integration sequence

Given that the integration sequence of high tidal range, the current speed could be also quite high in the location, while only a maximum of 0.5m/s was simulated for the Swansea Bay (Uncles, 2010, p.9). The maximum limit for positioning a jack-up vessel is 2kn ($\approx 1.03m/s$), whereby those currents would be still sufficient (Thomsen et al., 2014, p.231). A detailed operability study should also utilise detailed current data as all positioning activities of the jack-up, barge and floater might be challenging if the currents were stronger. Due to the lack of sufficient current data and the maximum current speed of 0.5m/s, currents are not regarded in this study.

To account for the uncertainty of the weather data, the so-called alpha factor is often applied to the operational limits, which were determined based on the design limits. This alpha factor is multiplied with the design limit and is also regarding the higher uncertainty for longer operations. It is very challenging to forecast accurately low significant wave heights as they have a lower resolution, while the numerical wave models are also less accurate in coastal areas (Alday et al., 2022, p.1). Therefore, the alpha factor for the turbine integration H_s limits is especially low to account for the higher uncertainty. The values of the alpha factors can be found in DNV-OS-H101 and are

presented for waves and wind in Table 18 and Table 19. T_{Pop} represents the planned operation time, which is below 12h for all operations in the integration sequence. For the wave alpha factor, the value should be calculated with linear interpolation if the H_s limit is in between it. The alpha factor for the wind is determined based on the relation of the ten-year maximum wind speed and the design wind speed limit.

Operation period	$H_s=1$	$H_s=2$	$H_s=4$	$H_s \geq 6$
$T_{Pop} \leq 12$	0.65	0.76	0.79	0.8
$T_{Pop} \leq 24$	0.63	0.73	0.76	0.78
$T_{Pop} \leq 36$	0.62	0.71	0.73	0.76
$T_{Pop} \leq 48$	0.6	0.68	0.71	0.74
$T_{Pop} \leq 72$	0.55	0.63	0.68	0.72

Table 18: Alpha factor for waves in the base case (DNV, 2011, p.32)

Operation period	Design wind seed V_d	
	$V_d < 0.5 V_{10yr}$	$V_d > 0.5 V_{10yr}$
$T_{Pop} \leq 24$	0.8	0.85
$T_{Pop} \leq 48$	0.75	0.8
$T_{Pop} \leq 72$	0.7	0.75

Table 19: Alpha factor for wind (DNV, 2011, p.33)

Table 20 represents the operational limits if the alpha factors were to be applied to the operational limits in Table 17. Especially for the turbine integration, the limits become very low. As the operability analysis is based on historical data, the operational limits of Table 17 with $\alpha = 1$ are used as the initial reference. The impact of the reduced limits will be further discussed in chapter 6.4.4, which will also discuss more relaxed operational limits for the turbine integration. In this case, only the alignment limits are applied to all operations, as the mating limits might be overly conservative for the tower and nacelle integration.

Operation task	H_s limit	T_p limit	Wind limit
Transit	2.7m	-	-
Positioning	1.06m	12s	-
Component transfer	1.92m	-	-
Floater connection	1.92m	-	-
Tower integration	0.52m	8.7s	6.4m/s
Nacelle integration	0.52m	8.7s	6.4m/s
Blade integration	0.52m	8.7s	6.4m/s
Commissioning	1.92m	-	-

Table 20: Operational limits with applied alpha factor

6.4.3 Results

The weather-restricted model is now run for both the shuttling and the feeder barge scenario with different assumptions for the installation time for the historical hindcast weather data from 2011 to 2020. The model is also determining the total waiting time as well as the waiting time of the individual task and also the cause for the waiting time. The outcomes of this study will be examined in this chapter.

Figure 67 and Figure 68 display the outcomes of the weather-restricted model in terms of total installation time and cost. The values are the average of the calculations for the ten different years, while also the standard deviation is displayed. The values are compared to the calm weather model to better understand the increase in time and cost due to the waiting on weather. The figures show that both the time and the cost are increasing substantially when regarding the weather limitations. The increase is even more significant for the scenarios with the increased operation time as this will require a good weather window for an even longer duration, while the relative increase with the reduced operation time is much lower as the good weather windows can be shorter.

In comparison to the calm weather model, the duration to install the eight wind turbines has more than doubled across all cases and lies in the mean at 42.1 days for the feeder scenario (calm: 16.5 days) and 47.09 days for the shuttling scenario (calm: 19.21 days). The time difference between both scenarios is the largest when comparing the short operation case (11.84%), while it is lower for the long operation case (7.02%). However, this difference has already gotten substantially smaller compared to the 17.8-19.6% time difference between both scenarios in the calm weather model. In theory, this could be accounted for the additional weather-restricted operation of the feeder operation when the components need to be transferred from the barge on the vessel. However, as Figure 71 shows, the transfer didn't have a single waiting hour for any of the feeder cases. Instead, this observation can be accounted to the total waiting times displayed in Figure 69. As can be seen, the average waiting time is very similar for the same case in the feeder and shuttling scenario, where for instance, the waiting time on the high case is only 0.4% different, while the others are also only 1.5% and 7.7% different. Those total wait hours are added on top of the theoretical calm weather model, where as mentioned, the shuttling scenario took 17.8-19.6% longer. Therefore, the relative increase of the shuttling scenario is smaller and thus the relative difference between the scenarios also became smaller.

The fact that the average waiting time is not completely the same between the two scenarios can be accounted to the different integration sequences of both scenarios, where the different starting times of each operation step lead to other operation time windows and thus also different weather windows which result in different waiting times. The standard deviation of the different installation scenarios is in the range of 136-272h. It is reasonable that the standard deviation of all cases is fairly similar as they all are based on the same years of weather data and thus all experience the same amount of harsh and good weather years. The fact that they all are not exactly the same, which could be expected as they are based on the same data, highlights again the importance and impact of the different integration sequences where different time windows for the operation lead to different waiting times.

Like the time, also the cost has substantially increased compared to the calm weather scenario. As the vessel cost per hour is lower for the shuttling, the additional waiting times also don't have

economically as much of an impact, whereby the shuttling is only 6.77% more expensive than the feeder, the min case costs 4.42% more and the max case is only 2.13% more. The integration sequence of the feeder scenario would cost €10.22 million, which is an increase of 155% and would make up now 2.58% of the total project CAPEX.

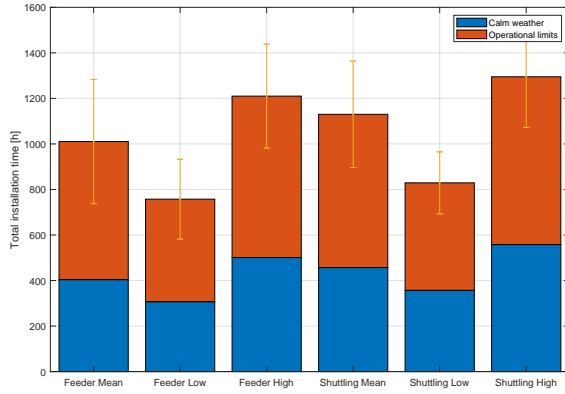


Figure 67: Average total installation time in the weather-restricted model

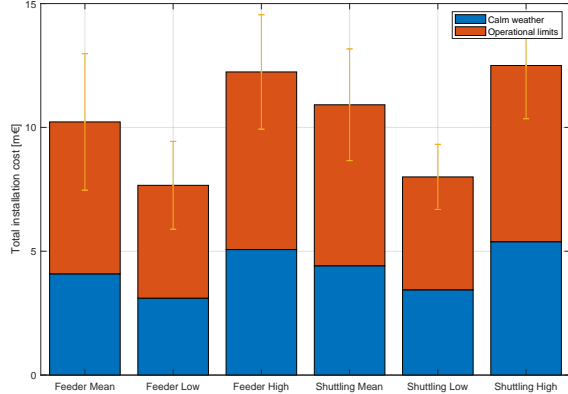


Figure 68: Average total installation cost in the weather-restricted model

In regards to the waiting time, Figure 69 shows the previously described observation that the waiting time also increases with the estimated duration of the task as longer weather windows have to be waited for. The causes for the waiting time in Figure 69 have been grouped in wind and waves in general, not H_s or T_p , as the waves always occur as a combined state where H_s and T_p are only two measures for the same wave. Generally, the model is accounting for a waiting time once any of the H_s , T_p or U limits are exceeded. To understand which condition was the cause for the waiting time, the model is checking if only the wind speed, only the waves or both are exceeding the operational limits. For the operations where the operational limits are only defined for waves it is accounted for the wave-only wait time. The figure shows that most often a pure exceedance of the wave limit is causing the waiting time as it accounts for 75.6-77.9% of the time that the operations have to halt to due environmental conditions. Further 15.5-17.7% of the waiting times are environmental conditions where both wind and waves exceed the limit. This can be accounted to the fact that the operational limits of the integration task were determined for the single blade installation, where especially the wave-induced motions of the floater lead very fast to the exceedance of the acceptable limits during mating, thus the operational limit for the waves is fairly harsh. The wind-only case makes only up 5.7-7.0% of the waiting time.

The operability of the vessels is determined when comparing the total installation time of the calm weather model (operability 100%) to the one of the weather-restricted model. The results are presented in Figure 70, where it can be seen that the operability drops down to the range of 38.1-47.8% once the weather restrictions are included. Therefore, the vessels can only be used less than half of the time while they are chartered. With the given integration sequence, it is also not possible to utilize the vessels in another way while they have to wait on suitable conditions especially as the turbine integration tasks are the main cause of the waiting time as Figure 71 shows. As the waiting time is increasing with the estimated duration of the operation, the operability of

the cases with the low time estimates is the highest while the high time estimates lead to the lowest operability. The operability of the shuttling scenario is higher than the feeder scenario as both have a very similar average waiting time but the calm weather shuttling integration sequence takes longer, therefore the relative operability is higher.

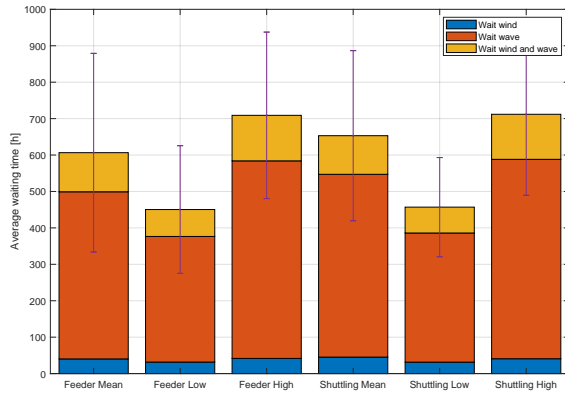


Figure 69: Average waiting time separated by wind and waves

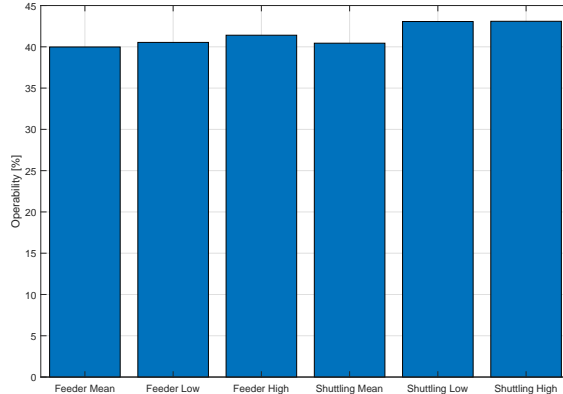


Figure 70: Average operability of the different scenarios and cases under weather restriction

As it can be seen in Figure 71, even the ten years average of the waiting times of the different operations can vary largely. This can be especially seen in the integration tasks when both the feeder and the shuttling have exactly the same operational time but the different integration sequences can lead to vastly different average waiting times. Generally, the low time case has the lowest waiting time per task, while the max has the highest as the weather windows need to be good for a longer duration. However, examples like the feeder waiting time for the nacelle integration also show, that this is not always the case as the waiting time of the high case is actually the lowest. This shows the importance of suitable weather windows and how random the waiting time can be from year to year. However, despite the variation in the average waiting time for the individual tasks, it is worth noting that the total waiting time is still following the trend that the waiting time increases with the assumed operation duration.

In regards to the individual operation tasks, during the shuttling scenario, the vessel never has to wait for good conditions as the operational limit is fairly high while the sea conditions are fairly moderate at the investigated location. In the shuttling scenario, the jack-up would need to be positioned and jacked-up several times which leads to additional waiting times which on average are in the range of 12.2-42.4h while the feeder scenario has no extra waiting time for the positioning. In the port location the component transfer from the barge onto the vessel, the connection of the floater and the commissioning can happen without any further delays due to weather restrictions. For both the feeder and the shuttling scenario the wind turbine integration is by far the largest cause for the waiting on weather. Even though the tower integration is assumed to be done 2h faster than the integration of the nacelle with the same operational limits, the waiting time for the tower integration is substantially larger on average. This is because the tower integration happens after the mooring connection where the limits were more relaxed. After a suitable weather window for the tower integration occurs, it is quite likely that the weather window remains fairly calm so

that also the nacelle integration takes place. However, after a certain time, the weather changes again which can be seen for the blade installation, which has a larger average waiting time than most of the cases of the nacelle integration even though the single blade installations of the three blades are considered separately.

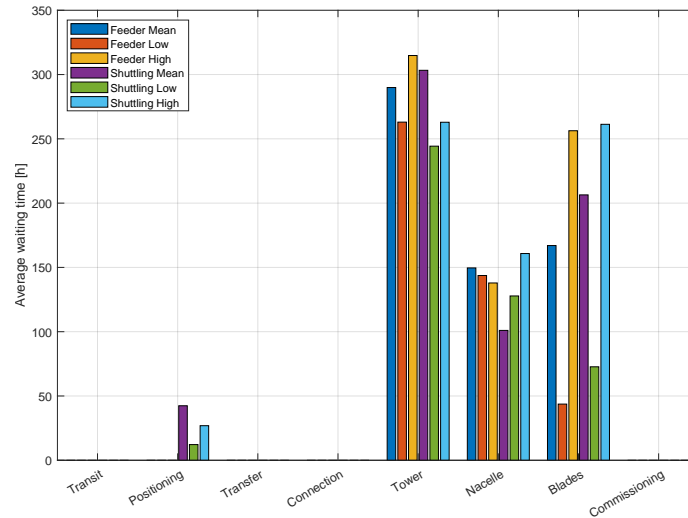


Figure 71: Waiting times of the different operations for all cases

To better understand how the waiting time is impacting the operational duration of each individual task of the integration sequence, Figure 72 is presenting the combination of the individual task and its associated average waiting time for both the mean feeder and mean shuttling scenario. Again it can be seen that mainly the wind turbine integration tasks are affected by the operational limits, where the installation times more than doubled for all the tasks and even increased more than sevenfold for the tower. Also, the impact of the shuttling scenario on the calm operation times becomes clear as also the transit time and the additional time of the multiple positioning operations (including jacking down) are visualised. However, in comparison to the wind turbine integration with the weather restrictions, those additional tasks are relatively short.

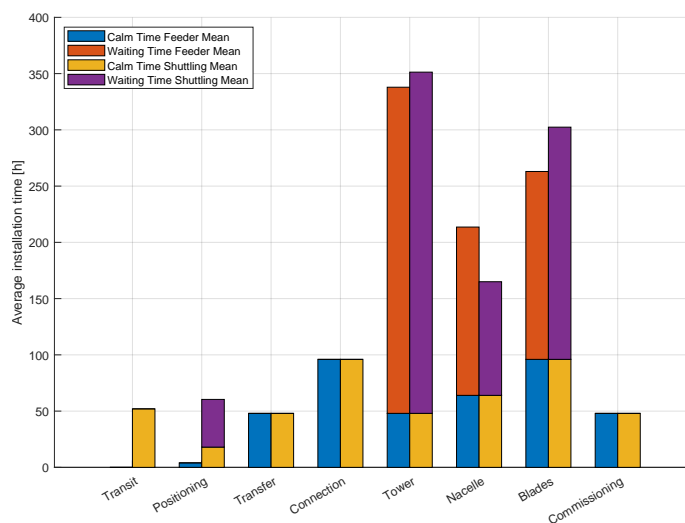


Figure 72: Waiting times of the different operations for all cases

6.4.4 Sensitivity analysis

The outcomes of the operability analysis are depending a lot on the assumptions and input parameters. While the sensitivity of the model can be tested by changing those parameters, the focus should be on three of them as they are related to some of the major assumptions of this work. The first factor is the large uncertainty of the operational limits which have been determined in this work. There is a lack of detailed studies on the tower and nacelle integration, and given that the single blade installation is very sensitive, it could be the case that the assumed operational limits for the integration are overly conservative. In contrast, also more restrictive operational limits should be tested as working with forecast data has a high uncertainty. The second major assumption was the starting time in May. As the operability analysis showed, some of the integration tasks are very sensitive to environmental loads. Therefore, it is of interest to know the impact of other starting dates in the year. Furthermore, it should be investigated what impact the size of the proposed wind farm has on the outcomes of the operability analysis. It could be beneficial if the concept is utilised for several smaller projects consecutive or even for large scale commercial scale projects, therefore the model is run on different project sizes. Other factors which could be investigated are different cost, environmental data from different sheltered locations, trying to account for the delays or change the number of vessels which are involved in the integration sequence. However, testing all factors would exceed the scope of this thesis.

Initially, alternative operability limits to the ones of chapter 6.4.2 shall be investigated. Case one are harsher operational limits, where the alpha factor is applied to the operational limit which were previously used. As the previous chapter has shown, already smaller H_s can cause issues for the wind turbine integration and generally, those smaller wave heights are harder to predict during the operations. Therefore, the lower alpha value has to be chosen, while the low operating time allows the higher values of the category. The second case is a scenario where more loose operational limits are used for the wind turbine integration, which is by far the largest factor for the waiting

time. Those operational limits are now set to the limits of the alignment procedure in chapter 5.6, which were: $H_{s,max} = 1.6m$, $T_{p,max} = 11s$ and $U_{max} = 12m/s$. The outcomes of the modelling with the different operational limits are displayed in Figure 73 to Figure 74 where the time and cost of the different operational limits as well as the default case are portrayed with the standard deviation of the most restrictive case. If the harsher limits were used, the total time to execute the integration sequence of the eight turbines would increase to around 48.6 to 81.9 days or 6 to 10 days per turbine. Given that the industry rule of thumb is usually to integrate one wind turbine within 24h, this represents a massive increase. Also, regarding estimated cost, this project would become significantly more expensive in the range of €11.8 to €19 million, which would make up 2.05-3.3% of the projected CAPEX.

The more loose boundaries decrease the estimated time and cost drastically because, as chapter 6.4.3 showed, the limitations on the wave conditions were governing the required waiting time for the turbine integration, which make up the majority of the waiting time of the integration sequence. By doubling the allowable H_s limit and also increasing the allowable T_p and U , the total installation time is now in the range of 17 to 31.5 days and the cost in a range of €4.1 to €7.3 million.

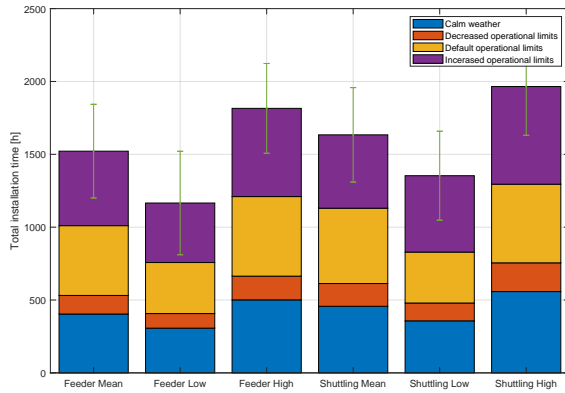


Figure 73: Average total installation time with different operational limits

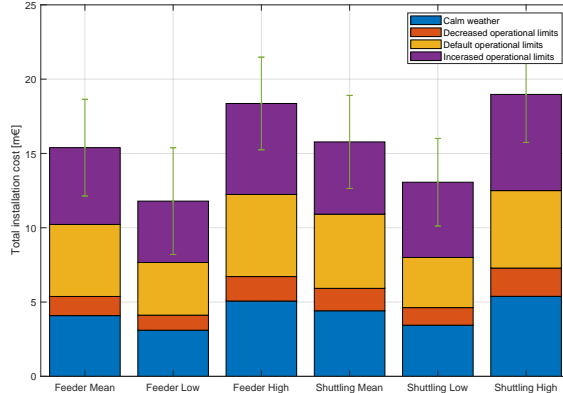


Figure 74: Average total installation cost with different operational limits

As can be expected, also the operability of the project is largely impacted by the operational limits. Figure 100 in Appendix R shows the operability of the different limits, where the increased waiting times due to the alpha-factored limits lead to an operability of 26.3 to 28.4%. Given the very high charter rates and the long required installation time in this case, it becomes very questionable whether it is still feasible to rent those very high-cost vessels if they are utilized only a quarter of the paid time. For the loosened-up operational limits, the waiting time substantially decreases. Thus, the operability is also still very high in the range of 73.9 to 76.03%. This high utilization rate makes it more promising that the project is more feasible, even though the very short installation time also imposes higher charter rates of the jack-up as the usually minimal charter time is 30 days.

The next aspect, which should be investigated, is the starting time of the entire integration sequence. As the installation time of the eight turbines is optimally fairly low and as the market

for the newer large installation vessels is very sparse, it might become hard to actually charter the jack-up during the favourable summer season. Therefore, Figure 75 investigates the total installation time if the mean feeder scenario would start at different times throughout the year. The starting day is always the first of the month at 10 am. The installation time follows a clear trend where during the winter months the installation time is higher and then steadily decreases with the calmer summer months approaching. The starting month with the fastest and thus cheapest integration sequence is July, with a total duration of 33.9 days which is equivalent to costs of € 7.99 million. If the operation would start in the months after July, the installation time would increase again, where a starting date in December would lead to the longest installation time of on average 104.95 days which would cost on average €25.48 million. Figure 75 shows a very large standard deviation for a starting time in October. This shows that a start of the operation in that month would make the integration sequence far less predictable in regards to cost and time as both a very calm and a very rough autumn weather are possible. If the wind turbine integration task should be executed outside of the highly demanded summer operation window, it is advisable to rather start earlier in the year, where a starting time in March has an 85% higher installation time than in July, and April is only 52% longer. Starting times in the months from October to February would result in installation times which, compared to July, would be 145% larger or even more, which certainly would have an effect on the feasibility of the operation.

Figure 101 in Appendix S is separating the average waiting time with the different starting times in its different components of wind-induced waiting times, wave induces waiting time and occasions where both exceed the limit. It can be seen that the portion of conditions, where only the wind is exceeding the limits remains very small, whereas in the majority of all month, the wave-only condition is causing the longest waiting time. This part is also the one that is varying the most throughout the year, showing that the sea states remain fairly calm in the summer while becoming more rough in winter.

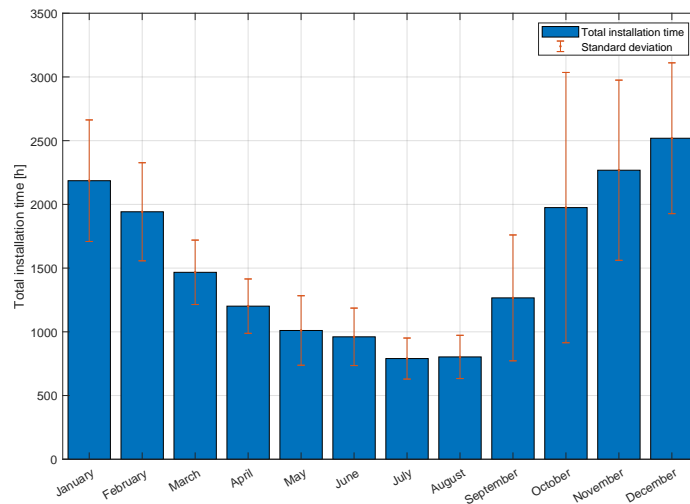


Figure 75: Installation time of the mean feeder scenario when starting at different times

The third sensitivity study should help to understand how the integration system would perform if

it should be used for the integration of larger wind farms than the 96MW one, which is assumed to only consist of eight turbines. Alternatively, it could also be the case that the integration system is utilized for the integration of the turbines of several different smaller wind farms consecutively. Therefore, the model is also run for larger wind farms consisting of sixteen and forty-one 12MW turbines, so a total capacity of 192MW and 492MW. The results of this study are presented in Figure 76 and Figure 77.

It can be seen that while doubling or even more than quintupling the number of turbines that need to be installed, the installation cost and time are not scaling proportionally with this increase. This is due to the fact that by having the default starting date in May, the more favourable summer working conditions are not fully utilized by the eight-turbine case. This can be also seen in Figure 78, which displays the operability of the different wind farm sizes where the 16-turbine project is constantly better than the 8-turbine project while it varies for the 41-turbine project. The 16 turbines are successfully integrated on average in 55.7 to 87.6 days, which means that that is done at the latest in July when assuming the longer operation times, whereby the better weather windows can be more utilized and thus the operability is also higher. The same case goes for the 41-turbine installation project, which is done on average in 128 to 304 days so early September to the end of February and therefore fully utilizing the summer operation window. The large gap between the different possible installation times for different scenarios occurs because the long duration estimate of the shuttling scenario reached into the winter season, whereby the waiting times substantially increase as it is described in Figure 101 in Appendix S. This shows again how important it is to make the installation processes as fast as possible because especially large-scale projects could otherwise experience substantially larger delays due to unfavourable weather conditions.

In regards to cost, the impact of a favourable weather window can be also observed based on those results. The 8-turbine project was mainly conducted in the slightly rougher month of May and thus cost in total 1.94 to 3.16% of the total project CAPEX. Under the same assumption of €4.12 million per MW, the 16 turbine project would cost 1.72 to 2.47% of CAPEX and the 41 turbine project would be 1.57 to 3.54% of the CAPEX, where the range is so large as some integration sequences go into the unfavourable winter month.

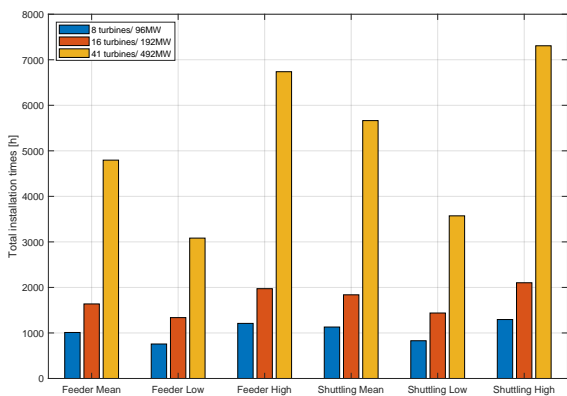


Figure 76: Installation times for the different amounts of turbines to be installed

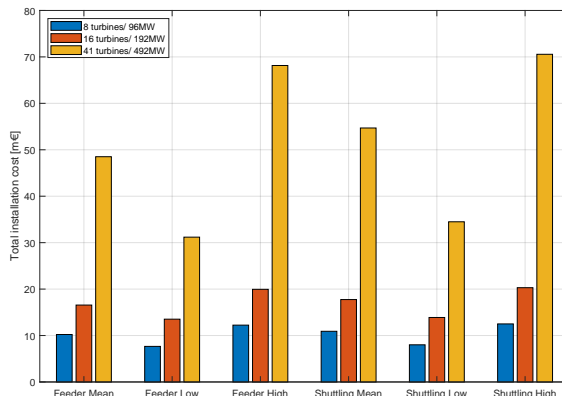


Figure 77: Installation costs for the different amounts of turbines to be installed

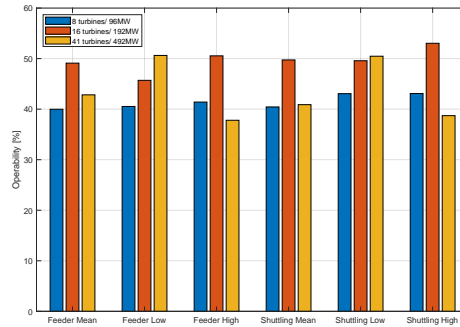


Figure 78: Operability for the different amounts of turbines to be installed

6.5 Discussion

After presenting the outcomes of the operability analysis, it is important to assess the impact of the made assumptions of chapter 6.2 on the simulation outcomes.

One major simplification that has been made is that the model is not using the environmental data from inside the port but a location which is around 2km outside of the port. Therefore, the wave conditions are not correctly represented as the breakwaters of the port of Port Talbot will result in much calmer wave regimes. However, the integration system was found to be mainly sensitive to the wave-induced motions of the floater, which also governs the operational limits. When applying those very restrictive operational limits to a site in open waters, most of the waiting time is due to the exceedance of this wave limitation (in this study on average 76.6%). As the wave regime within a sheltered area is very site-specific, it can not be quantified how the wave-induced waiting time within the port would be, only that it is most likely to be lower than in the open waters and that the calculated waiting times and cost are probably overly conservative. At least the wind-induced waiting times, which made up on average 140h of the total waiting (23.4%), can be applied with fair certainty to the operation within the port as the breakwaters have no effect on the wind.

A further simplification that has been made is not regarding the tides in the operational analysis. Quantifying the impact of the tides onto the integration sequence is hard, as it is not only impacting minimum draft requirements but also have a significant impact on the mooring system and the integration sequence due to the constant vertical variation. As previously described it is unlikely that the proposed mooring system would actually work on site, however this is not directly linked to weather-induced waiting times. For the operability, it could be more important that the integration could only take place if the tidal range is considerably small as too large vertical displacements can't be handled by the crane.

It is hard to factor in the potential added delays due to failures, supply chain issues or other factors as those happen randomized and are hard to predict. A more sophisticated model could regard those by adding an average waiting time of x hours per turbine, based on experience from previous projects, or include the stochastic effects in even more detail. The aim of this thesis is to create a general understanding of the system, where future work would need to investigate many

aspects in more detail. Therefore, those added delays are not regarded while being aware that they will increase the actual waiting time and project cost.

Assuming the same operational limits of the single blade installation for the tower and nacelle integration is probably fairly conservative, given that those operational limits were determined based on minimal allowable displacements of the mating procedure. However, due to the lack of other detailed investigations of the floater integration, those limits are adapted. Generally, the operational limits used in this work are more rough estimations and best guesses. A detailed operability analysis would require operational limits based on operational studies of the most probable sea states for every single operation of the integration sequence.

By not factoring in all the costs related to the integration sequence, the outcomes of the model can't represent a complete estimation of all associated cost. Determining the exact cost of an operation is very challenging as the vessels owners and other suppliers rarely are willing to share their cost to stay competitive within the market while the price structures are also often more complex than assumed in this work. Therefore, most publicly available cost assumptions are generally quite imprecise.

Conducting a detailed operational analysis would also require more detailed data of other local factors such as soil conditions, currents or detailed spatial plans of the port. Knowing those factors would help to map out the integration sequence in more detailed. However, all those factors are likely to increase the operation time as they complicate the sequence. The operational analysis is based on hindcast data, but when the actual operation should take place, historic data is only valuable to a certain extent as the operation needs to use forecast data, which has a higher uncertainty. Therefore, also the alpha-factored operational limits need to be used, which will increase the waiting time.

The integration sequence has been simplified to eight different tasks where durations and limits are determined for each one of them. However, those tasks can be split into several subtasks, which all have their own requirements and limitations. A detailed model should regard every completed task individually, but the eight defined tasks describe the system fairly sufficiently for a first understanding.

6.6 Economic feasibility

An economic feasibility study should assess the value of an investment before committing to a detailed study. It is important that the long-term gains overshadow the short-term costs as the economic feasibility is not given otherwise (Kendall & Kendall, 2011, p.63). Questions that can be asked in this regard are:

- What are the initial cost associated with the technology?
- How much cost could be saved by implementing the technology or are there potential efficiency gains?
- How does the technology compare to existing alternatives?
- How efficient is the technology?

- What are the uncertainties that may affect the financial viability of the concept?

The cost assumptions for the integration of the 96MW wind farm under weather restrictions lay in the range of €79806/MW to €130203/MW and as previously discussed those cost estimates probably won't even represent the full cost of the integration sequence. Generally, those cost can be regarded as fairly high, but they need a reference to be better understood. The initial best guess would be to compare these cost to a port-based integration. In their 2023 Guide to a Floating Offshore Wind farm, ORE Catapult is estimating a share of 1.9% of project CAPEX for a complete port-based turbine integration, which in total numbers is £68000/MW (\approx €79560/MW), where also the load out is included into the cost estimates (BVG Associates et al., 2023d). Those cost can be further divided into the port cost (£28000/MW), the cost of all required lifting equipment for load out and integration (£30000/MW) and cost associated to technicians and other port activities. Comparing these cost to the estimated cost of the operability analysis, which don't even factor in the load out, would make the solution look economically unfeasible. However, the entire premise of the proposed system is to utilize the jack-up in regions where the required port infrastructure is not existing. Therefore, those estimated cost can be more seen as a required investment that is needed to realize the floating offshore wind farm in the first place. The technology would largely contribute to the general success of the project, which has much larger benefits than the slightly larger installation cost (\approx 2.58% CAPEX). This is especially the case for small projects, where the total upfront investment for the proposed concept is still comparably small in absolute terms.

Once the number of turbines to be integrated increases, the absolute investment for larger wind farm projects would also be higher. The investigated large wind farm case with 41 turbines comes already in the range of 50 to 100 turbines integrated per year which Ramirez predicted as the required pipeline for large-scale port investments (Ramirez et al., 2020, p.31). The estimated cost of the larger integration sequence is in the range of €31.2 to €70.6 million. This is still substantially lower than the £400-600bn that Torr predicted for the required cost to upgrade existing port facilities for the requirements of floating wind (Torr, 2022, p.43). However, as previously discussed in the assumptions, the actual cost of the integration sequence is quite likely to be higher as not all costs are factored in. Using the proposed integration system barely creates some any long-term infrastructure, which can be utilized after the jack-up has left, while the concept is also only exclusively suited to the turbine integration. In contrast, the investment in the port infrastructure would also go into other facilities like storage spaces, manufacturing facilities and further equipment. This conflict is more acceptable for smaller projects as the temporary solution should function more like a kickstart for larger projects in the region. But for large wind farm projects, it is unlikely that it would be economically feasible to use the proposed integration system for installing turbines at a larger scale as the return on the investment seems to be too low while a sufficient pipeline of projects would already exist to justify large port investments.

This study has found the feeder vessel to be faster and cheaper than the shuttling concepts. However, the outcome of comparing both scenarios highly depends on the site and its condition. For instance, if in another site the travelling distances were the same for both while the transport vessel would also need to go through rougher sea conditions, it could be possible that the shuttling is cheaper as the jack-up is faster and can travel in rougher sea states.

To assess the efficiency of the system, the estimated time can be considered. If only a few turbines should be installed, this is executed in the best case in only 14 to 23 days and even though

the weather restrictions double this installation time, it is still a fairly small time frame, whereby the system can work efficiently within the summer months of March to September. The sensitivity analysis has shown, that the starting time of the operation has large impact on the installation time. As it is very sensitive to the environmental conditions, an operation in the winter months lead to very long, inefficient delays of the integration sequence. This can get especially problematic when large offshore wind projects should be integrated with this concept. In those scenarios, it might be more feasible and efficient to completely halt the integration sequence before the project is entering the winter months and only start chartering all vessels again once the winter is over. This is common practice within the industry and while the total duration of the integration sequence might increase, the projects operability is much higher and significant waiting costs can be saved. The difference in the installation time between the shuttling and feeder scenarios is comparably low and their difference might be even smaller if both scenarios would utilize the same storage port.

As it has been discussed in the previous chapter, the results of the operability analysis underlie a large range of assumptions. The hindcast data, which has been used, is not properly representing the environmental conditions of Port Talbot and as tides are not regarded. The breakwater is most likely calming down the waves within the port, which would reduce the wave-induced waiting time of the system, which has the largest share of the waiting times. As the model is working sequentially, it is inefficient as some operations could take place in parallel, which would decrease the installation time. At the same time, the alpha-factored limits will need to be used for the actual operation as it will need to rely on forecast data. Also the tides could lead to certain waiting times as a sufficient draft is required for all vessels to enter even if the floater would be lowered to the seabed. Both factors would increase the installation time, but in total, especially the breakwater is expected to drastically decrease the waiting time. Further studies are required to validate this theory. The assumed execution time of every integration task have found to have a drastic impact on the total integration time and cost. To reduce this uncertainty, a more detailed study of the required execution time should be conducted to know the execution times more precisely.

The cost estimations are based on very simplified assumptions where also only a portion of the actual total installation cost is included within the model. Further costs are associated with the investigated integration sequence in regards to preparation and storage spaces. Furthermore, those costs are also only a share of the total turbine assembly cost which also include the load-out. For a detailed conclusion on the financial feasibility of the integration system, the cost should be investigated in much more detail with more complex cost structures and further quantification of all associated costs.

When regarding all those uncertainties, it is very hard to ultimately determine the economic feasibility of the system in the location of Port Talbot or in general. Nevertheless, especially for smaller pre-commercial projects, the system has proven to be substantially cheaper than building out the port infrastructure. Therefore, even though the actual installation time might be lower while the cost per hour might be higher, it can be said that the economic feasibility of the general concept is given for pre-commercial wind farms up to 200MW. If a longer pipeline of projects should be executed, the required cost come closer to the port infrastructure cost. Therefore, for large projects it would be more feasible to build out the port infrastructure as the long-term benefit is much larger compared to the jack-up-based integration.

7 Conclusion

In this work, the novel concept of using a wind turbine installation vessel to integrate a floating semi-submersible wind turbine has been investigated. The main goal of the work is to create a holistic understanding of the system. Therefore, several sub questions have been introduced in chapter 1.1 whose answers can now be assessed.

It was found that current ports would struggle with the turbine integration tasks due to the limitation of cranes and draft requirements, while infrastructure upgrades will be very expensive. Jack-up vessels could help out in this case as less port infrastructure is required, where the vessel can be either utilized just as a crane or as a complete integration unit. The focus of this work was set on the latter, while the other application will most likely also see several implementations in the future. The system is characterised during the single blade installation by large displacements of the hub while the blade displacements are also considerable. The study found that it is very hard to implement a mooring system which sufficiently can restrict the floater motions, especially when being subject to tides. It was also found that it is very hard to restrict the relative motions during the mating procedure to a sufficient extent, especially as the required technology does not exist so far. Conducting a single blade installation of a FOWT with a jack-up vessel is highly limited by the wave induced motions of the floater, while also the wind loads lead to significant displacements of the blade. The operational limits were determined based on a few exemplary load cases. It was found that the limits of the integration task lead to substantial waiting times and cost increases when assessing the complete integration sequence. The cost and installation times of the entire sequence depend largely on the assumed wind farm size and parameters, but it was found that the integration sequence, which preferably should use a feeder concept, can take place at a sufficient time and cost if smaller projects are considered. Based on the outcomes of this work, it can be said that the integration of floating offshore wind turbines with a jack-up vessel can be economically feasible and is also technically possible under the right circumstances. The concept represents an attractive initial solution for locations with large floating wind ambitions, but so far insufficient port infrastructure, when pre-commercial wind farms should be realized as a first step.

The outcomes of this thesis are largely dependent on the variety of assumptions which have been made. Due to the novelty of the concept, there is no work for reference models, which the results can be compared to. It would be very beneficial to validate the outcomes of the numerical study in SIMA with simulations from a different software like ORCAFLEX and also investigate the integration with other floater concepts. The mooring system was found to be insufficient with the local, arguably very unique site conditions. The implementation of the system in other locations has not been investigated and more promising other mooring solutions, which fixate the floater, were not investigated. The simplified operational limits were only determined based on a few load cases while a proper investigation would examine a much larger range of sea states. The modelling was only focused on the single blade installation, where a very restrictive controller has been assumed, while the integration of the nacelle and the tower do require further detailed studies to determine the limitations of the operations. The outcomes of the operability analysis can not be considered as accurate for the investigated site in Port Talbot as the environmental data does not represent the site conditions of the sheltered area correctly. Furthermore, the large tidal range of the site was not considered within the model, whereby the impact of this environmental loading can not be properly judged. The cost assumptions of the system are based on fairly speculative numbers

from literature and most likely don't represent market prices, while the actual cost structure of the integration sequence is likely to be more complex.

Has the main goal of understanding the concept of integrating a floating wind turbine with a jack-up vessel been achieved? Despite the limited scope and the broad range of assumptions, it can be stated that this thesis did address all important aspects of the concept, which certainly does contribute to the understanding of the system. The limitation of the wave-induced floater motions will always play an important role for this integration sequence and it has been also pointed out that it is very challenging to implement a mooring system in shallow water which sufficiently reduces the floater motions. The site conditions of Port Talbot were not accurately represented due to a lack of data and limitations of the model, whereby a suitability of the concept in this location couldn't ultimately be determined. However, this case only served as an example, where the findings of this study should also be transferable to other site locations. Even though a general understanding of the concept has been established, the thesis also showed that the actual implementation of the system in a site require much more detailed studies of all involved components and processes which was not possible in this thesis due to the limited scope of the work.

The main scientific contribution of this work is an initial broad introduction of the concept of using a jack-up vessel for the integration of floating wind turbine. Furthermore, a novel mooring system has been investigated which is implemented in a numerical model that combined modified versions of already existing models. This model then used to conduct the first simplified, academic investigation of a single blade installation of a floating wind turbine in nearshore waters. Furthermore, the operability analysis of the complete integration sequence has been done by modifying and extending an existing model for the proposed floating wind application.

When conducting such a broad analysis of a system it is immanent that mistakes are made on the way and not all can be corrected within the limited time of a thesis. In this work, the load cases have been poorly defined in a method that is not well suited to determine the operational limits accurately. They should have been defined more methodically to represent the probable sea states. Also running the entire model for different wind directions was not of much value as the outcomes gave no clear result while significant computational time was used to also evaluate those direction. As the system is more sensitive to wave loads anyways, it would have been more valuable to assign this time for the calculation of more sea states.

7.1 Recommendations

So far, the concept of using a jack-up vessel for the wind turbine integration has seen no implementation in some projects as of June 2023. However, as highlighted, the number of floating offshore wind farms under development has increased drastically over the past years, with the large magnitude of projects only expected to be realized in the late 2020s or even later. Several of those projects will be first movers in regions that have not encountered floating wind. As this study has shown, it can be feasible to use a jack-up vessel for the integration to implement the concept in the near future. If this is the case, more detailed studies of the system would be required. This thesis had the motivation to create a more general understanding of the proposed concept. Due to the limited scope of this thesis, several simplifications were made and not all aspects of the concept were regarded. Some aspects that future studies of the concept could include would be:

- Numerical modelling of the nacelle and tower integration to understand the limitations of those operations.
- Testing the integration procedure with different semi-submersible or barge concepts to understand the dynamics of the different structures and how much the operation of the integration procedure depends on the floater.
- Different station-keeping systems should be evaluated for the system in detail to find the optimal solution for the integration procedure.
- If the concept should be implemented in areas with a large tidal range, the tides should also be considered in the numerical and operational analysis of the system.
- Some control measurement needs to be developed to sufficiently reduce the relative motions between the blade root and the hub during the mating operation so that the guide pin can be mated without collision.
- Verify the modelling results in a different simulation software like HAWC2.
- A detailed study of the operational limits each integration task needs to be conducted based on methodically well proven load cases or optimally even all probable sea states to understand the limits of the system accurately.
- Extending the operability analysis by factoring in other waiting times, such as unexpected delays due to technical failures, working hours or delayed supplies.
- The cost of the operation should be quantified in more detail with dynamic charter rates but also all other associated costs should be quantified to have a more detailed understanding of the cost.
- Investigate other use cases for the jack-up in floating wind like the use for the port-based wind turbine integration or major component exchanges during operation.
- Investigate the impact of the assumed installation setup with different alignments and distances between the jack-up and the floater.
- Investigate the working procedures of the integration sequence and all associated risks.
- Conduct more sensitivity studies on the integration sequence.

Even though the study of the system was made in a very simplified context, the outcomes of this work has shown that it is worth further investigations. A crucial recommendation for the implementation in future work is to restrict the floater motions as much as possible by fixating the floater in some way, as the wave-induced floater motions are the main cause for the waiting time during the wind turbine integration. This fixation also could alleviate the issue of the tides, which has proven to be a big problem at the investigated site. The study has shown that a jack-up vessel can efficiently perform the integration of small floating offshore wind farms task without much added infrastructure and thus could be an important tool for the the commercialization of floating offshore wind.

References

- 4C Offshore. (2023a). *Global offshore wind map*. Retrieved April 1, 2023, from <https://map.4coffshore.com/offshorewind/>
- 4C Offshore. (2023b). *Provence grand large floating wind farm*. Retrieved May 10, 2023, from <https://www.4coffshore.com/windfarms/france/provence-grand-large-france-fr65.html>
- 4C Offshore. (2023c). *White cross floating wind farm*. Retrieved April 9, 2023, from <https://www.4coffshore.com/windfarms/united-kingdom/white-cross-united-kingdom-uk50.html>
- ABP. (2023). *Swansea*. Retrieved June 2, 2023, from https://www.southwalesports.co.uk/Port_Information/Swansea
- ABP South Wales. (2023a). *Bristol channel tides*. Retrieved April 1, 2023, from https://www.southwalesports.co.uk/Marine_Information/Marine_Information/Bristol_Channel_Tides/
- ABP SouthWales. (2023b). *Port of port talbot*. Retrieved April 13, 2023, from https://www.southwalesports.co.uk/Port_Information/Port_Talbot/
- Ahn, D., Shin, S. C., Kim, S. Y., Kharoufi, H., & Kim, H. C. (2017). Comparative evaluation of different offshore wind turbine installation vessels for korean west–south wind farm. *International Journal of Naval Architecture and Ocean Engineering*, 9, 45–54. <https://doi.org/10.1016/j.ijnaoe.2016.07.004>
- Alday, M., Arduin, F., Dodet, G., & Accensi, M. (2022). Accuracy of numerical wave model results: Application to the atlantic coasts of europe. *Ocean Science*, 18(6), 1665–1689.
- Amaral Jr, J., & Moravia, W. (2020). Thermal properties of polypropylene and high modulus polyethylene fibers reinforced concretes. *Revista IBRACON de Estruturas e Materiais*, 13, 32–38.
- A&P Group. (2023). *A&P falmouth*. Retrieved April 1, 2023, from <https://www.ap-group.co.uk/facilities/ap-falmouth>
- APMG. (2023). *Appraising ppp projects*. Retrieved June 18, 2023, from <https://ppp-certification.com/ppp-certification-guide/appraising-ppp-projects>
- Armstrong, H. (2023). Personal communication [Moreld Ocean Wind].
- Associated British Ports. (2021). *Future ports: Port talbot transformational change for the next industrial revolution*.
- Associated British Ports. (2023). *Port talbot*. Retrieved April 9, 2023, from <https://www.abports.co.uk/locations/port-talbot/>
- Bak, C., Zahle, F., Bitsche, R., Kim, T., Yde, A., Henriksen, L. C., Nata-rajana, A., & Hansen, M. H. (2013). *Description of the dtu 10 mw reference wind turbine*.
- Bessone, M. B., Zaaijer, M., Terzi, D. V., Dykes, K., Jump, E., & Vire, A. (2022). Including installation logistics costs in the optimal sizing of semi-submersibles for floating wind farms. *Journal of Physics: Conference Series*, 2265.
- Bhaskaran, S., Shankar Verma, A., Yuan, S., Jiang, Z., & Henning Halse, K. (2023). A code-to-code comparison for dynamic modeling and response analysis of offshore wind turbine blade mating process. *Journal of Offshore Mechanics and Arctic Engineering*, 145(6), 062003.
- Blue H. (2023). *Historical development*. Retrieved June 27, 2023, from <http://www.blueengineering.com/historical-development.html>
- Boer, H. (2022). *Modelling and estimating the installation duration and cost for an offshore wind farm with and without the consideration of weather limits*. <https://github.com/HugoBoer/Research-Assignment>.
- Borisade, F., Bhat, J., & Matha, D. (2019). *D5.5 overall summary of the industrialization process*.

- Bortolotti, P., Tarrés, H., Dykes, K., Merz, K., Sethuraman, L., Verelst, D., & Zahle, F. (2019). *Iea wind tcp task 37: Systems engineering in wind energy-wp2.1 reference wind turbines*. National Renewable Energy Laboratory (NREL). <https://doi.org/10.2172/1529216>
- Buljan, A. (2022a). *Bold tern gets new crane*. Retrieved April 9, 2023, from <https://www.offshorewind.biz/2022/04/26/bold-tern-gets-new-crane/>
- Buljan, A. (2022b). *Floating wind lcoe to drop below usd 40/mwh by 2050, installed capacity to reach 264 gw*. Retrieved April 18, 2023, from <https://www.offshorewind.biz/2022/02/17/floating-wind-lcoe-to-drop-below-usd-40-mwh-by-2050-installed-capacity-to-reach-264-gw/>
- Buljan, A. (2022c). *Uk industry to explore storing fully assembled floating wind turbines offshore*. Retrieved April 18, 2023, from <https://www.offshorewind.biz/2022/09/09/uk-industry-to-explore-storing-fully-assembled-floating-wind-turbines-offshore/>
- Buljan, A. (2023). *Van oord's aeolus ready for 15 mw wind turbines with crane upgrade no. 2*. Retrieved June 13, 2023, from <https://www.offshorewind.biz/2023/01/20/van-oords-aeolus-ready-for-15-mw-wind-turbines-with-crane-upgrade-no-2/>
- BVG Associates, ORE Catapult, & The Crown Estate. (2019). *Wind farm costs*. Retrieved June 14, 2023, from <https://guidetoanoffshorewindfarm.com/wind-farm-costs>
- BVG Associates, ORE Catapult, The Crown Estate, & FOWCE. (2023a). *I.5 floating offshore wind turbine assembly*. Retrieved June 12, 2023, from <https://guidetofloatingoffshorewind.com/guide/i-installation-and-commissioning/i-5-floating-offshore-wind-turbine-assembly/>
- BVG Associates, ORE Catapult, The Crown Estate, & FOWCE. (2023b). *I.5.1 heavy lifting and moving equipment*. Retrieved June 12, 2023, from <https://guidetofloatingoffshorewind.com/guide/i-installation-and-commissioning/i-5-floating-offshore-wind-turbine-assembly/i-5-1-heavy-lifting-and-moving-equipment/>
- BVG Associates, ORE Catapult, The Crown Estate, & FOWCE. (2023c). *I.8 construction port*. Retrieved June 12, 2023, from <https://floating.pixelhouse.host/guide/i-installation-and-commissioning/i-8-construction-port/>
- BVG Associates, ORE Catapult, The Crown Estate, & FOWCE. (2023d). *Wind farm costs*. Retrieved June 9, 2023, from <https://guidetofloatingoffshorewind.com/wind-farm-costs/>
- Celtic Sea Cluster. (2023). *Ports*. Retrieved April 1, 2023, from <https://celticseacluster.com/ports/>
- CEN, E. C. f. S. (1991). EN 20273:1991 - Fasteners - Clearance Holes for Bolts and Screws.
- Christakos, K. (2021). *Welcome to metwaves's documentation!* Retrieved April 14, 2023, from <https://met-waves.readthedocs.io/en/latest/>
- C-Job. (2021). *C-job x ampelmann — offshore wind feeder vessel*. Retrieved June 5, 2023, from <https://c-job.com/projects/c-job-x-ampelmann-offshore-wind-feeder-vessel/>
- Collins, M., Ferentinos, G., & Banner, F. T. (1979). *The hydrodynamics and sedimentology of a high (tidal and wave) energy embayment (swansea bay, northern bristol channel)*.
- Cordis. (2022). *Offshore windfarm at vindeby*. Retrieved June 27, 2023, from <https://cordis.europa.eu/project/id/WE.-00375-87>
- Cranes Today. (2021). *Power boost*. Retrieved June 18, 2023, from <https://www.cranestodaymagazine.com/features/power-boost-8813944/>
- Cromarty Firth. (2022). *Fred. olsen 1848 backs opportunity cromarty firth's green freeport bid with plans for an innovative mobile port solution*. Retrieved June 12, 2023, from <https://opportunitycromartyfirth.co.uk/fred-olsen-1848-backs-opportunity-cromarty-firths-green-freeport-bid-with-plans-for-an-innovative-mobile-port-solution/>
- Crowle, A. P., & Thies, P. R. (2021). *Construction port requirements for floating offshore wind turbines*. <http://hdl.handle.net/10871/128092>

- Dalley, E. (2023). *47 formosa 2 owf turbines installed*. Retrieved May 8, 2023, from <https://www.projectcargojournal.com/offshore/2023/02/07/47-formosa-2-owf-turbines-installed/?gdp=accept>
- de Leeuw, K. (2019). Single lift blade alignment for large offshore wind turbines: A critical assessment of the alignment process of next generation wind turbine blades.
- Díaz, H., Serna, J., Nieto, J., & Soares, C. G. (2022). Market needs, opportunities and barriers for the floating wind industry. *Journal of Marine Science and Engineering*, 10.
- DNV. (2011). Dnv-os-h101: Marine operations, general.
- Eatough, L. (2021). *Floating offshore wind technology and operation review*.
- EMODnet. (2023). *Emodnet map viewer*. Retrieved April 17, 2023, from <https://emodnet.ec.europa.eu/geoviewer/>
- Equinor. (2022). *Equinor and technip energies enter strategic collaboration for floating wind substructures*. Retrieved April 14, 2023, from <https://www.equinor.com/news/equinor-technip-strategic-collaboration-floating-wind-substructures>
- Equinor. (2023). *Hywind scotland*. Retrieved June 27, 2023, from <https://www.equinor.com/energy/hywind-scotland>
- EuroStat. (2023). *Energy statistics - an overview*. Retrieved June 14, 2023, from https://ec.europa.eu/eurostat/statistics-explained/index.php?title=Energy_statistics_-_an_overview
- Faltinsen, O. (1993). *Sea loads on ships and offshore structures* (Vol. 1). Cambridge university press.
- Flotre, A. (2020). *Rystad energy - size matters in offshore wind, why costlier 14 mw turbines actually reduce the large-scale farm bill*. Retrieved June 18, 2023, from <https://energycentral.com/news/rystad-energy-size-matters-offshore-wind-why-costlier-14-mw-turbines-actually-reduce-large>
- FOWCE & ORE Catapult. (2021). *Floating offshore wind centre of excellence-industrial leadership: Unlocking the uk's floating wind potential*.
- FOWCE & ORE Catapult. (2022a). *Floating offshore wind centre of excellence-international market opportunities*.
- FOWCE & ORE Catapult. (2022b). *Floating offshore wind centre of excellence-manufacturing concrete floating wind foundations in scotland*.
- Fred Olsen 1848. (2023a). *Floating maintenance solution*. Retrieved June 12, 2023, from <https://www.fredolsen1848.com/technologies/floating-maintenance-solution/>
- Fred Olsen 1848. (2023b). *Mobile port solution*. Retrieved June 12, 2023, from <https://www.fredolsen1848.com/technologies/mobile-port-solution/>
- Fred. Olsen Windcarrier. (2022). *A closer look at bold tern's new crane*. Retrieved April 13, 2023, from <https://windcarrier.com/media/news/a-closer-look-at-bold-tern-s-new-crane/>
- Fred. Olsen Windcarrier. (2023a). *Blue tern - ready for your most challenging installations*. Retrieved May 8, 2023, from <https://windcarrier.com/fleet/blue-tern/>
- Fred. Olsen Windcarrier. (2023b). *Bold tern - now with a new 1600t crane*. Retrieved April 13, 2023, from <https://windcarrier.com/fleet/bold-tern/>
- Gao, Z. (2022). Hydrodynamic analysis of offshore wind turbines.
- Gao, Z., Guachamin Acero, W., Li, L., Zhao, Y., Li, C., & Moan, T. (2016). Numerical simulation of marine operations and prediction of operability using response-based criteria with an application to installation of offshore wind turbine support structures. *Proceedings of the Third Marine Operations Specialty Symposium (MOSS2016)*, Singapore, 20–21.

- Gaunaa, M., Bergami, L., Guntur, S., & Zahle, F. (2014). First-order aerodynamic and aeroelastic behavior of a single-blade installation setup. *Journal of physics: conference series*, 524(1), 012073.
- GE Renewable Energy. (2023). *Haliade-x offshore wind turbine*. Retrieved April 14, 2023, from <https://www.ge.com/renewableenergy/wind-energy/offshore-wind/haliade-x-offshore-turbine>
- Gibson, S., & O'loan, W. B. D. (2022). *National ports study*.
- Goh, K. (2022). *Current developments of wind turbine installation vessels*.
- Goward Brown, A., Calverley, M., Creswell, D., Grignon, L., Herson, J., Jeans, G., Leggett, I., Mardell, G., Nicholls, A., O'Cathain, M., Parker, J., Roberts, Z., Stagg, A., & Wakefield, R. (2018). *Metocean procedures guide for offshore renewables*.
- Guachamin Acero, W., Li, L., Gao, Z., & Moan, T. (2016). Methodology for assessment of the operational limits and operability of marine operations. *Ocean Engineering*, 125, 308–327.
- Guachamin Acero, W. I., Gao, Z., & Moan, T. (2017). Numerical study of a novel procedure for installing the tower and rotor nacelle assembly of offshore wind turbines based on the inverted pendulum principle.
- Gucma, S., Gralak, R., Przywarty, M., & Ślkaczka, W. (2022). Maximum safe parameters of out-bound loaded vessels for wind turbine installation. *Applied Sciences*, 12(8), 3868.
- GWEC, Lathigara, A., & Zhao, F. (2022). *Floating offshore wind-a global opportunity*.
- Ha, K. (2020). Reduction of stress concentration factor (scf) on the bolted joint connection for a large wind turbine rotor blade through various design modifications. *Applied Sciences (Switzerland)*, 10. <https://doi.org/10.3390/APP10186588>
- Ha, K., Truong, H. V. A., Dang, T. D., & Ahn, K. K. (2021). Recent control technologies for floating offshore wind energy system: A review. *International Journal of Precision Engineering and Manufacturing-Green Technology*, 8(1), 281–301.
- Hannon, M., Topham, E., Dixon, J., McMillan, D., & Collu, M. (2019). Offshore wind, ready to float? global and uk trends in the floating offshore wind market.
- Hansen, M. O. (2015). *Aerodynamics of wind turbines*. Routledge.
- Harvey, M., Strivens, S., Evans, H., Morris, A., Wendt, F., Matha, D., Phillips, S., Hawkes, G., Sowman, J., Borgarino, B., Lemmer, F., Robic, H., & Raach, S. (2022). *Floating wind joint industry project - phase iv summary report*. www.carrenoir.com
- H-Blix. (2022). *Offshore wind vessel availability until 2030: Baltic sea and polish perspective - final report*.
- Henley, J. (2023). European countries pledge huge expansion of north sea wind farms.
- Hong, S., Zhang, H., Nord, T. S., & Halse, K. H. (2022). Effect of fender system on the dynamic response of onsite installation of floating offshore wind turbines. *Ocean Engineering*, 259, 111830.
- Hutchinson, M., & Zhao, F. (2023). *Gwec global wind report 2023*. www.gwec.net
- Ideol. (2023). *Floating is the future of offshore wind solutions*. Retrieved April 13, 2023, from <https://www.bw-ideol.com/en/technology>
- Ikhennicheu, M., Lynch, M., Doole, S., Borisade, F., Matha, D., Dominguez, J. L., Vicente, R. D., Habekost, T., Ramirez, L., Potestio, S., Molins, C., & Trubat, P. (2020). *D2.1 review of the state of the art of mooring and anchoring designs, technical challenges and identification of relevant dlcs*.
- Irish Offshore Operators Association. (2023). *The irish offshore seabed*. Retrieved April 1, 2023, from <https://iooa.ie/irelands-offshore/#history-of-irish-offshore-exploration>

- James, R., Weng, W., Spradbery, C., Jones, C., Matha, M., Mitzlaff, A., Ahila, R., Frampton, M., & Lopes, M. (2018). *Floating wind joint industry project phase i summary report*.
- Jiang, Z. (2018). The impact of a passive tuned mass damper on offshore single-blade installation. *Journal of Wind Engineering and Industrial Aerodynamics*, 176, 65–77.
- Jiang, Z. (2021). *Installation of offshore wind turbines: A technical review*. Elsevier Ltd.
- Jiang, Z., Gao, Z., Ren, Z., Li, Y., & Duan, L. (2018a). *A parametric study on the final blade installation process for monopile wind turbines under rough environmental conditions*.
- Jiang, Z., Gao, Z., Ren, Z., Li, Y., & Duan, L. (2018b). A parametric study on the final blade installation process for monopile wind turbines under rough environmental conditions. *Engineering Structures*, 172, 1042–1056. <https://doi.org/10.1016/j.engstruct.2018.04.078>
- Kendall, K., & Kendall, J. (2011). *Systems analysis and design*.
- Kikuchi, Y., & Ishihara, T. (2019). Upscaling and levelized cost of energy for offshore wind turbines supported by semi-submersible floating platforms. *Journal of physics: conference series*, 1356(1), 012033.
- Kim, T. (2021). *Installation of an offshore wind turbine blade using a jack-up installation vessel in water depth of 60m*.
- Kim, Y.-K., Shin, J.-R., & Yoon, D.-Y. (2012). *A design of windmill turbine installation vessel using jack-up system*. <http://onepetro.org/ISOPEIOPEC/proceedings-pdf/ISOPE12/All-ISOPE12/ISOPE-I-12-060/1605852/isope-i-12-060.pdf/1>
- Lacal-Arántegui, R., Yusta, J. M., & Domínguez-Navarro, J. A. (2018). Offshore wind installation: Analysing the evidence behind improvements in installation time. *Renewable and Sustainable Energy Reviews*, 92, 133–145.
- Lee, K., Cassidy, M., & Randolph, M. (2013). Bearing capacity on sand overlying clay soils: Experimental and finite-element investigation of potential punch-through failure. *Geotechnique*, 63(15), 1271–1284.
- Liu, T., Halse, K. H., Leira, B. J., Jiang, Z., Chai, W., Brathaug, H.-P., & Hildre, H. P. (2023). Dynamic response of a swath vessel for installing pre-assembled floating wind turbines. *Marine Structures*, 88, 103341.
- Mammoet. (2022). Assembling the world’s largest floating offshore wind farm. Retrieved June 18, 2023, from <https://www.mammoet.com/cases/assembling-the-worlds-largest-floating-offshore-wind-farm/>
- Mammoet. (2023). *Building the world’s tallest floating turbines*. Retrieved June 20, 2023, from <https://www.youtube.com/watch?v=e8eRNUblyDA>
- Mammoet World. (2021a). Ensuring floating wind realizes its potential. Retrieved June 11, 2023, from <https://world.mammoet.com/articles/ensuring-floating-wind-realizes-its-potential/>
- MammoetWorld. (2021b). The path to maturity for floating offshore wind. Retrieved June 18, 2023, from <https://world.mammoet.com/articles/ensuring-floating-wind-realizes-its-potential/>
- Matha, D., Brons-Illig, C., Mitzlaff, A., & Scheffler, R. (2017). Fabrication and installation constraints for floating wind and implications on current infrastructure and design. *Energy Procedia*, 137, 299–306.
- Miceli, F. (2019). *Blades installation: More options than you might think*. Retrieved May 7, 2023, from <https://www.windfarmbop.com/blades-installation-more-options-than-you-might-think/>
- Muhabie, Y. T., Rigo, P., Cepeda, M., de Almeida D’Agosto, M., & Caprace, J.-D. (2018). A discrete-event simulation approach to evaluate the effect of stochastic parameters on offshore wind farms assembly strategies. *Ocean Engineering*, 149, 279–290.

- Musial, W., Butterfield, S., & Boone, A. (2003). Feasibility of floating platform systems for wind turbines: Preprint. <https://www.osti.gov/biblio/15005820>
- Naess, A., & Gaidai, O. (2008). Monte carlo methods for estimating the extreme response of dynamical systems. *Journal of Engineering Mechanics*, *134*(8), 628–636. [https://doi.org/10.1061/\(ASCE\)0733-9399\(2008\)134:8\(628\)](https://doi.org/10.1061/(ASCE)0733-9399(2008)134:8(628))
- Natarajan, A., Hansen, M. H., & Wang, S. (2016). Design load basis for offshore wind turbines.
- Ocergy. (2023). *Sustainable offshore solutions*. Retrieved April 13, 2023, from <https://ocg-wind.com/>
- ORE Catapult. (2020). *Benefits of floating offshore wind to wales and the south west - supply chain report*. https://c.ymcdn.com/sites/www.renewableuk.com/resource/resmgr/publications/Offshore_Wind_Investment_V4.pdf
- Palmer, M. R., Stephenson, G. R., Inall, M. E., Balfour, C., Düsterhus, A., & Green, J. (2015). Turbulence and mixing by internal waves in the celtic sea determined from ocean glider microstructure measurements. *Journal of Marine Systems*, *144*, 57–69.
- Pingree, R., & Mardell, G. (1985). Solitary internal waves in the celtic sea. *Progress in Oceanography*, *14*, 431–441.
- Pinnegar, J., Blanchard, J., Tidd, A., Trenkel, V. M., Pinnegar, J. K., Blanchard, J. L., & Tidd, A. N. (2004). *Can multispecies models be expected to provide better assessments for celtic sea groundfish stocks?* <https://www.researchgate.net/publication/267303278>
- Port of Milford Haven. (2023). *Port of milford haven*. Retrieved April 1, 2023, from <https://www.mhpa.co.uk/>
- Principle Power. (2023a). *Projects*. Retrieved April 14, 2023, from <https://www.principlepower.com/projects>
- Principle Power. (2023b). *The windfloat advantage: Performance - high performance under extreme conditions*. Retrieved April 14, 2023, from <https://www.principlepower.com/windfloat/advantage/performance>
- QuestFWE. (2022). *Floating wind designs of the world*. Retrieved April 13, 2023, from <https://questfwe.com/pbi-fwdi/>
- QuestFWE. (2023). *Floating wind energy projects of the world 2022*.
- Ramachandran, R. C., Desmond, C., Judge, F., Serraris, J.-J., & Murphy, J. (2021). Floating offshore wind turbines: Installation, operation, maintenance and decommissioning challenges and opportunities.
- Ramirez, L., Cecchinato, M., & Potestio, S. (2020). Ports: A key enabler for the floating offshore wind sector.
- Ramirez, L., Fraile, D., & Brindley, G. (2021). *Offshore wind in europe - key trends and statistics 2020*.
- Ren, Z., Jiang, Z., Gao, Z., & Skjetne, R. (2018). Active tugger line force control for single blade installation. *Wind Energy*, *21*(12), 1344–1358.
- Ren, Z., Skjetne, R., Verma, A. S., Jiang, Z., Gao, Z., & Halse, K. H. (2021). Active heave compensation of floating wind turbine installation using a catamaran construction vessel. *Marine Structures*, *75*, 102868.
- RenewableUK. (2022). *Energypulse insights: Offshore wind october 2022 preview copy*.
- Rodrigues, F. (2023). The path to maturity for floating offshore wind. Retrieved June 18, 2023, from <https://world.mammoet.com/articles/the-path-to-maturity-for-floating-offshore-wind/>

- Rognstad, A. T., & Nakstad, I. S. (2020). *Numerical study for single blade installation of an offshore wind turbine comparing a jack-up and a semi-submersible crane vessel in intermediate water depths*.
- RWE. (2022). *Rwe forges partnerships with abp and port of milford haven to deliver floating wind for wales*. Retrieved June 2, 2023, from <https://www.rwe.com/en/press/rwe-renewables/2022-03-31-rwe-forges-ports-partnerships-to-deliver-floating-wind/>
- Sander, A., Haselsteiner, A. F., Barat, K., Janssen, M., Oelker, S., Ohlendorf, J.-H., & Thoben, K.-D. (2020). Relative motion during single blade installation: Measurements from the north sea. *International Conference on Offshore Mechanics and Arctic Engineering, 84416*, V009T09A069.
- Sarker, B. R., & Faiz, T. I. (2017). Minimizing transportation and installation costs for turbines in offshore wind farms. *Renewable Energy, 101*, 667–679.
- SENSEWind. (2023). Sense floating offshore [Online; accessed 11-June-2023].
- Ship Technology. (2016). *Rotra vente roll-on/roll-off vessel*. Retrieved June 2, 2023, from <https://www.ship-technology.com/projects/rotra-vente-roll-onroll-off-vessel/>
- Sieros, G., Chaviaropoulos, P., Sørensen, J. D., Bulder, B. H., & Jamieson, P. (2012). Upscaling wind turbines: Theoretical and practical aspects and their impact on the cost of energy. *Wind Energy, 15*(1), 3–17. <https://doi.org/https://doi.org/10.1002/we.527>
- Silva de Souza, C., Berthelsen, P., Eliassen, L., Bachynski, E., Engebretsen, E., & Haslum, H. (2021). Definition of the ino windmoor 12 mw base case floating wind turbine. *Tech. Rep. OC2020 A-044*.
- Simons, H. (2022). *Feeding the beast optimising the supply chain for offshore wind installation*.
- Skrzypiński, W., Gaunaa, M., & Heinz, J. (2016). Modelling of vortex-induced loading on a single-blade installation setup. *Journal of physics: conference series, 753*(8), 082037.
- Snieckus, D. (2021). Concrete progress: Floating wind spars ready for 'oil-greening' hywind tampen array. Retrieved June 18, 2023, from <https://www.rechargenews.com/wind/concrete-progress-floating-wind-spars-ready-for-oil-greening-hywind-tampen-array/2-1-1069663>
- Solis Boado, Y. (2023). Personal communication [Havfram Wind].
- Spearman, D., Strivens, S., Matha, D., Cosack, N., Macleay, A., Regelink, J., Patel, D., & Walsh, T. (2020). *Phase ii summary report - floating wind joint industry project*.
- Sreenivasan, A., & Voogt, A. (2022). Numerical simulations of offshore wind turbine component lifts to determine installation operability. *International Conference on Offshore Mechanics and Arctic Engineering, 86618*, V001T01A027.
- Statista. (2023). *Renewable electricity mix in the european union from 2013 to 2021, by energy source*. Retrieved June 14, 2023, from <https://www.statista.com/statistics/610362/renewable-electricity-mix-in-eu-28/>
- Stehly, T., & Duffy, P. (2022). 2021 cost of wind energy review.
- Stiesdal. (2023). *Tetra offshore foundations for any water depth*. Retrieved April 13, 2023, from <https://www.stiesdal.com/offshore/tetra-offshore-foundations-for-any-water-depth/>
- Strivens, S., Northridge, E., Evans, H., Harvey, M., Camp, T., & Terry, N. (2021). *Phase iii summary report - floating wind joint industry project*. www.carrenoir.com
- TEHO. (2023). *Magnaro[®] hmpe ropes*. Retrieved May 12, 2023, from <https://www.tehoropes.nl/product/magnaro-hmpe-ropes/>
- The Crown Estate. (2023). *Floating offshore wind*. Retrieved April 1, 2023, from <https://www.thecrownestate.co.uk/en-gb/what-we-do/on-the-seabed/floating-offshore-wind/>

- Thethys. (2022). *Swansea bay tidal lagoon (sbtl)- physical environment*. Retrieved April 17, 2023, from <https://tethys.pnnl.gov/project-sites/swansea-bay-tidal-lagoon-sbt1>
- Thomas, H. (2023). Wales freeports for milford haven-port talbot, anglesey. *BBC*.
- Thomsen, K. E., York, N., & Diego, S. (2014). *Offshore wind - a comprehensive guide to successful offshore wind farm installation*.
- TideTimes. (2023). *Port talbot tide times*. Retrieved May 12, 2023, from <https://www.tidetimes.co.uk/port-talbot-tide-times>
- Tjaberings, J., Fazi, S., & Ursavas, E. (2022). Evaluating operational strategies for the installation of offshore wind turbine substructures. *Renewable and Sustainable Energy Reviews, 170*, 112951.
- Torr, R. (2022). *Strategic infrastructure and supply chain development*.
- Tugdock. (2023). Tugdock. Retrieved June 18, 2023, from <https://tugdock.com/>
- Uncles, R. (2010). Physical properties and processes in the bristol channel and severn estuary. *Marine Pollution Bulletin, 61*(1-3), 5–20.
- van der Kaaij, I. (2023). Evaluating the workability of on-site assembly of a 15mw wind turbine blade on a semi-submersible floating wind turbine using a crane vessel.
- Vanderheggen, K., Janssen, J., & Meredith, N. (2021). *Lifting operations with wind turbine installation jack-ups using real-time data*.
- Verma, A. S., Jiang, Z., Ren, Z., Gao, Z., & Vedvik, N. P. (2020). Effects of wind-wave misalignment on a wind turbine blade mating process: Impact velocities, blade root damages and structural safety assessment. *Journal of Marine Science and Application, 19*, 218–233.
- Verma, A. S., Jiang, Z., Vedvik, N. P., Gao, Z., & Ren, Z. (2019). Impact assessment of a wind turbine blade root during an offshore mating process. *Engineering Structures, 180*, 205–222. <https://doi.org/https://doi.org/10.1016/j.engstruct.2018.11.012>
- Welsh Ports Group. (2023). *Port talbot harbour*. Retrieved April 9, 2023, from <https://directory.welshports.org.uk/ports/port-talbot-harbour>
- White Cross. (2023). *White cross*. Retrieved April 9, 2023, from <https://whitecrossoffshorewind.com/>
- Williams, R., Zhao, F., & Lee, J. (2022). *Gwec global offshore wind report 2022*. www.gwec.net
- WindSpider. (2023). Products. Retrieved June 18, 2023, from <https://windspider.com/products/>
- Wyatt, L. R. (1995). The effect of fetch on the directional spectrum of celtic sea storm waves. *Journal of physical oceanography, 25*(6), 1550–1559.
- Xu, K., Gao, Z., & Moan, T. (2018). Effect of hydrodynamic load modelling on the response of floating wind turbines and its mooring system in small water depths. *Journal of Physics: Conference Series, 1104*.
- Zhang, M. H. (2015). *Wind resource assessment and micro-siting: Science and engineering*. John Wiley & Sons.
- Zhao, Y. (2019). Numerical modeling and dynamic analysis of offshore wind turbine blade installation - doctoral thesis.
- Zhao, Y., Cheng, Z., Sandvik, P. C., Gao, Z., Moan, T., & Buren, E. V. (2018). Numerical modeling and analysis of the dynamic motion response of an offshore wind turbine blade during installation by a jack-up crane vessel. *Ocean Engineering, 165*, 353–364.

Appendix A: Stabilization concepts for floaters

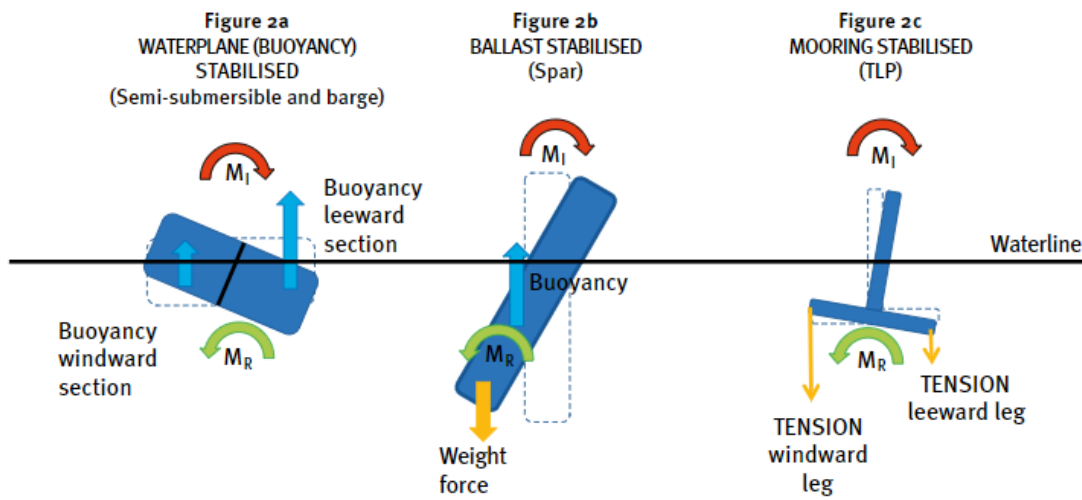


Figure 79: Sketch of the different stabilization types for floating substructures (Hannon et al., 2019, p.18)

Appendix B: Synergies of port facilities

Facility / Infrastructure	Synergies Through Co-location	Impact of Proximity to Project Site on LCOE
Steel substructure component fabrication facility	↑ ↓	M
Concrete substructure construction facility (may be supplied with pre-cast elements from elsewhere)		H
Steel substructure assembly facility	↑ ↓	H
FOWT marshalling, assembly, integration and load out facility		H
Chain manufacturing facility	↑ ↓	L
Synthetic rope manufacturing facility		L
Mooring component manufacturing facility	↑ ↓	L
Mooring marshalling, assembly, integration and load out facility		M
Dynamic cable manufacturing facility	↑ ↓	L
Dynamic cable component manufacturing facility		L
Dynamic cable system marshalling, assembly, integration and load out facility	↑ ↓	M
Operations, maintenance and minor repair support facility		H
Major component exchange facility (and / or sheltered water facility)		H
Decommissioning facility		M

Figure 80: Impact of co-location and proximity to site (H = high, M = moderate, L = low, full line = synergy, dashed line = limited synergy)(Torr, 2022, p.33)

Appendix C: Site distance

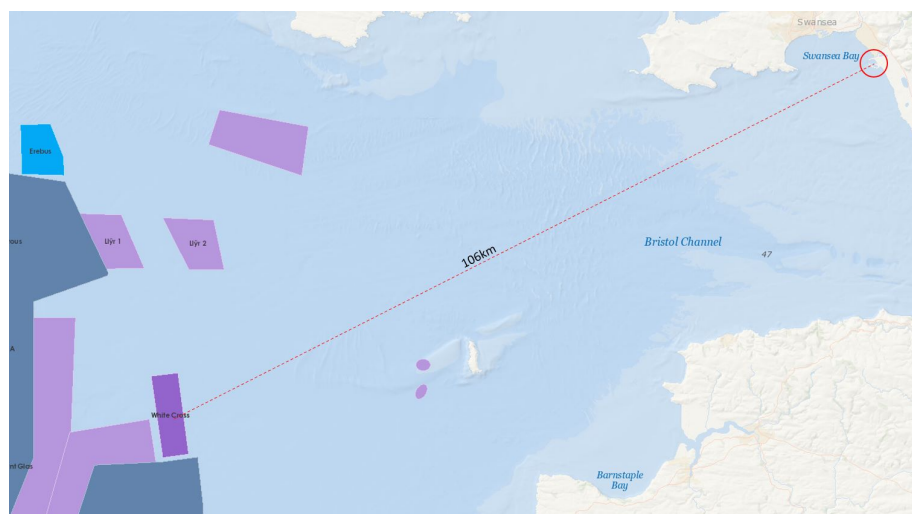


Figure 81: Distance between White Cross site and Port Talbot (4C Offshore, 2023a)

Appendix D: Metocean data on site

Total		0,00	0,00	0,08	1,65	4,12	7,77	11,37	7,39	9,95	12,36	13,77	13,24	10,00	5,03	2,29	0,00	0,74	0,21	0,00	0,03	0,00	0,00	0,00	0,00	0,00	100,00
Hs min [m]	Hs max [m]																										
11,7	12																										
11,4	11,7																										
11,1	11,4																										
10,8	11,1																										
10,5	10,8																										
10,2	10,5																										
9,9	10,2																										
9,6	9,9																										
9,3	9,6																										
9	9,3																										
8,7	9																										
8,4	8,7																										
8,1	8,4																										
7,8	8,1																										
7,5	7,8																										
7,2	7,5																										
6,9	7,2																										
6,6	6,9																										
6,3	6,6																										
6	6,3																										
5,7	6																										
5,4	5,7																										
5,1	5,4																										
4,8	5,1																										
4,5	4,8																										
4,2	4,5																										
3,9	4,2																										
3,6	3,9																										
3,3	3,6																										
3	3,3																										
2,7	3																										
2,4	2,7																										
2,1	2,4																										
1,8	2,1																										
1,5	1,8																										
1,2	1,5																										
0,9	1,2																										
0,6	0,9																										
0,3	0,6																										
0	0,3																										
Tp max [s]		1	2	3	4	5	6	7	8	9	10	11	12	13	14	15	16	17	18	19	20	21	22	23	24	25	
Tp min [s]		0	1	2	3	4	5	6	7	8	9	10	11	12	13	14	15	16	17	18	19	20	21	22	23	24	Total

Figure 82: Scatter diagram of the White Cross site depicting percentage occurrence of significant wave height H_s versus peak wave period T_p , data from NORA3

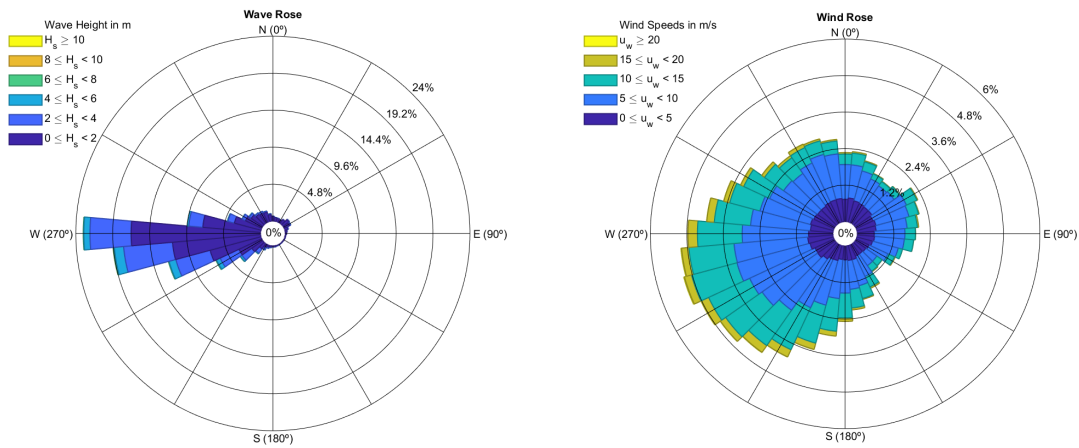


Figure 83: Wave rose of the wind farm site, data from NORA3 **Figure 84:** Wind rose of the wind farm site, data from NORA3

Condition	Duration [h]	Jan	Feb	Mrz	Apr	Mai	Jun	Jul	Aug	Sep	Okt	Nov	Dez	Average
Hs<1.5	3	26,75%	19,40%	46,37%	66,00%	66,65%	70,06%	75,80%	65,84%	62,72%	42,26%	33,96%	20,83%	49,72%
Hs<1.5	6	24,39%	17,28%	44,21%	63,56%	64,13%	67,36%	73,82%	63,08%	59,92%	39,80%	31,25%	19,18%	47,33%
Hs<1.5	12	20,10%	13,64%	40,36%	59,16%	59,85%	62,28%	70,21%	57,94%	54,78%	35,67%	26,45%	16,32%	43,06%
Hs<1.5	24	14,44%	8,33%	34,48%	52,02%	52,94%	53,74%	63,83%	48,85%	46,52%	28,75%	18,98%	11,78%	36,22%
Hs<1.5	48	8,65%	2,89%	26,12%	40,08%	42,06%	40,32%	54,60%	35,44%	35,26%	19,24%	10,27%	6,14%	26,76%
Hs<1.5	72	5,94%	1,32%	20,53%	30,56%	33,01%	31,24%	47,86%	25,26%	28,88%	11,89%	5,79%	3,34%	20,47%

Figure 85: Monthly distribution of the significant wave height below the threshold of 1.5m in the White Cross site, data from NORA3

Appendix E: Velocity triangle

In the velocity triangle L represents the lift force, D the drag force, α the angle of attack, V_{inf} the incoming flow velocity and c the chord.

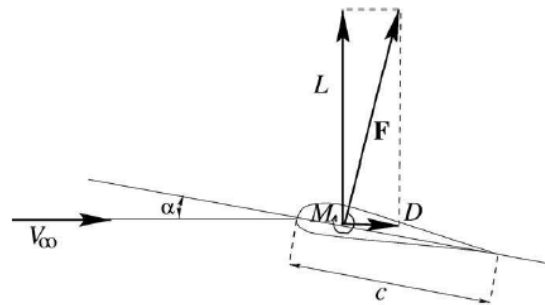


Figure 86: Velocity triangle of a 2D wind turbine blade (Hansen, 2015, p.8)

Appendix F: Blade decay tests

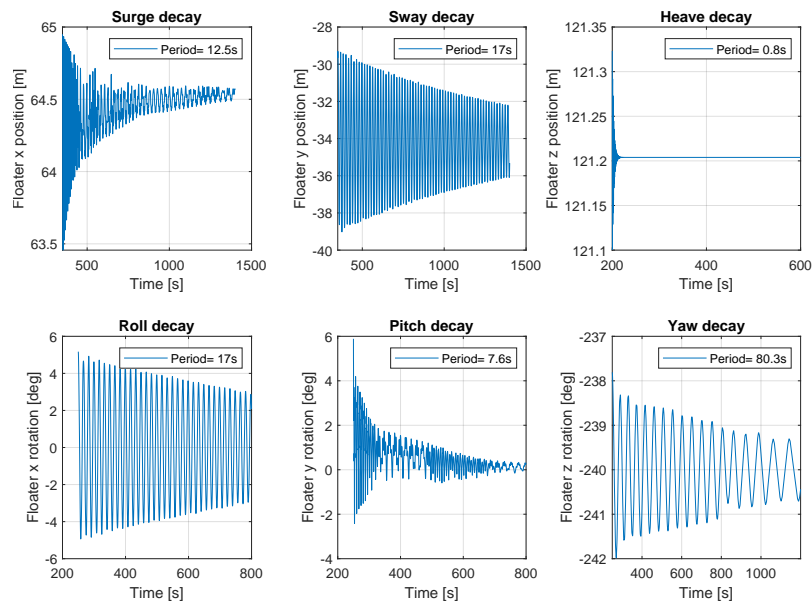


Figure 87: Time series of the blade decay test in all 6 DOF

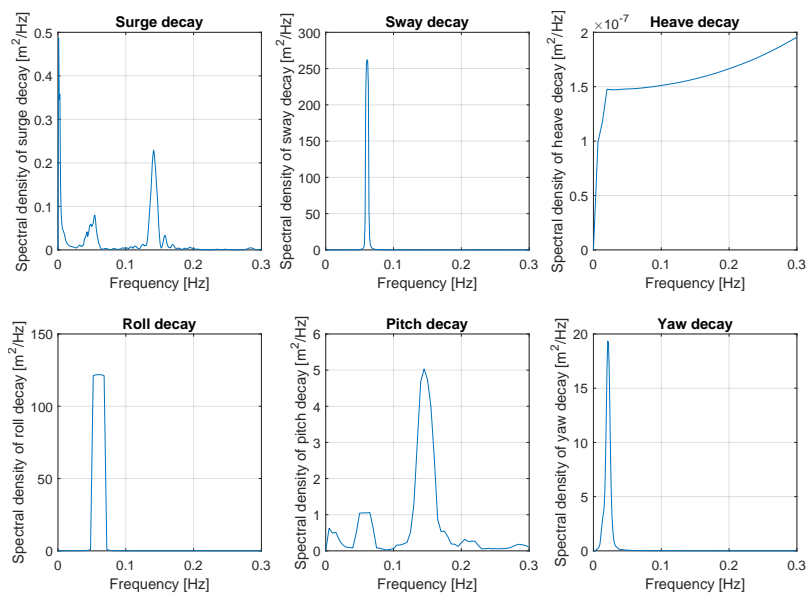


Figure 88: Response amplitude operators of the blade decay test

Appendix G: Crane tip PSDs

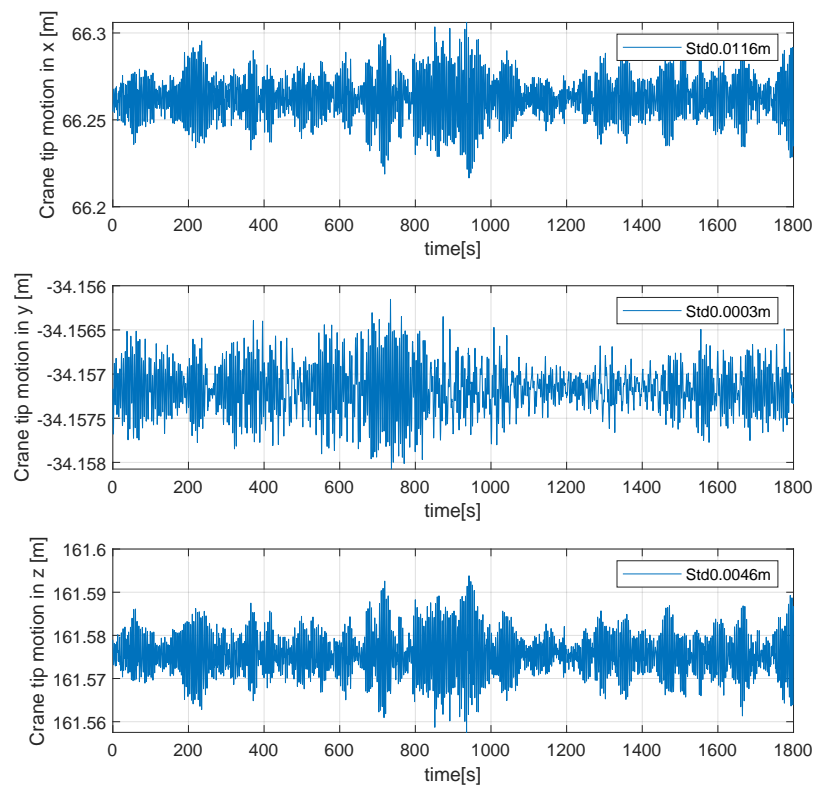


Figure 89: Time series of the crane tip motions at LC14

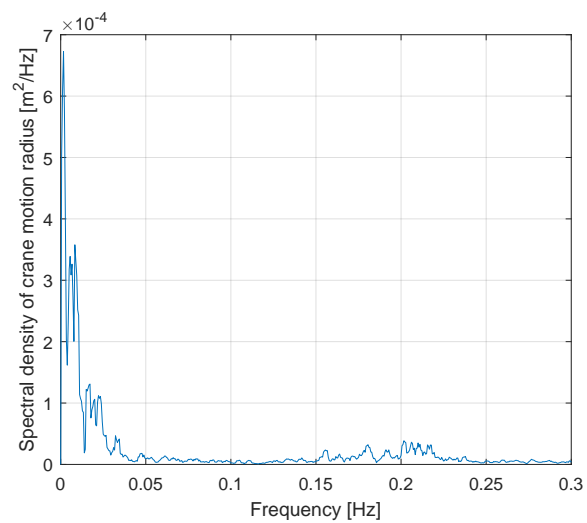


Figure 90: PSD of the relative crane time motion in the xz-plane at LC14

Appendix H: Impact of blade modelling assumptions

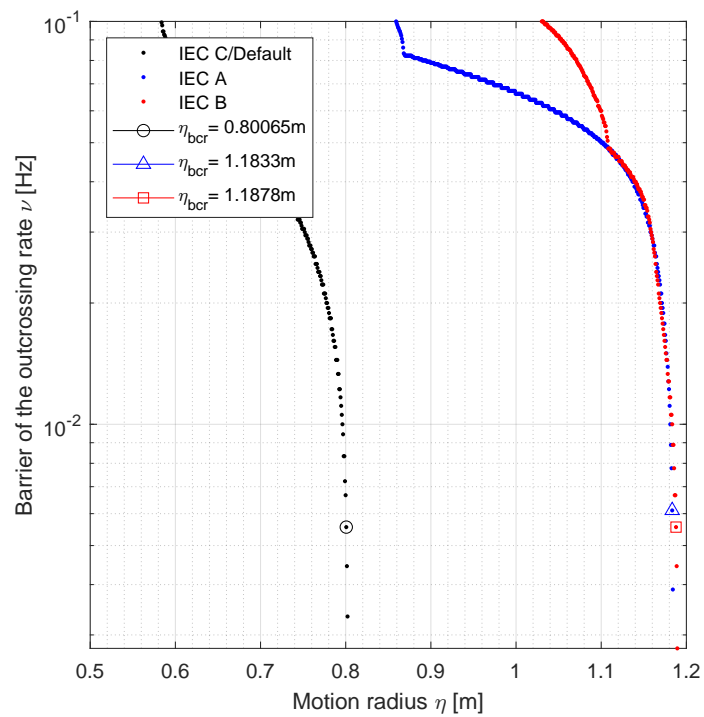


Figure 91: Critical blade root motion at LC14 for different turbulence intensities

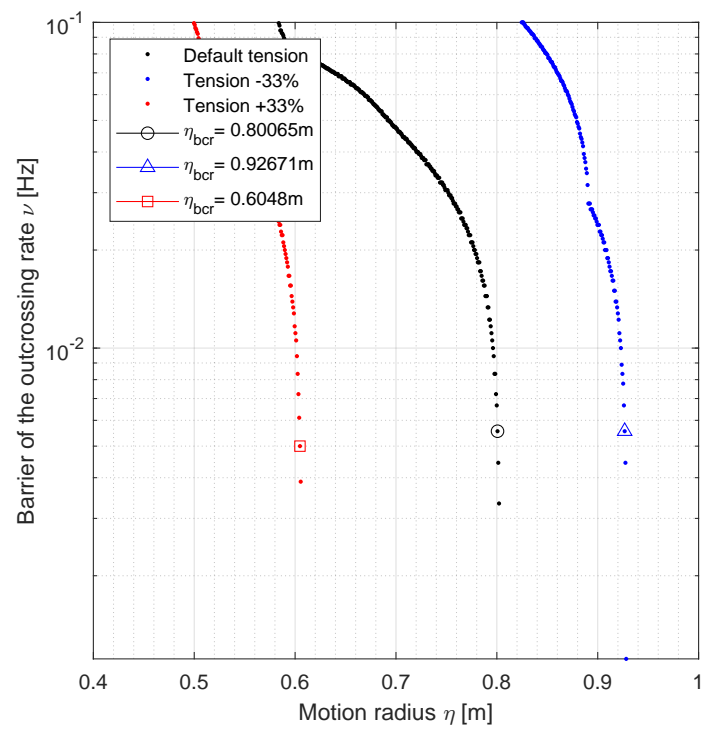


Figure 92: Critical blade root motion at LC14 for different tug line pretensions

Appendix I: Floater decay tests

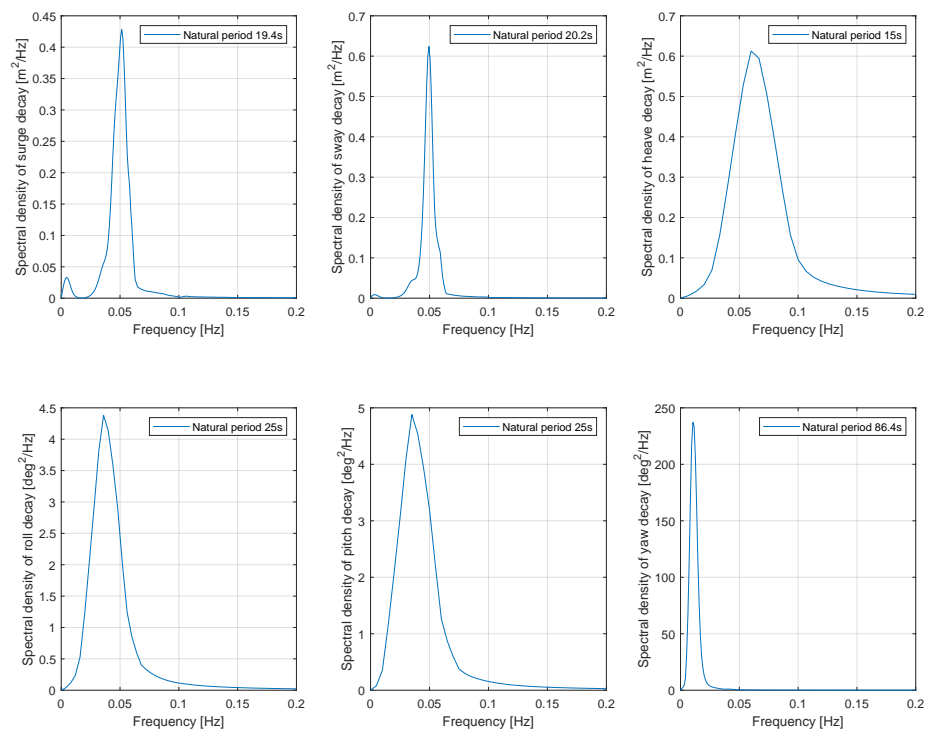


Figure 93: PSDs of the floater motions from the decay test

Appendix L: Mooring line time series

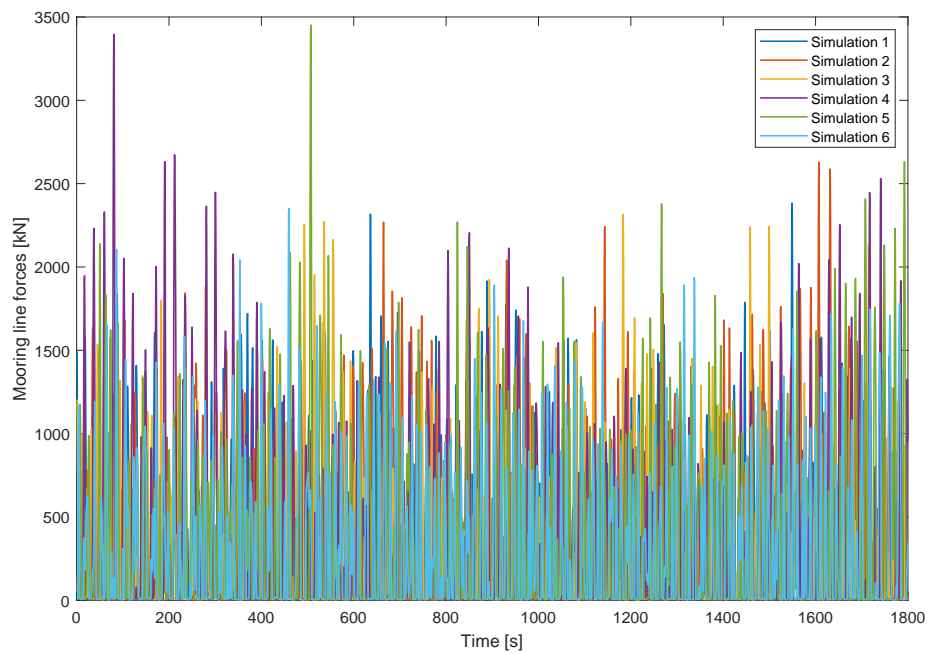


Figure 94: Time series of the mooring line forces of line 2 at LC14 for different simulations

Appendix M: Hub motion statistics

LC	Case	Hs [m]	Tp [s]	Mean [m]	Max [m]	Std [m]	Skewness	Kurtosis
1	A	0.53	8.67	0.8	0.15	0.04	0.05	2.8
2	B	0.7	7.44	0.8	0.18	0.05	-0.02	3
3	C	0.57	11.7	0.82	0.52	0.15	0.08	3.06
4	A	0.79	7.55	0.8	0.21	0.06	-0.01	3.02
5	B	1.1	8.86	0.81	0.52	0.14	0.13	3.53
6	C	1.02	10.2	0.82	0.58	0.16	0.18	3.18
7	A	1.19	7.86	0.8	0.41	0.12	0.02	3.14
8	B	1.6	9.14	0.82	1.01	0.28	0.12	3.71
9	C	1.41	10.6	0.83	0.97	0.29	0.13	3.11
1	A	1.60	8.6	0.81	0.78	0.21	0.1	3.64
11	B	2.2	10.04	0.84	1.39	0.42	0.1	3.2
12	C	1.94	11.6	0.86	1.43	0.41	0.13	3.05
13	A	2.03	9.12	0.82	1.03	0.32	0.06	3.19
14	B	2.7	10.31	0.84	1.57	0.45	0.08	3.21
15	C	2.29	12.3	0.87	1.81	0.53	0.11	3.02

Table 21: Statistics of the hub motion radius, Case A: Mean H_s , Case B: $H_s + 35\%$, Case C: $T_p + 35\%$

Appendix O: Relative motion PSDs for different environmental loads

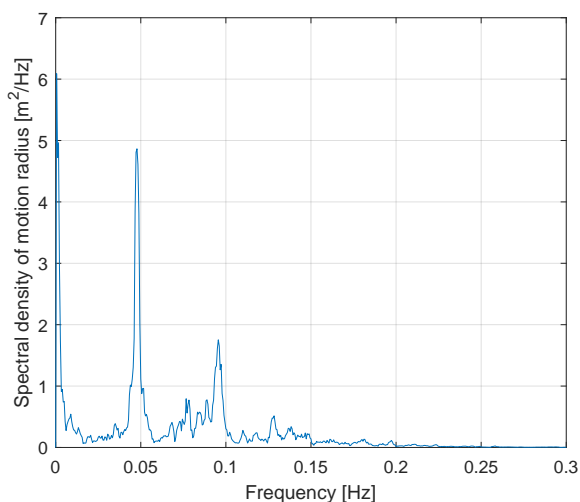


Figure 95: PSD of the relative motion in the xz-plane at LC14 when only considering wave loads

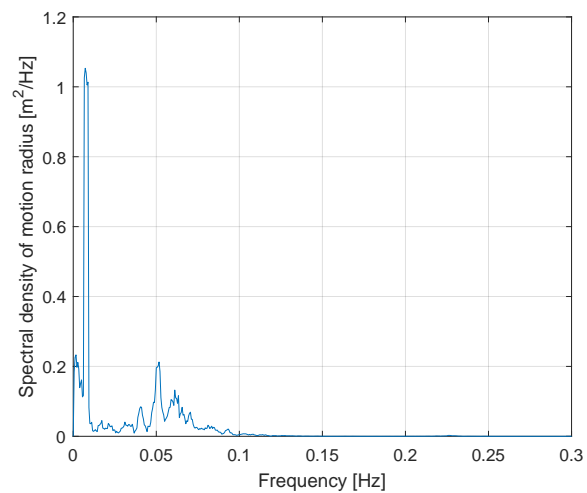


Figure 96: PSD of the relative motion in the xz -plane at LC14 when only considering wind loads

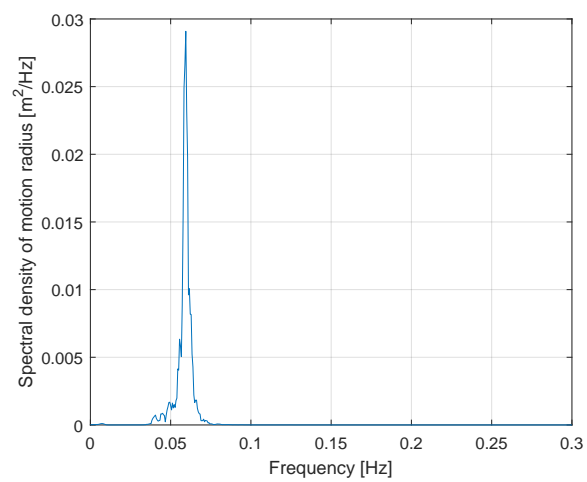


Figure 97: PSD of the relative motion in the xz -plane at LC14 when only considering currents

Appendix P: Pin flange critical motions for 0.3Hz

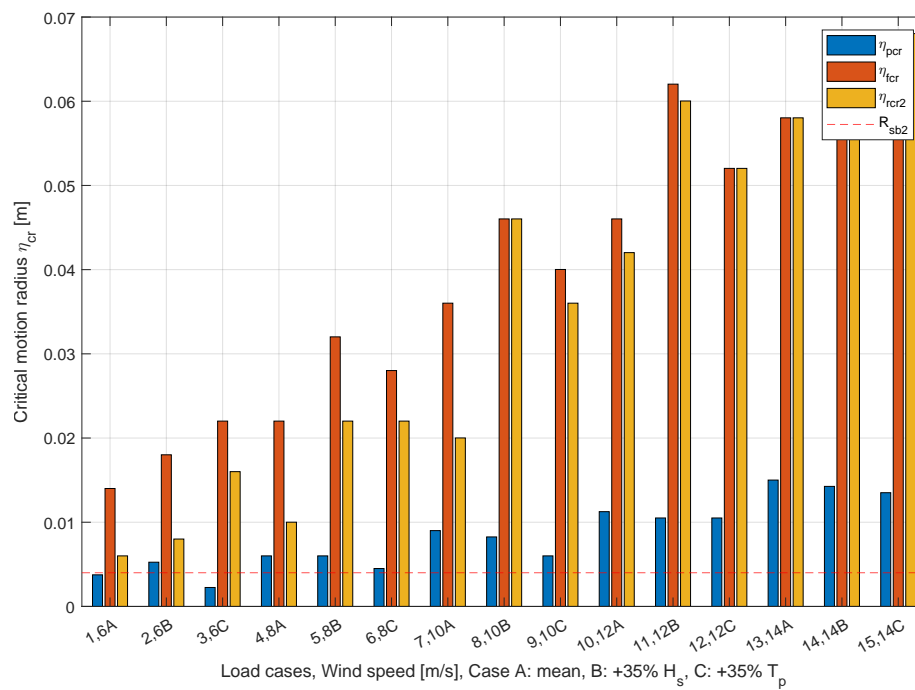


Figure 98: Critical pin-flange motion radii for all considered load cases with a filter of 0.3Hz, $\beta_{wind} = 0^\circ$ and the safe boundary of $R_{sb2} = 4mm$

Appendix Q: Detailed allowable sea states

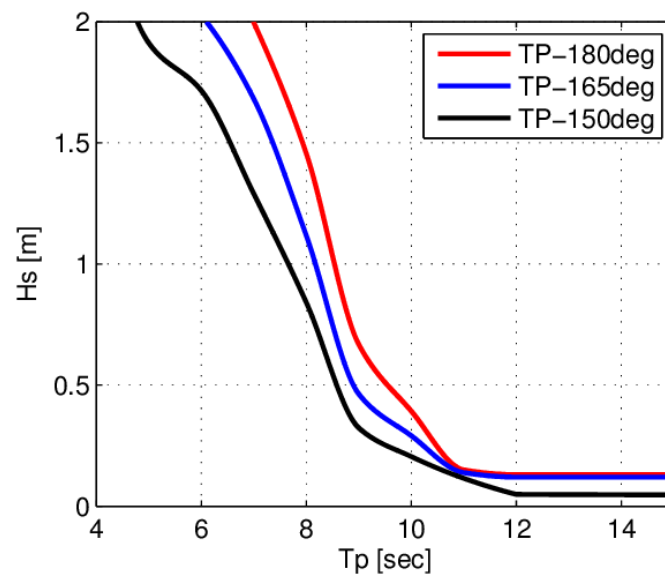


Figure 99: Detailed allowable sea states for the transition piece installation with different heading angles (W. Guachamin Acero et al., 2016, p.323)

Appendix R: Operability of the installation sequence with different limits

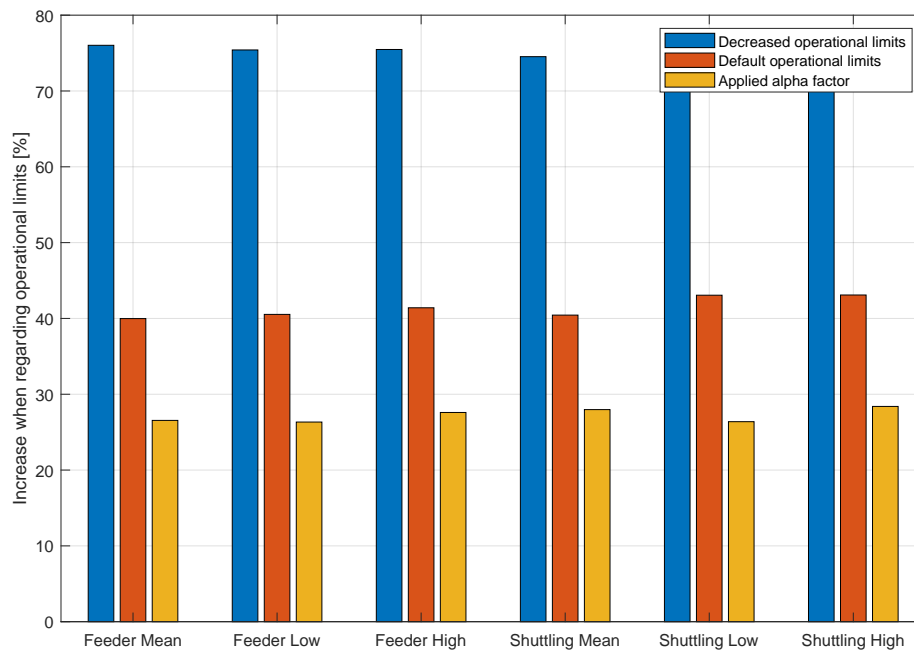


Figure 100: Operability with the different operational limits

Appendix S: Waiting time distribution through out the year

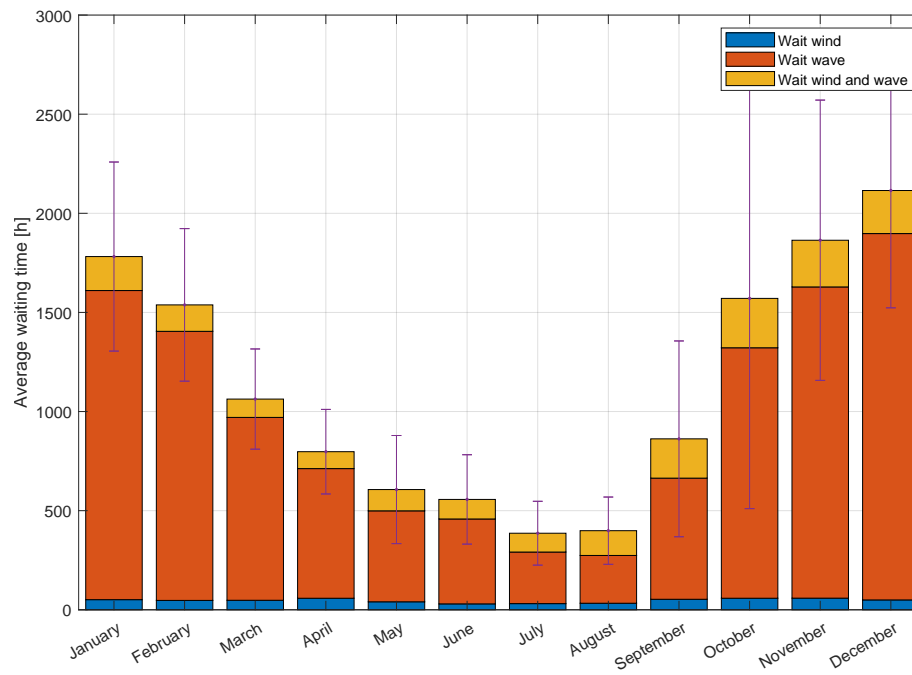


Figure 101: Waiting time per month, separated by the different causes for the waiting time